Chem Soc Rev

REVIEW ARTICLE

View Article Online
View Journal | View Issue

Cite this: *Chem. Soc. Rev.*, 2025, **54**, 10427

Radical retrosynthesis: a powerful strategy for modern assembly of terpenoid natural products

Yong Zhang,†[ab] Yanbo Zhang †[b] and Chao Li *[bc]

Radical retrosynthesis has emerged as a powerful strategy for the modern assembly of complex natural products, offering a one-electron logic that complements traditional polar disconnections. This review highlights recent advances—particularly developed over the past decade—in radical methodologies and their strategic applications in the total synthesis of terpenoid natural products. Emphasis is placed on how various radical precursors, including alkenes, carboxylic acids, halides, alcohols, carbonyl compounds, and alkanes, have been transformed through innovative processes such as photoredox catalysis, metal–hydride hydrogen atom transfer (MHAT), redox-active ester (RAE) chemistry, cross-electrophile couplings (XEC), and HAT-based C–H functionalization. By organizing the discussion around precursor classes and corresponding reaction modes, we illustrate how radical-based synthetic strategies enable efficient construction of quaternary stereocenters and modular assembly of complex polycyclic scaffolds.

Received 2nd July 2025

DOI: 10.1039/d5cs00760g

rsc.li/chem-soc-rev

1. Introduction

Retrosynthetic analysis, since its formalization by E. J. Corey,[1,2] has traditionally rested on polar disconnections as the foundation of synthetic planning. These intuitive disconnections rely on charged synthons, often requiring prefunctionalization and relatively harsh conditions to generate ionic intermediates (Scheme 1(A)). Radical retrosynthesis---articulated by Baran and co-workers in 2018—offers a complementary one-electron framework that exploits innate radical reactivity.[3] Radical intermediates can frequently be accessed under milder, more functional-group-tolerant conditions, enabling bond formations such as radical additions, metal-catalyzed cross-couplings, and cascade sequences. Recent advances—including MHAT,[4–6] RAE chemistry,[7,8] metallaphotoredox catalysis,[9] cross-

[a] *Academy for Advanced Interdisciplinary Studies, Peking University, Beijing 100871, China*
[b] *National Institute of Biological Sciences, Beijing, 102206, China. E-mail: lichao@nibs.ac.cn*
[c] *Tsinghua Institute of Multidisciplinary Biomedical Research, Tsinghua University, Beijing, 100084, China*
† These authors contributed equally to this work.

Yong Zhang

Yong Zhang earned his BSc in Pharmacy from Hebei University of Science and Technology in 2013 and his Master's degree under Prof. Yunfei Du from Tianjin University in 2018. He is currently a PhD candidate at the National Institute of Biological Sciences, Beijing (NIBS) and Peking University, supervised by Prof. Chao Li. His research focuses on 3d metal-catalyzed cross-coupling reactions and radical retrosynthesis strategies for natural product synthesis.

Yanbo Zhang

Yanbo Zhang graduated from The High School Affiliated to Renmin University of China in 2025 and has recently begun his undergraduate studies in the Weinberg College of Arts and Sciences at Northwestern University. He is also enrolled in the Integrated Science Program and is majoring in chemistry. Prior to starting his undergraduate studies, he conducted research as an intern in Dr. Chao Li's laboratory, where he focused on organic synthesis and methodology development. His academic interests center on the design and development of novel synthetic strategies in organic chemistry.

electrophile couplings (XEC),[10] and HAT-based C–H functionalization[11,12]—have expanded the radical synthesis toolbox and begun to address longstanding selectivity challenges.[13] By providing alternative disconnections and harnessing the unique reactivity of radicals, this approach is reshaping synthetic logic and opening new avenues for the efficient assembly of complex natural products.[14,15]

Terpenoid natural products represent one of the most structurally and functionally diverse classes of secondary metabolites.[16] Biosynthetically derived from simple isoprene units, terpenoids give rise to an astonishing array of carbon skeletons, often characterized by densely functionalized frameworks, multiple contiguous stereocenters, and complex polycyclic scaffolds. Representative examples such as taxol and artemisinin not only exemplify the architectural complexity of terpenoids but also underscore their potent biological activities (Scheme 1(B)). Beyond their inherent diversity, terpenoids also serve as precursors to structurally elaborate natural products, including terpenoid-alkaloids,[17] meroterpenoids,[18] and steroids,[19] further expanding their structural and functional landscape.

The remarkable structural complexity and diversity of terpenoids, combined with their potent biological activities,[20] have positioned them as enduring targets in synthetic chemistry.[21–24] Over the years, several reviews have summarized strategies for the chemical synthesis of terpenoids, focusing on bioinspired logic,[25] convergent assembly tactics,[26] radical cascade processes,[14] or chiral pool-based approaches.[27,28] In contrast, retrosynthetic strategies that systematically incorporate radical logic remain largely underrepresented in this context. While the concept of radical retrosynthesis was articulated in Baran's seminal 2018 *Acc. Chem. Res.* article,[3] that perspective was not specific to terpenoid synthesis and primarily laid the conceptual foundation for broader applications of radical disconnections. In the years since, however, radical chemistry has undergone remarkable methodological advances, and its utility in the total synthesis of complex terpenoids has begun to emerge more prominently. At this juncture, a comprehensive review of radical retrosynthesis as a strategic platform for assembling terpenoid natural products is timely and warranted.

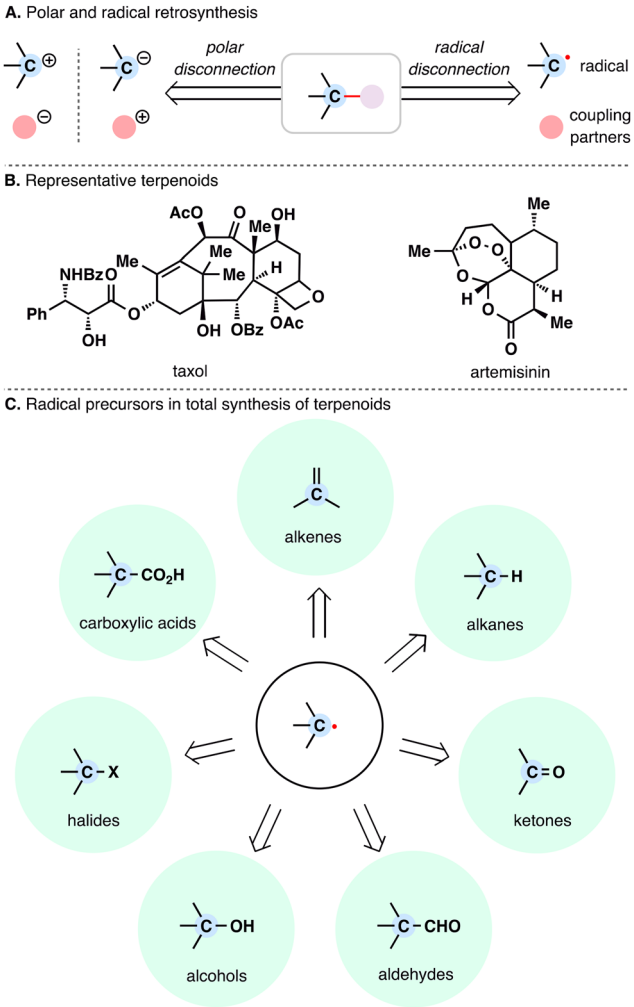

Scheme 1 (A) Polar and radical disconnection strategies. (B) Representative terpenoid-based drugs. (C) Modern radical precursors employed in the total synthesis of terpenoids.

From the perspective of radical retrosynthesis, a given chemical bond can be strategically disconnected into radical fragments, thereby simplifying complex molecular architectures. The success of this tactic hinges on the identification of suitable and stable radical precursors—readily available building blocks that can be converted into the corresponding radical species under controlled conditions. In the forward direction, appropriate radical generation methods and coupling paradigms enable the re-formation of the target bond through a variety of radical transformations. Guided by this logic, the present review is organized around the classes of radical precursors commonly employed in terpenoid synthesis (Scheme 1(C)), including alkenes, carboxylic acids, halides, alcohols, aldehydes, ketones, and alkanes. Within each category, representative examples are discussed according to the types of radical transformations utilized, such as Giese-type radical additions, metal-catalyzed cross-coupling reactions, and radical-polar crossover processes.

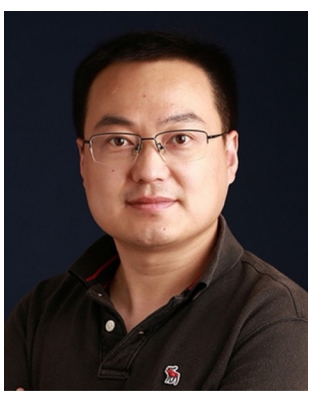

Chao Li

Chao Li received his BS from Qingdao University of Science and Technology in 2008 and earned his PhD in Organic Synthesis in 2013 under the supervision of Prof. Xiaoguang Lei at Tianjin University and the National Institute of Biological Sciences (NIBS), Beijing. He then carried out postdoctoral research with Prof. Phil S. Baran at Scripps Research. In late 2017, he joined NIBS as an Assistant Investigator and was promoted to Associate Investigator in 2023. His research focuses on the total synthesis of complex natural products and the development of novel, efficient synthetic methods.

By articulating this framework, we aim to highlight the synthetic flexibility and strategic versatility that radical retrosynthetic analysis offers in assembling terpenoid skeletons. While numerous studies have demonstrated the growing impact of radical chemistry in total synthesis,[15,29–34] this review focuses specifically on advances in radical chemistry made over the past decade—summarizing representative methodologies that have enabled the efficient assembly of complex terpenoid scaffolds. We hope this perspective offers a constructive framework for appreciating the potential of radical strategies in natural product synthesis, and encourages both experienced practitioners and newcomers to further explore and develop this promising area.

2. Alkenes as radical precursors

Alkenes, long revered for their ubiquity and chemical versatility, have ascended as privileged radical precursors in modern synthetic design, offering a dynamic platform to forge intricate molecular architectures. Their innate electronic polarization—paired with exceptional stability under diverse reaction regimes—renders them uniquely adept at generating carbon-centered radicals. Over the past decade, innovations such as MHAT have catalyzed a paradigm shift, redefining alkenes from passive structural units into strategic linchpins for radical-mediated transformations. This section delineates two recently emerged strategies—MHAT and dealkenylative fragmentation—that exploit alkenes as radical precursors, each offering distinct solutions to key synthetic challenges in terpenoid assembly.

2.1. MHAT reactions

The MHAT reaction has revolutionized the functionalization of unactivated alkenes, converting C=C bonds into reactive carbon-centered radicals under remarkably mild conditions.[4–6,35] By employing abundant transition metals (*e.g.*, Fe, Co, Mn) to deliver hydrogen atoms to alkenes *via* metal–hydride intermediates,[36,37] MHAT circumvents traditional ionic mechanisms reliant on carbocations or carbanions, thereby obviating harsh acidic/basic conditions and prefunctionalization requirements. Pioneered by Tabushi in 1979 for alkene hydration and refined by Mukaiyama in 1989 using silicon hydrides,[38–41] this radical-based paradigm was systematically expanded by researchers including Carreira,[42–48] Boger,[49–52] Norton,[53–57] Baran,[58–62] Shenvi,[63–69] Herzon,[70–73] and Pronin,[74–76] among many others,[77–81] who demonstrated its versatility in forging diverse bonds (C–O, C–N, C–C, C–H) through radical intermediates, even within polyfunctional molecular landscapes.

A transformative leap occurred in 2014 with Baran's reductive olefin coupling (BROC),[59,60] which enabled the direct coupling of unactivated alkenes with electron-deficient partners (*e.g.*, Michael acceptors) using $Fe(acac)_3$ as the catalyst and $PhSiH_3$ as the hydrogen source. This method allowed for the modular construction of sterically congested motifs—such as quaternary centers, bicyclic systems, and cyclopropanes—with high chemoselectivity. In the years that followed, MHAT chemistry emerged as a powerful strategy for assembling complex terpenoid architectures. Its ability to engage unactivated alkenes under mild conditions has proven particularly valuable in constructing polycyclic frameworks with high efficiency and step economy.[80] Today, MHAT-based transformations play an increasingly central role in radical-mediated approaches to terpenoid synthesis.

From the lens of radical retrosynthesis, sterically congested motifs such as quaternary carbons—long considered synthetic bottlenecks—can be strategically deconstructed into two modular fragments: a bulky carbon radical and a tailored radical coupling partner. The former is readily generated *via* MHAT activation of alkenes, while the latter encompasses a diverse array of electrophilic or nucleophilic partners that dictate bond-forming selectivity (Scheme 2). In terpenoid synthesis, key radical coupling partners include electron-deficient olefins (*e.g.*, α,β-unsaturated carbonyls), nitriles, alkenes (as linchpins for radical cascades), alkenylsilanes, carbonyls (ketones/aldehydes), electron-deficient or electron-rich arenes (depending on radical polarity), benzyliron (TPP) (for S_H2 homolytic substitution), and quinone monoacetals (for C–O bond formation)—each enabling distinct bond-forming events. The following case studies illustrate how these partnerships, orchestrated *via* MHAT, overcome steric and electronic challenges in terpenoid assembly. Note that, given the prolific application of MHAT in terpenoid skeleton construction over the past decade, we categorize MHAT-enabled reactions into four classes based on mechanistic parallels: MHAT-radical additions, MHAT-radical-polar crossover cascades, MHAT-S_H2 homolytic substitution, and MHAT-fragmentations cascades.

2.1.1. MHAT-radical additions. Shortly after the Baran group disclosed the HAT-initiated conjugate addition, the Pronin group leveraged this radical-based tactic to enable a concise total synthesis of paxilline indole diterpenes (±)-emindole SB (**1**).[81] As shown in Scheme 3, the commercially available **2** was elaborated in three steps to afford diene **3**. A strategic Fischer indole synthesis was then employed to incorporate an indole N–H group, which served as a stereochemical anchor for the ensuing radical addition, furnishing polycycle **4**. Oxidation of the primary alcohols under Parikh–Doering conditions, followed by mild

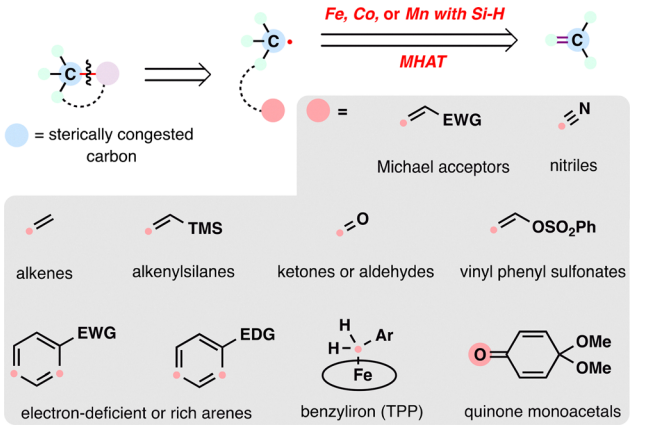

Scheme 2 Contemporary radical retrosynthesis of sterically congested carbon employing the MHAT reaction.

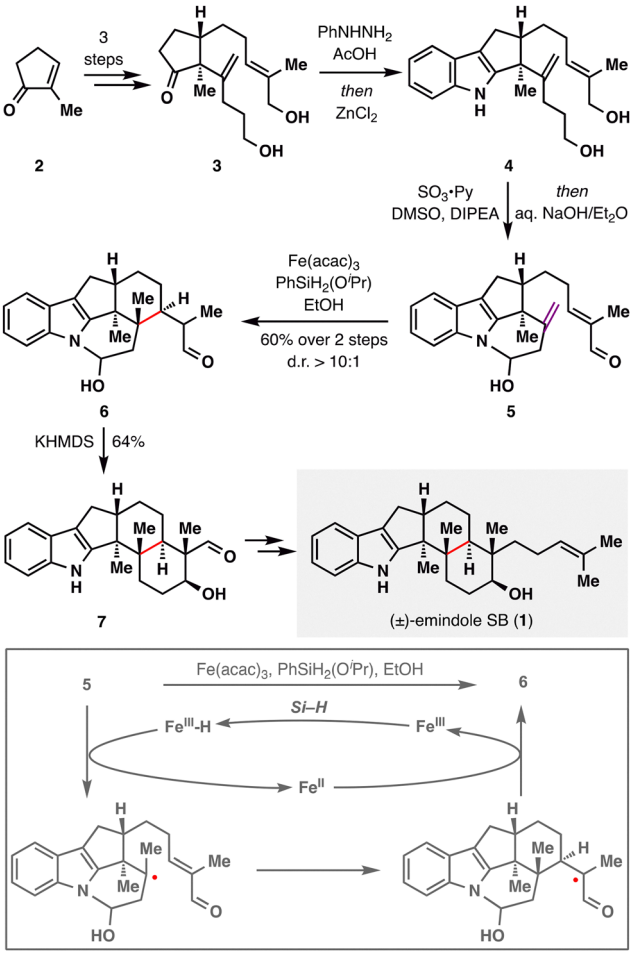

Scheme 3 Total synthesis of (±)-emindole SB (**1**) by Pronin and co-workers.

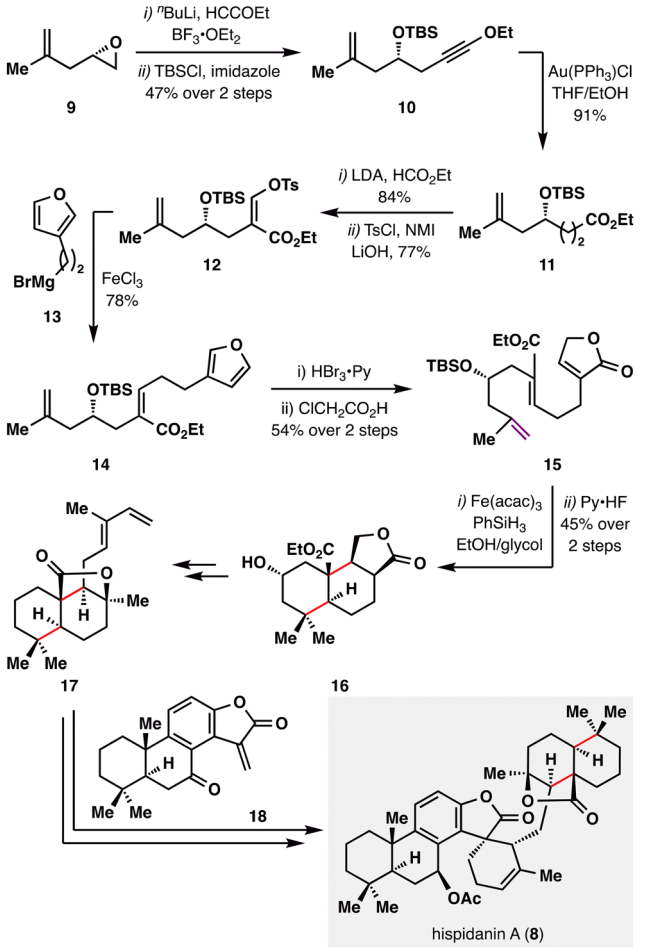

Scheme 4 Liu's synthesis of (−)-hispidanin A (**8**).

basic workup, furnished the cyclic hemiaminal **5**. The key functionalized pentacycle **6**, featuring the challenging quaternary stereocenter, was then secured *via* an intramolecular BROC radical cyclization. This critical sequence proceeded in 60% yield with excellent diastereoselectivity (d.r. > 10:1), a result of stereocontrol imparted by the cyclic hemiaminal.

Taking this reaction as an illustrative case, the mechanism of BROC, although intricate and influenced by solvent effects, can be outlined as follows:[58] $Fe(acac)_3$ first reacts with a silane in an alcoholic solvent to generate an Fe(III)–H intermediate. This species engages the donor olefin to produce a tertiary carbon radical along with an Fe(II) complex. The resulting radical then undergoes an intramolecular Giese-type addition to form an α-aldehyde radical, which is subsequently reduced by the Fe(II) species and protonated to afford the desired product. Treatment of **6** with KHMDS induced an intramolecular aldol reaction to deliver pentacycle **7**, which was advanced to (±)-emindole SB (**1**) in a few further steps.

Hispidanin A (**8**) is a dimeric diterpenoid isolated from the rhizomes of *Isodon hispida*, notable for its polycyclic structure with eleven stereocenters.[82] One of the monomeric units features a polycyclic structure that can be efficiently assembled *via* an MHAT-enabled radical cascade.[83,84] As illustrated in Scheme 4, B. Liu and co-workers initiated the synthesis with an epoxide opening of **9**, followed by TBS protection of the resulting propargyl alcohol to furnish alkynyl ether **10**. Au(I)-catalyzed hydration afforded ester **11**, which was then formylated and tosylated to yield enol tosylate **12**. Kumada cross-coupling of **12** with furanyl Grignard reagent **13** efficiently delivered *Z*-alkene **14**. The furan moiety subsequently underwent oxidative elaboration followed by acid-mediated rearrangement to generate lactone **15**. A BROC radical cyclization, initiated at the *gem*-disubstituted terminal alkene bearing the least steric hindrance and greatest electron density, then constructed the tricyclic core **16**. This radical cascade forged two carbocyclic rings and installed four contiguous stereocenters in a single operation, efficiently assembling the labdane scaffold with high stereocontrol. Further manipulations of **16** provided compound **17** bearing a diene fragment, which engaged in a Diels–Alder cycloaddition with totarane-type dienophile **18**, furnishing the complex polycyclic framework of hispidanin A (**8**) through a concise, strategically orchestrated sequence featuring high *endo*-selectivity and mild conditions.

Another noteworthy example of employing BROC radical cyclization to construct complex polycyclic frameworks is the total synthesis of aplysiasecosterol A (**19**) reported by A. Li and

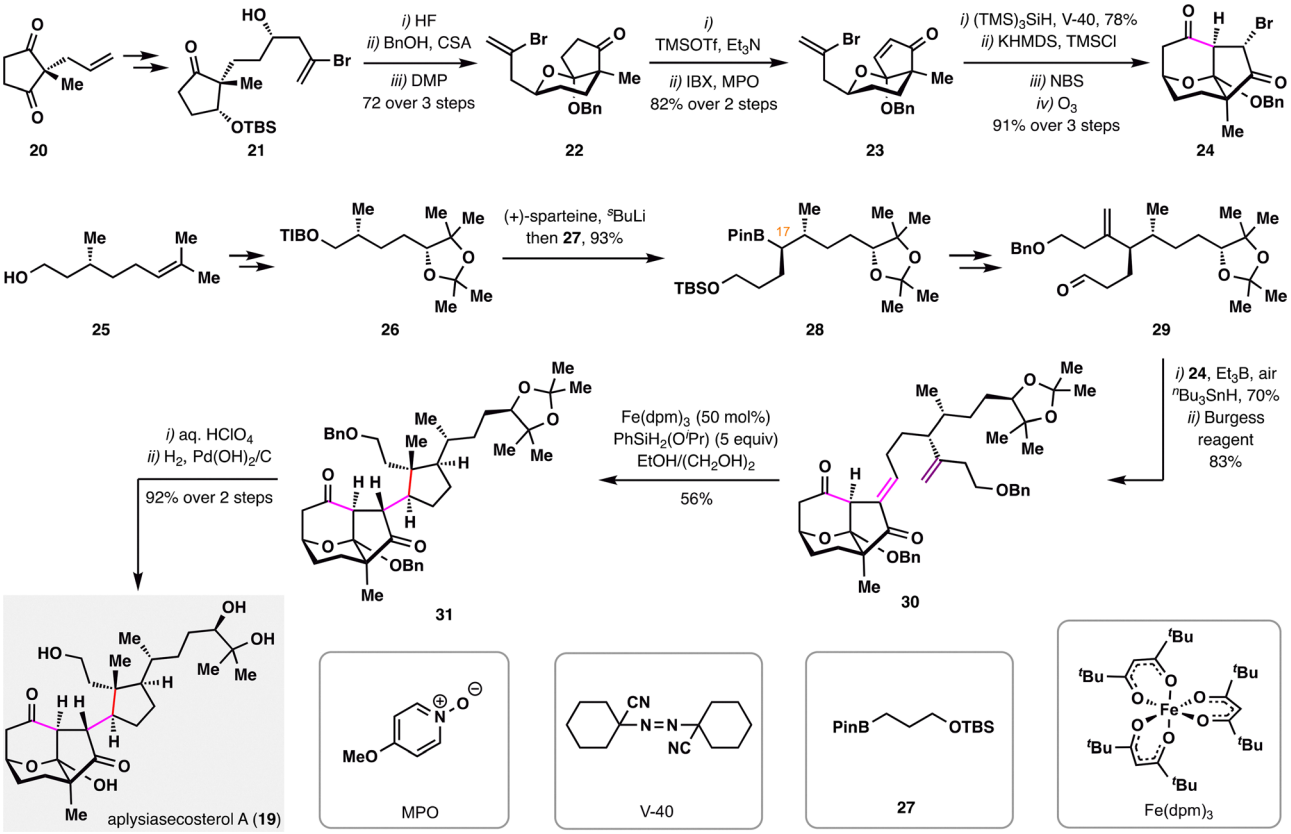

Scheme 5 Total synthesis of aplysiasecosterol A (**19**) by A. Li and co-workers.

co-workers (Scheme 5),[85] in which three contiguous stereocenters—including a quaternary carbon center—were forged in a single step. The synthesis adopted a convergent strategy, involving the preparation of two polyoxygenated fragments **24** and **29**, each bearing multiple stereocenters. The left-hand fragment **24** was constructed from compound **20** through a sequence involving key desymmetrizing reduction, asymmetric 2-bromoallylation, ketalization, and IBX dehydrogenation to furnish intermediate **23**, which then underwent intramolecular radical cyclization, bromination, and ozonolysis. The right-hand fragment **29** was derived from (+)-citronellol, with an Aggarwal lithiation–borylation serving as the key transformation to install the C17 stereocenter.[86] Coupling of fragments **24** and **29** *via* a radical-initiated Reformatsky-type reaction furnished the adduct,[87] which was subjected to Burgess dehydration to give compound **30**. Subsequent treatment of **30** with a modified BROC cyclization protocol [$Fe(dpm)_3$ and $PhSiH_2(O^iPr)$] provided tricyclic product **31** in 56% yield with high diastereoselectivity. Final deprotections of **31** delivered aplysiasecosterol A (**19**) in high yield.

The stereospecific MHAT radical addition directed by a quaternary center has been effectively explored by Snyder and co-workers in their elegant construction of the conidiogenone family (**32–34**).[88] As illustrated in Scheme 6, enone **35** underwent a BROC radical cyclization to afford bicyclic ketone **36**. Due to the steric bias imparted by the adjacent quaternary center, the tertiary radical generated under $Fe(acac)_3/PhSiH_3$ conditions approached exclusively from the bottom face, furnishing **36** as a single diastereomer in 83% yield. Subsequent functional group manipulations converted **36** into enol triflate **37**, bearing a terminal alkene, which underwent a Pd-catalyzed ring closure to construct the tricyclic scaffold **38**. This intermediate was then elaborated to alkenyl iodide **40**, which participated in a reductive Heck coupling to generate **42**—a versatile branching point for the divergent synthesis of three structurally related natural products: conidiogenone B (**32**), conidiogenone (**33**), and conidiogenol (**34**).

Meroterpenoids represent a vast and structurally diverse class of hybrid terpene natural products, many of which exhibit notable biological activities.[89] Among them, taondiol (**43**) and chevalone A (**44**) share a characteristic C3-oxidized *ent*-isocopalane core. Recently, Renata and co-workers employed an intramolecular BROC to stereoselectively construct the synthetically challenging adjacent C8 and C14 stereocenters (Scheme 7).[90] Starting from sclareol (**45**), a readily available diterpene with an isocopalane-like framework, a concise three-step sequence transformed it into lactone **46**, thereby establishing the structural platform for a BROC radical cyclization. Under classical conditions, the resulting tertiary radical underwent a highly diastereoselective top-face addition to the enone, furnishing compound **47** as a single diastereomer in 95% yield. This selectivity was attributed to rapid conformational reorganization of the tertiary radical intermediate and conformational control imposed by the rigid *trans*-decalin and butyrolactone

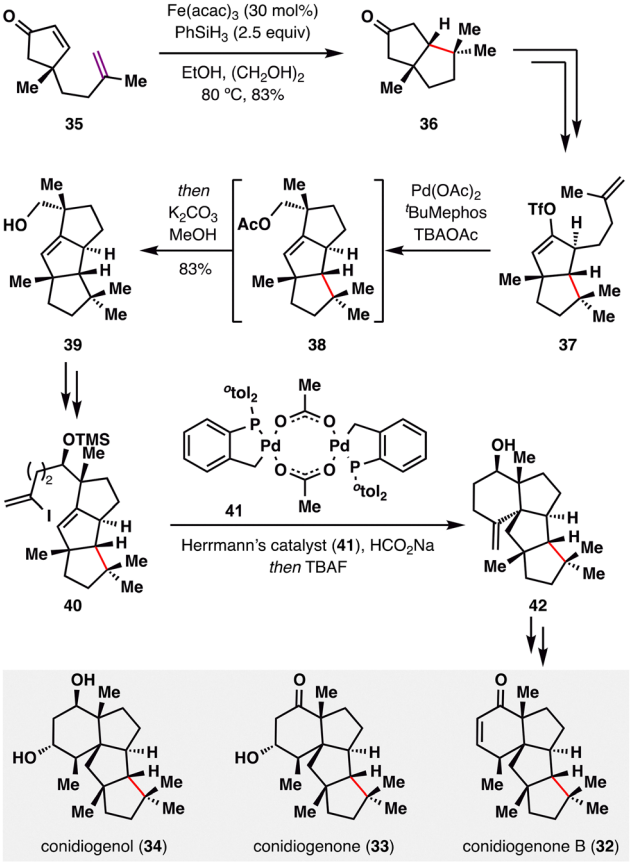

Scheme 6 Quaternary-center-guided synthesis of conidiogenones (**32–34**) by Snyder and co-workers.

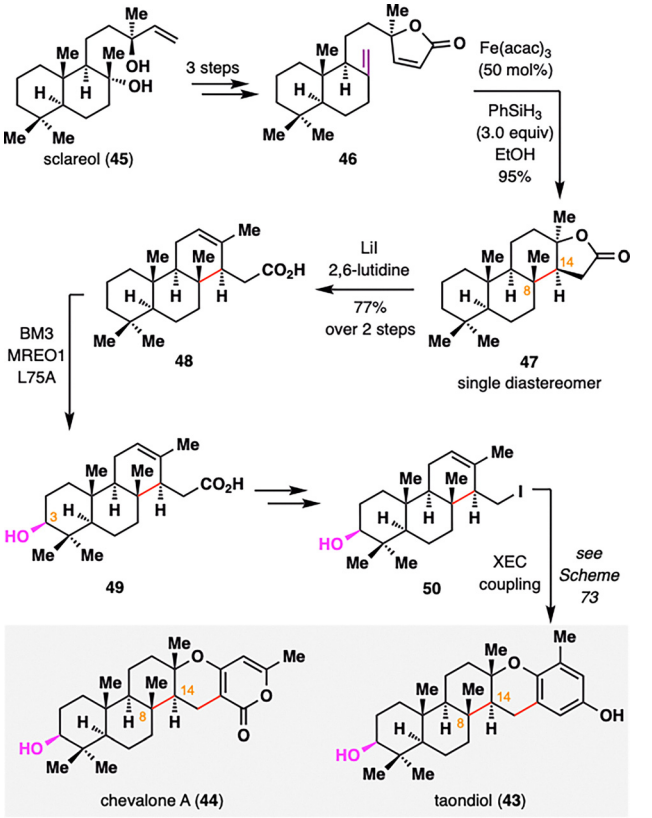

Scheme 7 Renata's synthesis of taondiol (**43**) and chevalone A (**44**).

motifs. Subsequent lactone opening *via* elimination yielded carboxylic acid **48**, completing the construction of the *ent*-isocopalane core. Site-selective C3 oxidation of **48** was achieved using the engineered biocatalyst MERO1 L75A, delivering compound **49** in 62% yield. Further functionalization furnished iodinated intermediate **50**, which served as a common precursor for the synthesis of both taondiol (**43**) and chevalone A (**44**) *via* cross-electrophile coupling (XEC), as outlined in Scheme 7**3**.

Daphnezomines A (**51**) and B (**52**), first isolated by Kobayashi and co-workers from the leaves of *Daphniphyllum humile*, feature a rare and synthetically formidable aza-adamantane core (Scheme 8).[91] Our group addressed this challenge through a late-stage construction of the topologically strategic C8–C9 bond *via* BROC radical cyclization.[92] The synthesis commenced from commercially available chiral pool material (*S*)-(+)-carvone (**53**). A sequence involving hydrogenation, Sharpless allylic amination,[93,94] and palladium-catalyzed oxidative cyclization furnished azabicyclo[3.3.1]nonane scaffold **55**. The bridgehead ketone was subsequently transformed into an olefin, and an enone moiety was installed to set the stage for the BROC radical cyclization. Notably, the use of low concentrations of $Fe(acac)_3$ and $Ph(^iPrO)SiH_2$ proved optimal, delivering compound **57** in moderate yield. This transformation simultaneously established two stereocenters at C8–C9 and completed the construction of the tetracyclic skeleton in a single operation. Final

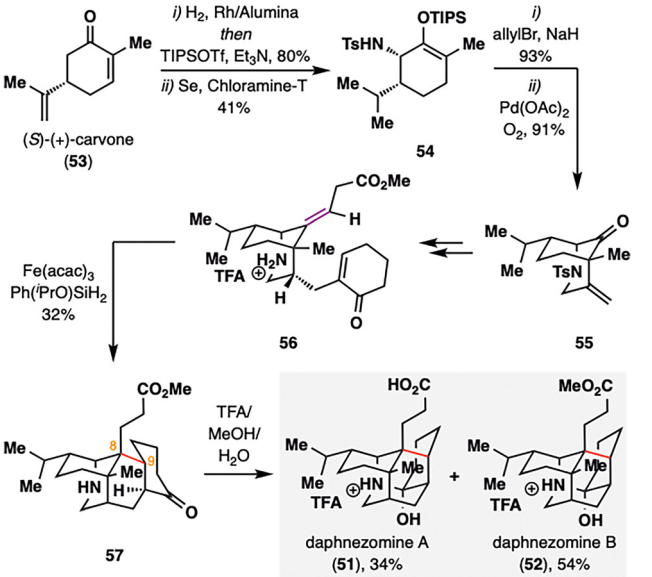

Scheme 8 C. Li's total synthesis of daphnezomines A (**51**) and B (**52**).

treatment of **57** with trifluoroacetic acid in methanol furnished the natural products daphnezomine A (**51**) and daphnezomine B (**52**) in 34% and 54% yields, respectively.

Gedunin (**58**), a member of the tetranortriterpenoid family, features a highly oxidized and structurally rearranged limonoid scaffold that poses a significant synthetic challenge. Renata

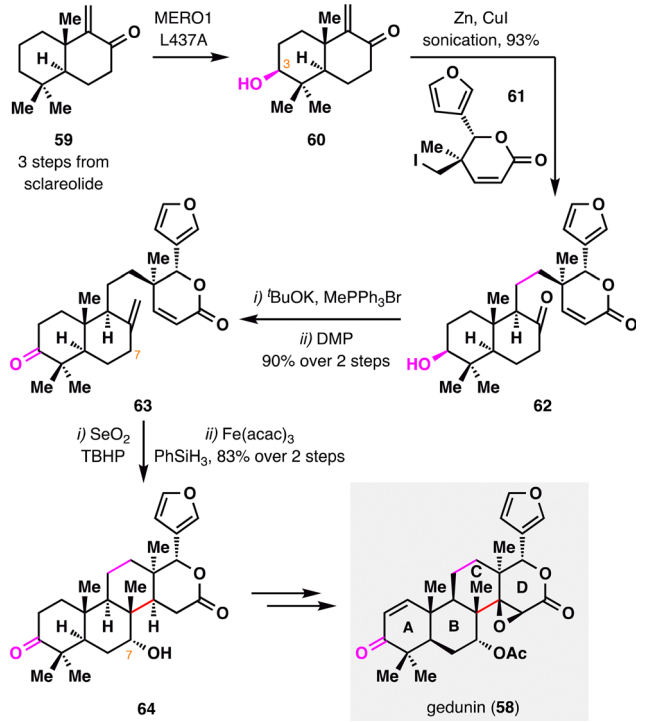

Scheme 9 Chemoenzymatic synthesis of gedunin (**58**) by Renata and co-workers.

and co-workers achieved the first total synthesis of gedunin (**58**),[95] through a combination of BROC radical cyclization and enzyme-catalyzed C–H oxidation. As outlined in Scheme 9, the synthesis commenced from bicyclic enone **59**, readily prepared from commercially available sclareolide. A bioengineered enzyme-catalyzed C3 hydroxylation of **59** furnished alcohol **60**, which was coupled with lactone **61** *via* Luche's protocol to deliver ketone **62** as a single diastereomer in 93% yield.[96] Methylenation of the ketone followed by a second C3 oxidation provided intermediate **63**. Subsequent C7 allylic oxidation, followed by treatment of the resulting allylic alcohol with $Fe(acac)_3$ and $PhSiH_3$, successfully established the crucial quaternary stereocenter and the sterically congested C/D-ring junction with excellent diastereoselectivity and high efficiency. Final double desaturation of the A and D rings, followed by diastereo- and chemoselective epoxidation, delivered the natural product gedunin (**58**) in a highly streamlined and efficient sequence.

MHAT-radical addition also plays a central role in the synthesis of longiborneol sesquiterpenoids (**65–73**) *via* a "functionalized camphor" strategy, as reported by Sarpong and co-workers (Scheme 10).[97,98] Notably, this work revealed vinyl sulfonates as viable radical acceptors, thereby expanding the scope of MHAT chemistry to include polarity-reversed enol alkylation. The synthesis commenced with epoxidation of (*S*)-carvone (**53**), followed by a Ti(III)-mediated intramolecular reductive cyclization of the resulting epoxy-carvone to yield cyclobutanol **76**.[99] A Brønsted acid-promoted semipinacol rearrangement of **76** furnished 8-hydroxycamphor (**77**), which was further elaborated to compound **78**, bearing a skipped diene

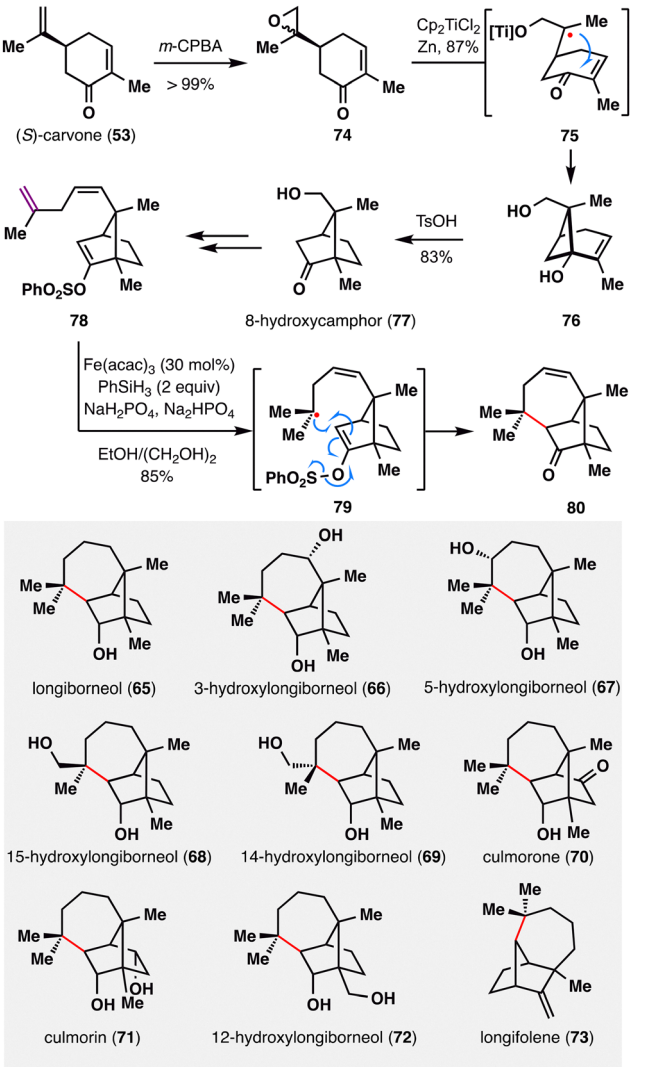

Scheme 10 Collective synthesis of longiborneol sesquiterpenoids (**65–73**) by Sarpong and co-workers.

and an enol vinyl phenyl sulfonate. Exposure of **78** to BROC radical cyclization conditions delivered compound **80** in excellent yield. This transformation proceeded *via* HAT from an Fe(III)–H species to the terminal position of the 1,1-disubstituted alkene, generating a tertiary radical that underwent intramolecular addition into the vinyl sulfonate. Subsequent homolytic cleavage of the S–O bond furnished the corresponding ketone. The successful application of MHAT in this "functionalized camphor" strategy highlights its versatility in enabling the total synthesis of structurally diverse longiborneol sesquiterpenoids (**65–73**) bearing the bicyclo[2.2.1]bornane core.

Pleuromutilin (**81**), a diterpenoid natural product isolated from *Clitopilus* species, is well known for its antibacterial activity.[100] Pronin and co-workers achieved rapid access to its core perhydroindanone framework through a sequence featuring an intermolecular Diels–Alder cycloaddition followed by a key BROC radical cyclization.[101] As outlined in Scheme 11, the Diels–Alder reaction between diene **82** and dienophile **83** afforded bicyclic adduct **84** in 41% yield with moderate diastereoselectivity

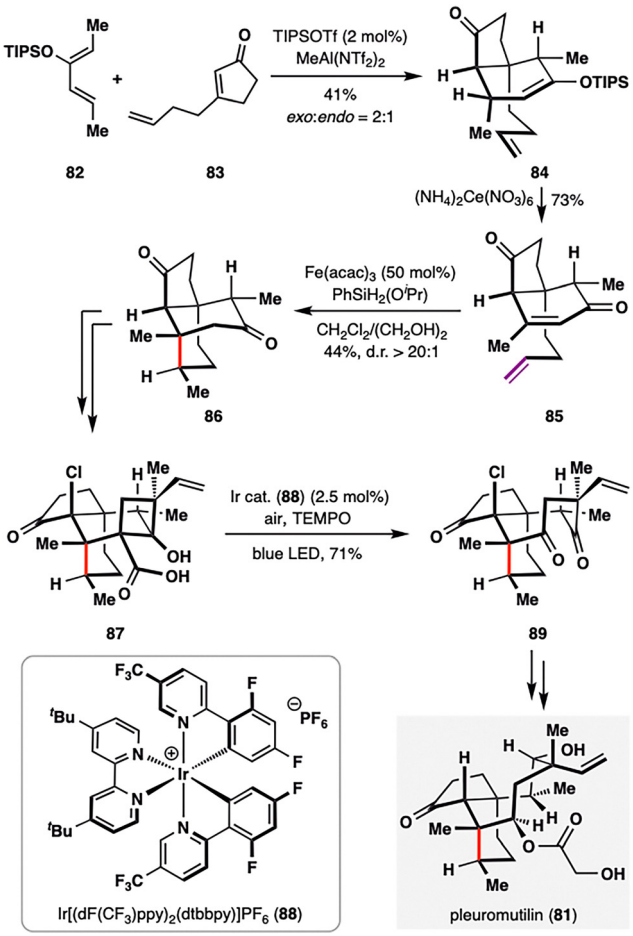

Scheme 11 Pronin's synthesis of pleuromutilin (**81**).

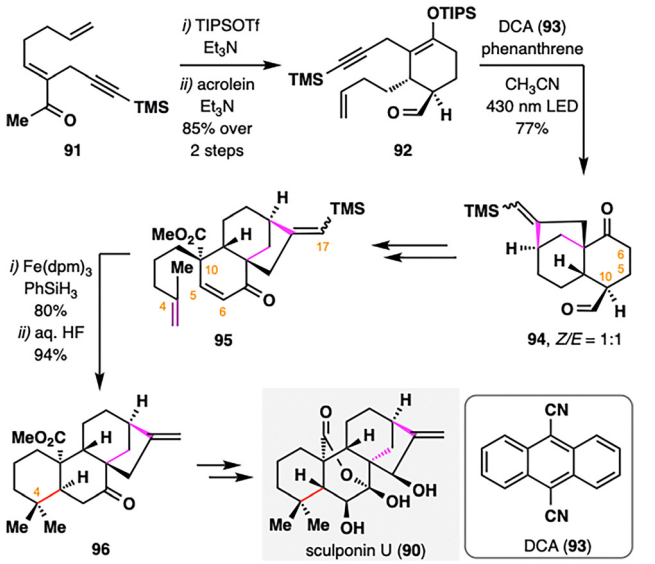

Scheme 12 Total Synthesis of sculponin U (**90**) by Liu, Fu, and co-workers.

(*exo*: *endo* = 2:1). Oxidation of the resulting enol ether yielded enone **85**, bearing both a terminal alkene and an enone moiety poised for BROC cyclization. Treatment of **85** with $Fe(acac)_3$/$PhSiH_2(O^iPr)$ delivered tricycle **86** in 44% yield and excellent diastereoselectivity (d.r. > 20:1). This radical cyclization proceeded *via* formation of a secondary radical at the terminal alkene, which added to a sterically hindered β-disubstituted enone—demonstrating the power of MHAT in challenging radical additions. From **86**, formation of a strained four-membered ring in **87** enabled a photoredox-catalyzed oxidative decarboxylation (air/TEMPO/Ir cat. **88**), generating a cyclobutyl radical intermediate that was trapped by TEMPO or oxygen. The resulting intermediate underwent Grob-type fragmentation to furnish functionalized cyclooctane **89**. Final elaboration of **89** completed the total synthesis of pleuromutilin (**81**) in three additional steps.

B. Liu and co-workers reported the total synthesis of sculponin U (**90**),[102] an *ent*-kaurane-type diterpenoid characterized by a distinctive 7,20-lactone–hemiketal bridge. The synthetic strategy prominently features a radical cascade initiated by photoinduced electron transfer (PET) and a subsequent BROC radical cyclization as key transformations. As outlined in Scheme 12, silyl enol ether formation from intermediate **91**, followed by a Diels–Alder reaction with acrolein, furnished adduct **92**. The core bicyclo[3.2.1]octane scaffold **94** was then constructed *via* a PET-mediated radical cyclization developed by the Mattay group,[103] employing 9,10-dicyanoanthracene (**93**) as photosensitizer under 430 nm irradiation. Remarkably, the transformation proceeded exclusively through a 6-*endo*-trig cyclization followed by a 5-*exo*-dig closure. Subsequent steps included dehydrogenation at C5–C6 and installation of a terminal alkene at C10, thereby setting the stage for BROC radical cyclization. Treatment of **95** with $Fe(dpm)_3$/$PhSiH_3$, followed by desilylation at C17, furnished compound **96** in excellent yield. Notably, the steric hindrance from the bulky TMS group at C17 effectively suppressed undesired hydrogenation of the C16═C17 double bond under HAT conditions, thus ensuring the chemoselectivity of the radical cyclization. Final elaboration, including conversion of the *cis*- to the *trans*-A/B ring fusion, completed the total synthesis of sculponin U (**90**).

Beyond the construction of the C4 quaternary center in the aforementioned synthesis of sculponin U (**90**), BROC radical cyclization also demonstrates powerful utility in forging the C10 quaternary carbon in other tetracyclic diterpenoids. In 2023, C. Fan and co-workers developed an asymmetric strategy for the divergent synthesis of nine C8-ethano-bridged tetracyclic diterpenoids, including natural products **97–101**, with MHAT-mediated BROC radical cyclization as a key step.[104] As illustrated in Scheme 13, the bicyclo[3.2.1]octane scaffold **103** was efficiently assembled from readily accessible cyclohexenone **102** *via* a Au(I)-catalyzed Conia-ene cyclization. Subsequent functional group manipulation of **103** furnished intermediate **104**, which underwent intermolecular reductive coupling with fragment **105** to generate a mixture of C7 diastereomers, **106a** and **106b**. Strategic application of BROC radical cyclization on **106a** and **106b** delivered the corresponding tetracyclic products **107** and **108**, each bearing a C10 quaternary center, in good yields and with high diastereoselectivity. Notably, the optimized protocol—employing $Fe(dbm)_3$ and $Ph(^iPrO)SiH_2$ in the presence of Na_2HPO_4—proved

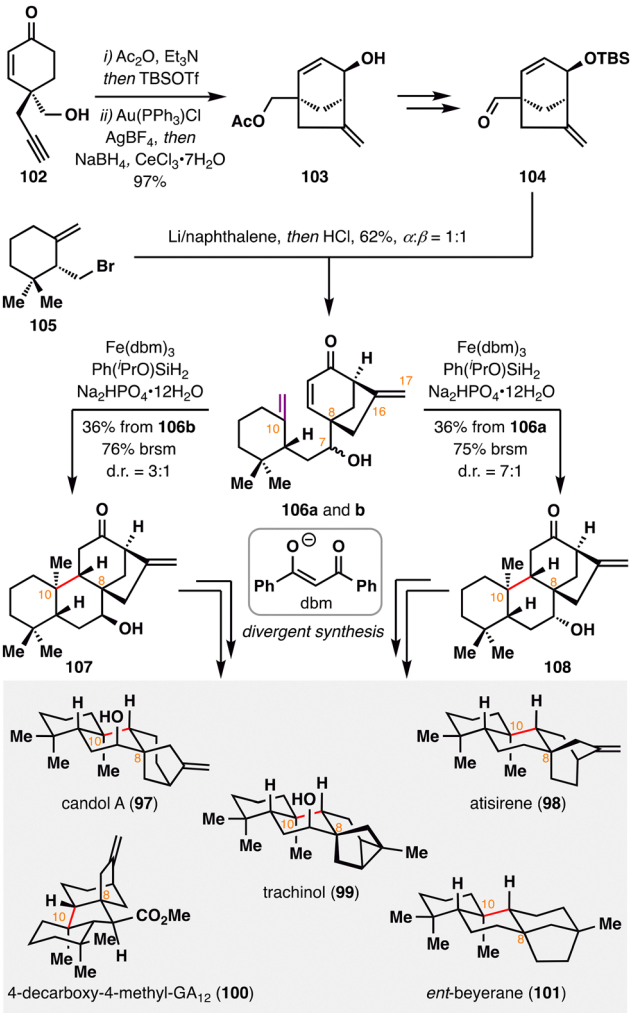

Scheme 13 C. Fan's divergent synthesis of *ent*-kaurane-, *ent*-atisane-, *ent*-beyerane-, *ent*-trachylobane-, and *ent*-gibberellane-type diterpenoids (**97–101**).

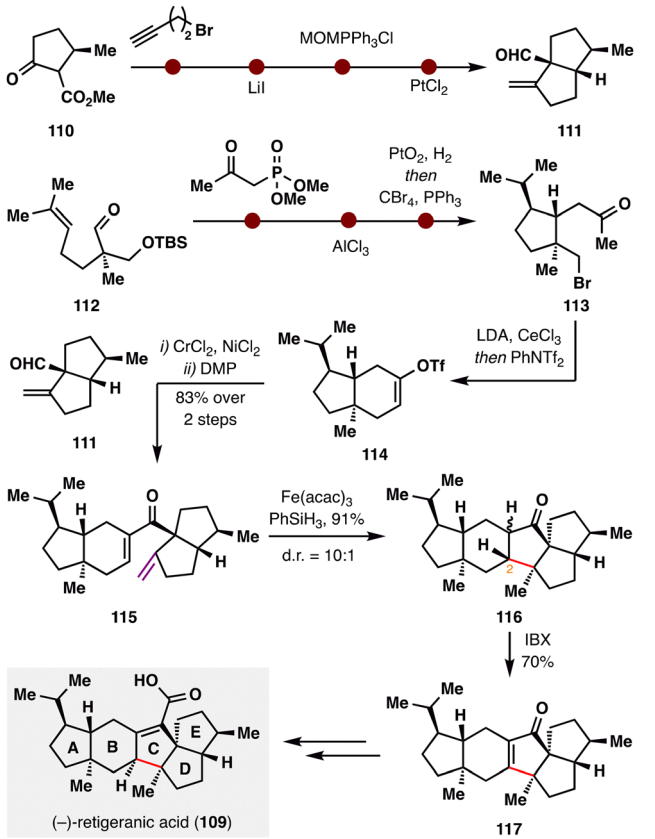

Scheme 14 Total synthesis of (–)-retigeranic acid (**109**) by X. Chen, S.-H. Wang, and co-workers.

crucial in suppressing both the formation of undesired diastereomers at C10 and over-reduction of the C16═C17 olefin, thereby ensuring excellent regio- and stereocontrol. Tetracycles **107** and **108** subsequently served as versatile intermediates for the downstream collective synthesis of C8-ethano-bridged diterpenoids.

(–)-Retigeranic acid A (**109**), isolated from *Himalayan lichens*,[105] features a unique pentacyclic architecture comprising an angular triquinane subunit and eight stereocenters—rendering it an exceptionally challenging and attractive synthetic target. Recently, the groups of S.-H. Wang and X. Chen collaboratively achieved its total synthesis,[106] highlighted by a late-stage 5-*endo*-trig BROC radical cyclization—an anti-Baldwin closure that is topologically disfavored (Scheme 14). The synthesis commenced from ester **110**, which underwent α-substitution, Krapcho decarboxylation, Wittig olefination, and a Conia–ene cyclization to furnish the [5.5]-fused D/E ring system **111**. In parallel, aldehyde **112** was elaborated into the A/B ring fragment **113** *via* a sequence comprising Horner–Wadsworth–Emmons (HWE) homologation, Prins cyclization, hydrogenation, and Appel chlorination. Intramolecular substitution followed by triflation with $PhNTf_2$ afforded vinyl triflate **114**, which underwent Nozaki–Hiyama–Kishi (NHK) coupling with fragment **111**. Subsequent DMP oxidation furnished ketone **115**. The pivotal BROC radical cyclization was then applied to forge the central C ring in **116** *via* a topologically disfavored 5-*endo*-trig pathway, proceeding in an impressive 91% yield and showcasing the unique capability of this radical approach in accessing otherwise inaccessible ring systems. Although the resulting stereochemistry at C2 was epimeric relative to the natural product, a subsequent IBX dehydrogenation installed enone **117**, enabling downstream stereochemical correction. With the core skeleton fully constructed, a final four-step sequence completed the synthesis of (–)-retigeranic acid A (**109**).

Cycloaurenones and dysiherbols represent a class of sesquiterpene quinones/quinols characterized by a fused 6/6/5/6 tetracyclic framework that incorporates either a *cis*- or *trans*-decalin motif and four contiguous stereocenters.[107] Recently, the Lu group reported the first enantioselective and divergent total synthesis of these natural products,[108] featuring a desymmetrizing BROC radical cyclization and a newly developed copper-catalyzed enantioselective conjugate addition. In their synthesis of cycloaurenones (Scheme 15(A)), the route commenced with the installation of two nonadjacent 1,4-stereocenters *via* a desymmetrizing enantioselective hydrogenation of bis-α,β-unsaturated Weinreb amide

121, delivering **122** in d.r. > 99:1 and 99% e.e. Subsequent transformations converted **122** into cyclohexadienone **124**, thereby setting the stage for the key BROC radical cyclization. Treatment of **124** with $Fe(acac)_3$ and $PhSiH_3$ induced an intramolecular cyclization to furnish fused tricyclic intermediate **125** in 85% yield. The high stereoselectivity of this desymmetrizing radical cyclization was attributed to pseudo-1,3-diaxial interactions between the methyl groups at C5 and C9, which directed the formation of the stereogenic quaternary center at C9. Further elaboration of **125**, including SeO_2-mediated allylic oxidation and Pd-catalyzed reductive Heck coupling, yielded the tetracyclic intermediate **126**, which was advanced to cycloaurenones (**118–120**). In the synthesis of dysiherbols (Scheme 15(B)), a Cu-catalyzed desymmetrizing 1,4-conjugate methylation to **124** furnished **132**, which upon exposure to the same BROC radical cyclization conditions delivered fused decalin **133** in 78% yield as a single diastereomer. Subsequent IBX dehydrogenation followed by an intramolecular conjugate addition furnished common intermediate **135**, which was further functionalized to afford dysiherbols (**127–131**). In both sequences, BROC radical cyclization proved pivotal in constructing the polycyclic cores and establishing multiple stereocenters in a single transformation, thereby enabling a concise and modular approach to these architecturally complex sesquiterpenoids.

Building upon these elegant applications of MHAT chemistry in assembling complex polycyclic terpenoid frameworks, Dai and co-workers further demonstrated its versatility in addressing one of the most formidable topological challenges in diterpenoid synthesis: the stereoselective construction of a sterically congested cyclopropane ring (Scheme 16).[109] (−)-Peyssonnoside A (**137**), a sulfated diterpene glycoside isolated from the red alga *Peyssonnelia* sp.,[110] features an unprecedented 5/6/3/6 tetracyclic carbon skeleton incorporating a highly hindered pentasubstituted cyclopropane moiety—posing a significant synthetic challenge. Dai and co-workers addressed this complexity by leveraging a counterintuitive BROC radical cyclization to forge the cyclopropane ring with remarkable stereocontrol. The synthesis commenced from 2-methylcyclopentenone (**138**), which underwent asymmetric conjugate addition of $^{i}PrMgCl$ in the presence of $Cu(OTf)_2$/chiral N-heterocyclic carbene,[111] alkylation with alkyne **139**, and Pd-catalyzed *syn*-hydroarylation of the alkyne with aryl boronic acid **140** to furnish alkene **141**.[112] Subsequent Ir-catalyzed asymmetric hydrogenation delivered intermediate **142** with exceptional diastereoselectivity (d.r. = 51:1). The MHAT precursor **144** was assembled in three steps from **142**, involving vinyl triflation, demethylation, and a Pd(II)/RuPhos-catalyzed dearomative cyclization.[113] Upon treatment with BROC radcial cyclization conditions, a tertiary radical was generated that underwent an intramolecular Giese-type addition to the adjacent enone, constructing the tetracyclic product **145** in 65% yield as a single diastereomer. The success of this unusual transformation was attributed to rapid single-electron reduction of the radical intermediate to a stabilized carbanion, thereby preventing fragmentation of the newly formed cyclopropane ring. A final six-step sequence completed the total synthesis of (−)-peyssonnoside A (**137**) in just 13 steps from **138**.

As illustrated in the previous example, the BROC radical cyclization has proven particularly effective for constructing

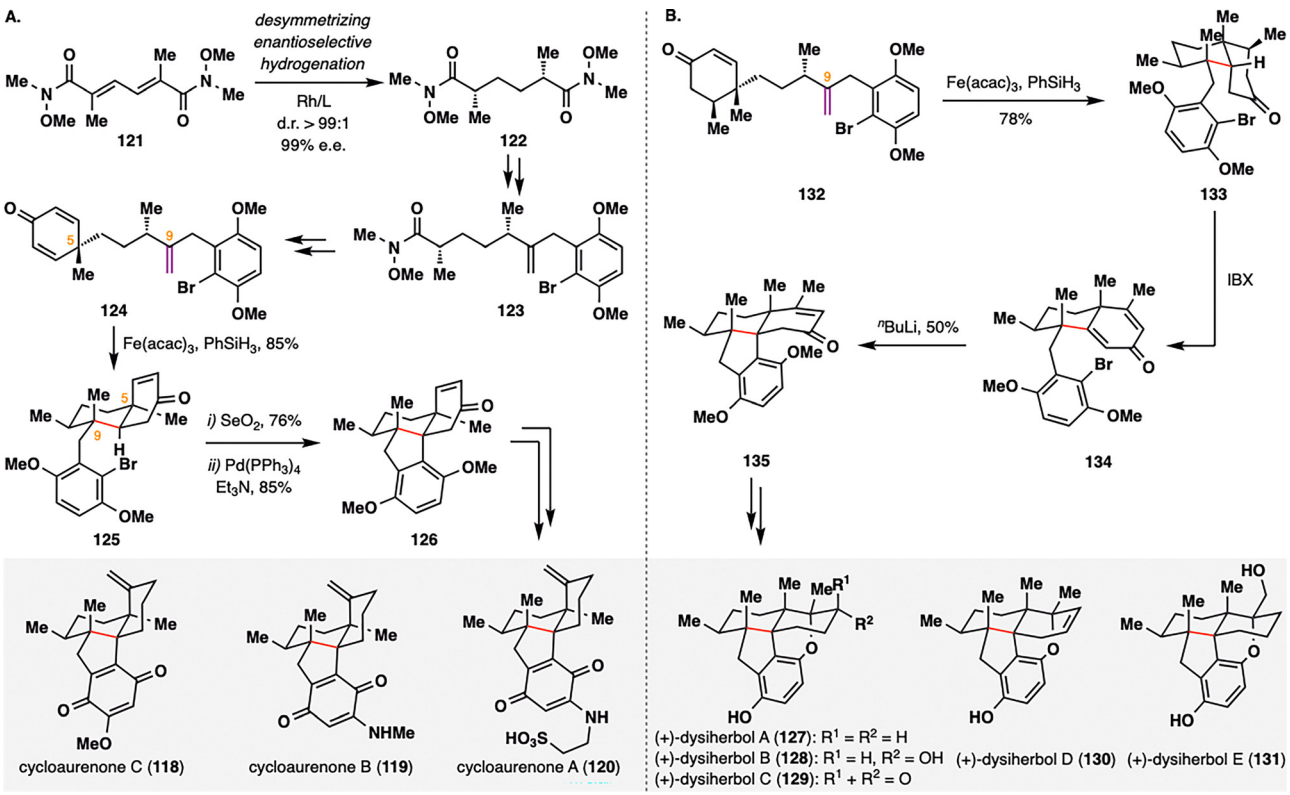

Scheme 15 Lu's collective total synthesis of cycloaurenones (**118–120**) and dysiherbols (**127–131**).

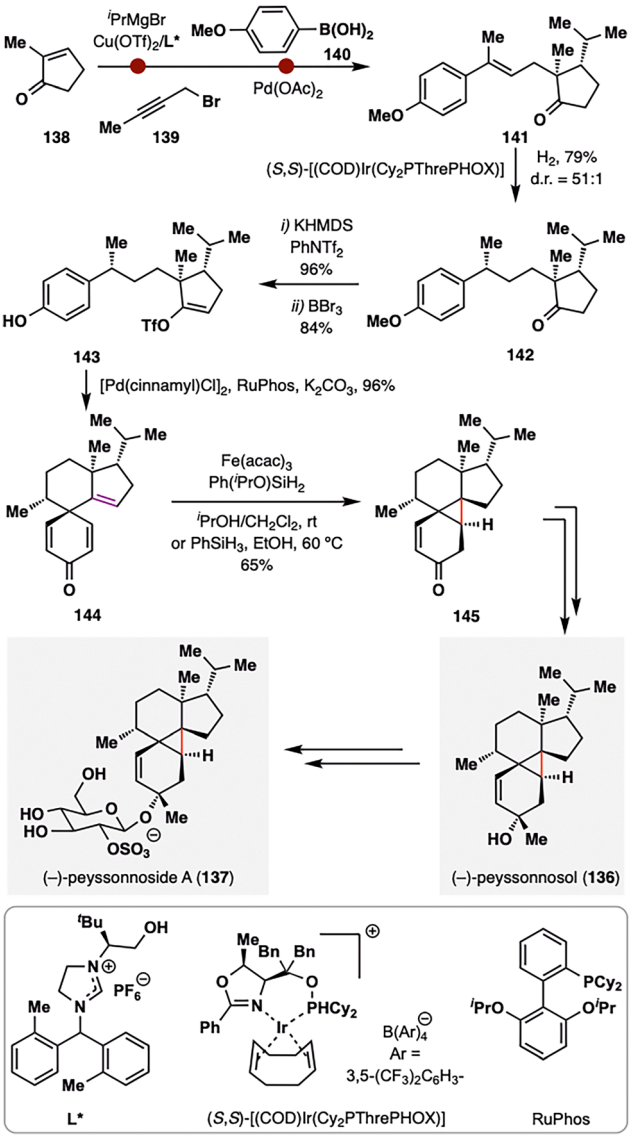

Scheme 16 Dai's total synthesis of (–)-peyssonnoside A (**137**).

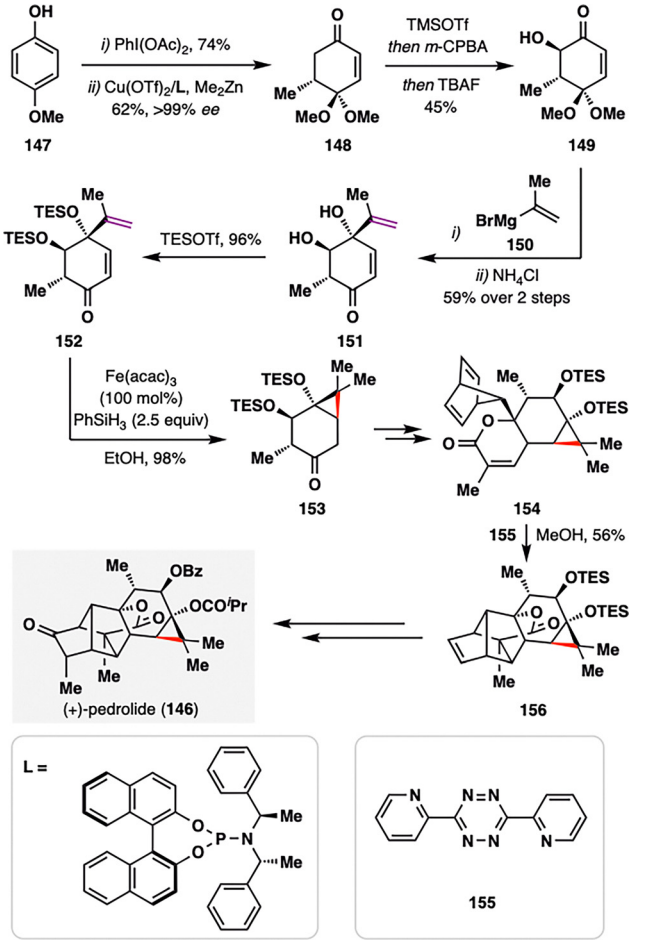

Scheme 17 Carreira's total synthesis of (+)-pedrolide (**146**).

small-ring cycloalkanes with substantial ring strain. Building on this strategy, Carreira and co-workers achieved the first total synthesis of (+)-pedrolide (**146**, Scheme 17),[114] a densely substituted carane-containing diterpenoid isolated from *Euphorbia pedroi*.[115] The carane scaffold, frequently encountered in spurge-family natural products, has long been regarded as a formidable challenge for synthetic chemists due to its strain and stereochemical complexity. The synthesis began with the efficient construction of ketone **152** from intermediate **147** through a sequence involving oxidative dearomatization, enantioselective 1,4-conjugate methyl addition, Rubottom oxidation, a diastereoselective Grignard addition, and TES protection of the resulting diol. Treatment of **152** with $Fe(acac)_3$ and $PhSiH_3$ under BROC radical cyclization conditions enabled a MHAT-driven radical addition into the adjacent enone, furnishing the highly strained cyclopropyl ketone **153** in an impressive 98% yield. This transformation underscores the utility of MHAT-based radical chemistry in assembling highly functionalized carane skeletons with exceptional efficiency. A late-stage, strategically designed Diels–Alder cascade was then employed to elaborate intermediate **156**, ultimately culminating in the concise total synthesis of (+)-pedrolide (**146**).

Recently, Ma and co-workers completed the total synthesis of *ent*-polytrichastrene B (**157**), a structurally complex natural product bearing a highly strained and sterically congested tetrasubstituted cyclopropane motif, featuring MHAT-based key transformations (Scheme 18).[116] The installation and stereochemical control of this feature posed significant synthetic challenges, which were elegantly addressed through the BROC radical cyclization similar to previous examples. The synthesis commenced with the asymmetric construction of cyclohexenone-aldehyde **161**, achieved *via* a redox-relay Heck alkenylation between enone triflate **158** and a homoallylic alcohol **159** under Sigman's conditions.[117] Following a series of elaborations, the core framework of *ent*-polytrichastrene B was efficiently assembled. The pivotal diastereoselective reduction of a highly hindered, unactivated tetrasubstituted olefin of **162** was accomplished using MHAT-initiated hydrogenation, enabling stereocontrolled access to the desired intermediate **163**. Subsequent seven-step manipulations led to the formation of an unsaturated

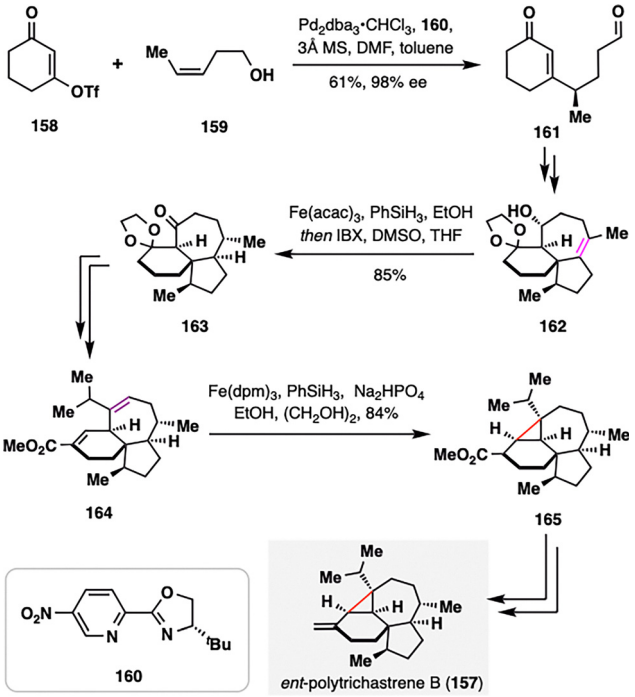

Scheme 18 Z. Ma's asymmetric synthesis of *ent*-polytrichastrene B (**157**).

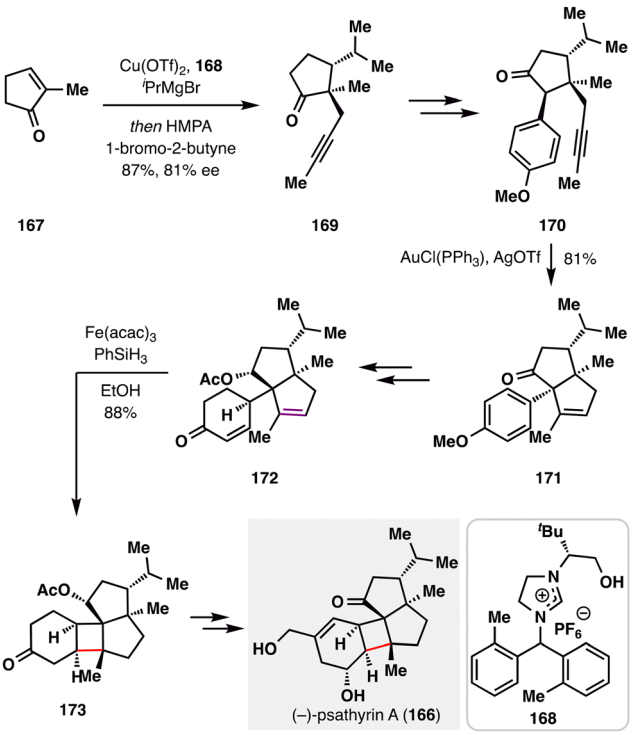

Scheme 19 Dai's asymmetric total synthesis of psathyrin A (**166**).

ester **164**, which underwent a successful 3-*exo*-trig radical cyclization under BROC conditions, furnishing tetracyclic intermediate **165** as a single diastereomer. This intermediate, featuring the target cyclopropane motif, was converted to *ent*-polytrichastrene B (**157**) in two additional steps.

Building on their prior success in strained cyclopropane construction, Dai and co-workers recently extended this strategy to forge a cyclobutane motif in their total synthesis of psathyrin A (**166**),[118] a diterpene natural product featuring an unique 6/4/5/5 tetracyclic carbon skeleton isolated from the fermentation broth of *Psathyrella candolleana*.[119] As outlined in Scheme 19, the synthesis began with a copper-catalyzed enantioselective conjugate addition of an isopropyl Grignard reagent to cyclopentenone **167**, followed by propargylation with 1-bromo-2-butyne to afford **169**. Subsequent elaboration provided intermediate **170**, which underwent a gold(I)-catalyzed Conia-ene cyclization to furnish **171**. Birch reduction of the aromatic ring in **171**, accompanied by alkene migration, gave **172** and established the requisite alkene–enone pairing for the forthcoming cyclization. Subjecting **172** to BROC conditions successfully delivered the strained cyclobutene **173**, overcoming the intrinsic ring strain of this scaffold. From this intermediate, further elaboration completed the synthesis of psathyrin A (**166**). This achievement underscores the power of BROC cyclization for constructing highly strained carbocycles in complex diterpene architectures.

MHAT radical cyclization can extend beyond traditional alkene–enone systems to encompass alkene–nitrile couplings, as exemplified in the total synthesis of cyclopianes (**32–34**) by Zhai and co-workers (Scheme 20).[120] These architecturally complex natural products—previously addressed in Snyder's synthesis (Scheme 6)—pose significant synthetic challenges due to their dense, angular polycyclic frameworks. Zhai's synthesis began with the asymmetric Corey–Bakshi–Shibata (CBS) reduction of readily available trimethylcyclopentenone (**174**), followed by a tandem vinylation/Claisen rearrangement and van Leusen homologation to furnish nitrile **177**, thereby establishing the crucial alkene–nitrile coupling motif. Subjecting **177** to BROC radical cyclization conditions [$Fe(acac)_3$, $PhSiH_3$] effected an intramolecular radical cyclization followed by acid-

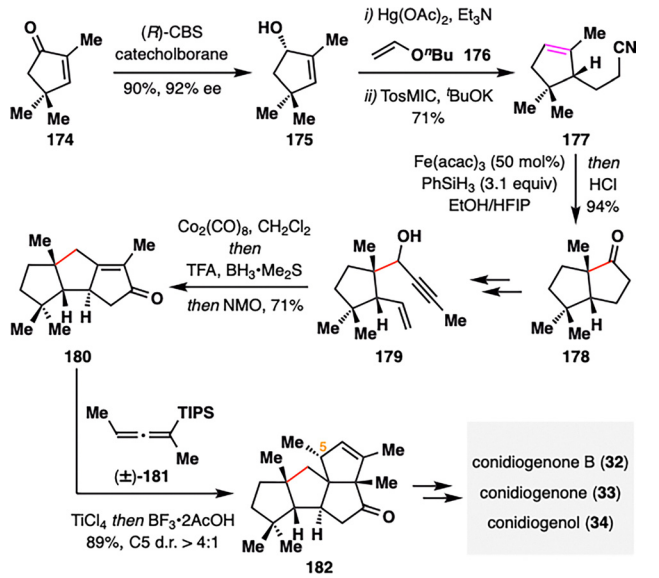

Scheme 20 Zhai's total synthesis of cyclopianes (**32–34**).

mediated hydrolysis to deliver the *cis*-biquinane scaffold **178** in 94% yield as a single diastereomer, establishing a new quaternary center with excellent stereocontrol. Subsequent elaboration of **178** yielded **179**, featuring an alkene–alkyne system primed for a Co-mediated Nicholas/Pauson–Khand reaction, which efficiently assembled the triquinane core **180**. A final Danheiser annulation with cumulene **181** forged the highly strained angular triquinane skeleton **182** in 89% yield and with good diastereoselectivity (d.r. > 4:1), thus completing the construction of the core cyclopiane framework. Final functional group manipulations converted **182** into natural products **32–34**.

As the scope of MHAT chemistry continues to expand beyond classical radical acceptors, its compatibility with unconventional motifs—such as alkenylsilanes—further underscores its versatility in complex molecule construction. (−)-Habiterpenol (**183**), a microbial G2 checkpoint inhibitor isolated from *Phytohabitans* sp.,[121] was synthesized by Nagamitsu, Ohtawa, and co-workers *via* a key MHAT-initiated redox radical cyclization involving an atypical alkene–alkenylsilane pairing (Scheme 21).[122] The synthesis commenced with the coupling of readily available aldehyde **185** and allylsilane **186**, followed by DMP oxidation to furnish alkenylsilane **187** with moderate diastereoselectivity at C3 (d.r. = 1.2:1). Subjecting **187** to BROC radical cyclization conditions [$Fe(acac)_3$, $PhSiH_3$] triggered a redox radical cyclization that efficiently forged the central six-membered ring and simultaneously established two stereocenters with excellent diastereocontrol (single diastereomer), affording pentacyclic intermediate **188** in 73% yield. Final deoxygenation steps completed the total synthesis of (−)-habiterpenol (**183**). Beyond enabling this total synthesis, the success of this transformation highlights the potential of MHAT chemistry to engage previously unreactive functional groups, thereby opening new avenues for radical-based bond constructions.

While prior examples of MHAT-based radical cyclization largely relied on 1,1-disubstituted or monosubstituted alkenes as radical donors, Gui and co-workers strategically employed a rare diene moiety as a radical donor in the total synthesis of swinhoeisterols A–C (**189–191**),[123] complex marine-derived steroids isolated from the Xisha sponge *Theonella swinhoei*,[124,125] thereby broadening the synthetic utility of MHAT chemistry (Scheme 22). These natural products feature a synthetic challenging seven-membered ring and three contiguous stereocenters at C13, C17, and C20. To address this, Gui's team employed a BROC radical cyclization, treating **193** with $Fe(dpm)_3$ and $Ph(^iPrO)SiH_2$, which furnished the desired intramolecular cyclized intermediate as a mixture of diastereomers with a ratio of 2.3:1 at C17 and a ratio of 1:1.5 at C20. Upon treatment with ^{t}BuOK, base-induced epimerization at C20 selectively furnished the desired (*S*)-configured isomer **194** with high diastereoselectivity (7.7:1). Interestingly, the *E*/*Z* geometry of **193** had minimal effect on stereochemical outcome. This strategy enabled construction of the key 6/6/5/7 tetracyclic core in 44% yield over two steps. Subsequent functional group manipulations from this common scaffold allowed for the divergent synthesis of swinhoeisterols A–C (**189–191**).

The expanding scope of MHAT-based radical additions—from classical alkene–enone systems to more unconventional partners such as nitriles, alkenylsilanes, and vinyl phenyl sulfonates—has enabled new retrosynthetic strategies for assembling structurally diverse natural products. A striking example of this versatility is the application of MHAT chemistry to alkene–ketone pairs, as demonstrated by Bradshaw and co-workers in their concise total synthesis of (−)-4-*epi*-presilphiperfolan-8α-ol (**195**),[126] a fungal-derived sesquiterpenoid featuring a fused

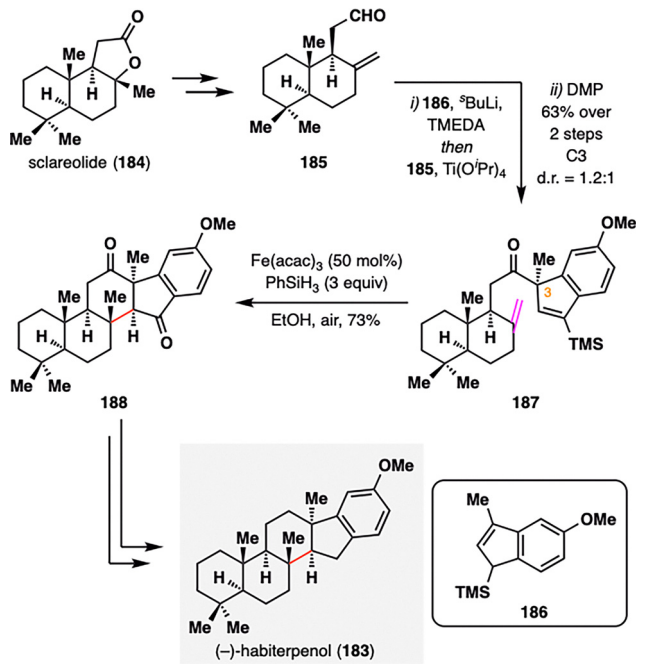

Scheme 21 Synthesis of (−)-habiterpenol (**183**) by Nagamitsu, Ohtawa, and co-workers.

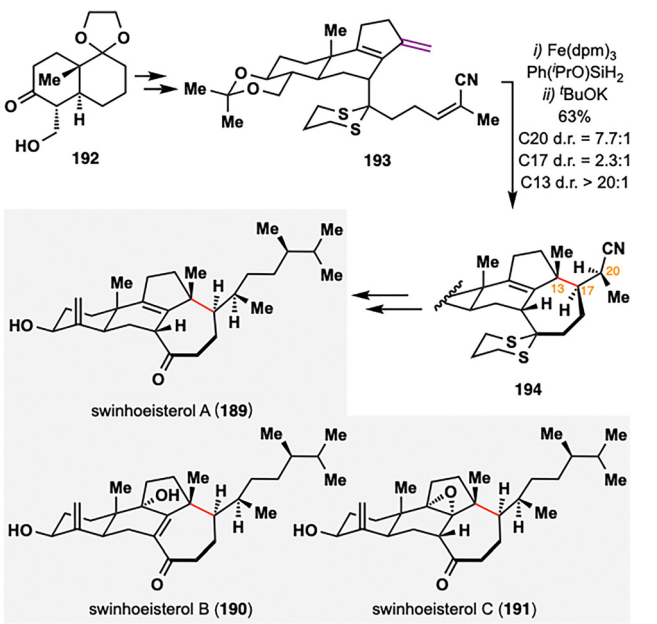

Scheme 22 Gui's total synthesis of swinhoeisterols A–C (**189–191**).

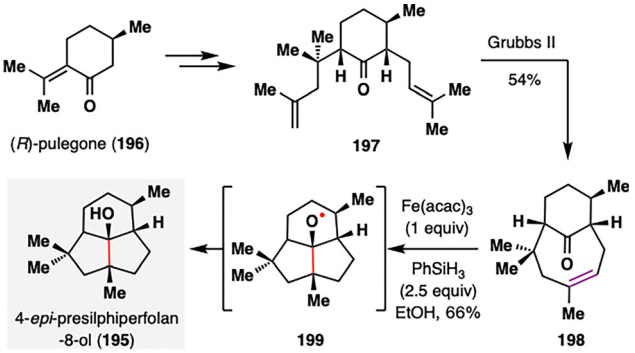

Scheme 23 Bradshaw's synthesis of (−)-4-*epi*-presilphiperfolan-8α-ol (**195**).

6/5/5 tricyclic core (Scheme 23). The synthesis commenced from (*R*)-pulegone (**196**), which was transformed into diene **197** *via* the installation of two requisite alkene units. A ring-closing olefin cross-metathesis using the Grubbs II catalyst efficiently forged the eight-membered bridged ring, affording the key keto–alkene intermediate **198** in 54% yield. Exposure of **198** to BROC radical cyclization conditions [$Fe(acac)_3$, $PhSiH_3$] generated a tertiary alkyl radical, which underwent a transannular cyclization onto the ketone to form alkoxy radical intermediate **199**. Subsequent reduction delivered (−)-4-*epi*-presilphiperfolan-8α-ol (**195**) as a single diastereomer in 66% yield. Notably, this transannular radical cyclization proceeded with excellent efficiency and stereocontrol, further exemplifying the potential of MHAT-based strategies in constructing complex and strained polycyclic architectures.

Beyond classical thermal conditions, photochemical activation has recently emerged as a powerful strategy for modulating MHAT reactivity—enabling new catalytic manifolds and improving functional group compatibility. In this context, Luo and co-workers employed a visible-light-promoted, Co(TPP)-catalyzed MHAT radical addition in their total synthesis of (−)-triptonide (**200**),[127] offering valuable mechanistic and synthetic insights into the optimization of MHAT-initiated coupling reactions (Scheme 24). The synthesis began with the preparation of enone **206** from ketone **201** *via* a sequence involving vinylMgBr addition, bromination, allylation, and acetal deprotection. Initial attempts at MHAT-mediated radical cyclization using conventional BROC radical cyclizayion conditions [$Fe(acac)_3$, $PhSiH_3$] furnished tricyclic product **208** in only 41% yield. To improve the synthetic efficiency, the authors investigated a cobalt-catalyzed alternative. Remarkably, the combination of Co(TPP), $PhSiH_3$, and visible light enabled the cyclization to proceed efficiently, affording **208** in 68% yield as a single diastereomer. This enhanced performance was attributed to photoexcitation-assisted homolysis of the Co–C bond, which facilitated effective radical generation and efficient turnover of the active catalyst. Final transformations—including acid-mediated deprotection, an intramolecular Friedel–Crafts cyclization, and global oxidation—completed the concise synthesis of (−)-triptonide (**200**).

Building upon the expanding versatility of MHAT chemistry, its application has recently been extended to the synthesis of

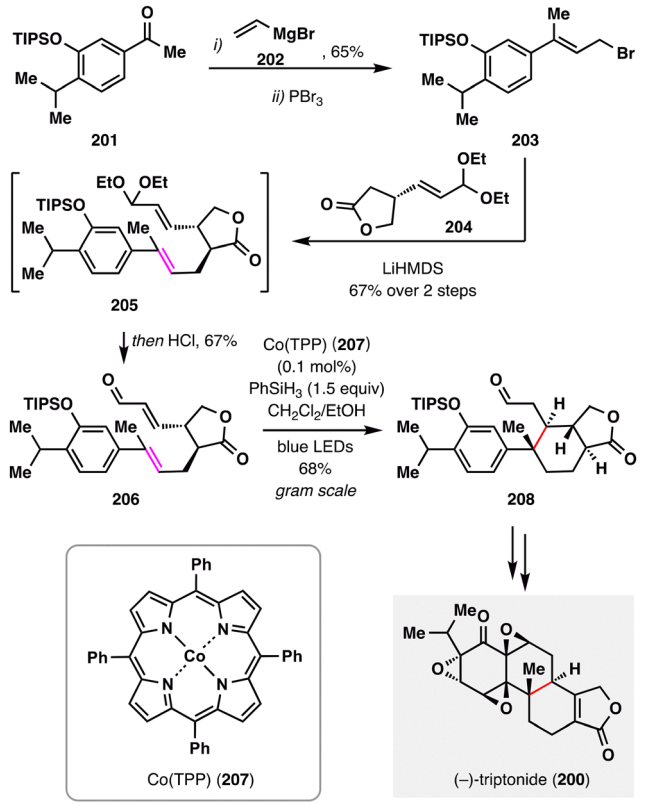

Scheme 24 Luo's total synthesis of (−)-triptonide (**200**).

aromatic steroids—a structural class traditionally considered less amenable to radical-based strategies. Viridin (**209**),[128] isolated from *Gliocladium virens*, and its biogenetic congener viridiol (**210**) feature a highly oxygenated steroidal framework incorporating a fused furan ring.[129] In a pioneering study, Gao and co-workers reported the first strategic use of MHAT radical cyclization in the synthesis of aromatic steroids, providing a new platform for the rapid construction of terpenoid architectures such as aromatic abietane diterpenoids (Scheme 25).[130] The synthesis began with an intramolecular [3+2] cycloaddition of readily accessible precursor **211**, furnishing compound **212** bearing a densely substituted six-membered ring. Subsequent functional group manipulations delivered **213**, which underwent coupling with dihydroindenol fragment **214** to yield ketone **215**—the substrate for the pivotal MHAT step. Subjecting **215** to Co-catalyzed MHAT cyclization promoted intramolecular radical addition between the terminal alkene and the aromatic ring, forging a new six-membered ring and establishing an all-carbon quaternary center. Notably: (i) the transformation proceeded with excellent substrate-controlled stereoselectivity *via* a twisted boat-like transition state that minimized 1,3-diaxial interactions between the OTBS group and the nascent methyl substituent; (ii) only catalytic amounts of Co-catalyst and $PhSiH_3$ were required, as the aromatization-driven process released a hydrogen atom, thus regenerating Co–H. This highly efficient sequence furnished tetracyclic intermediate **216** in 79% overall yield across the MHAT cyclization, deprotection, and oxidation steps. Final elaboration,

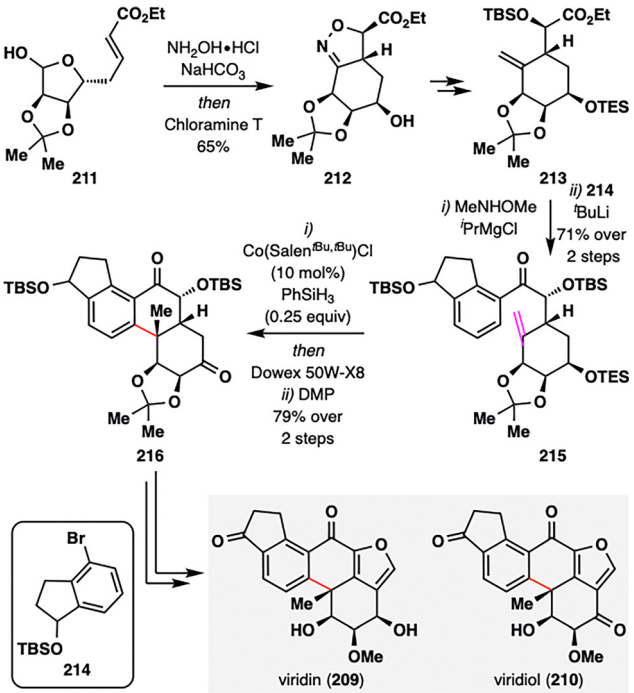

Scheme 25 Gao's total synthesis of viridin (**209**) and viridiol (**210**).

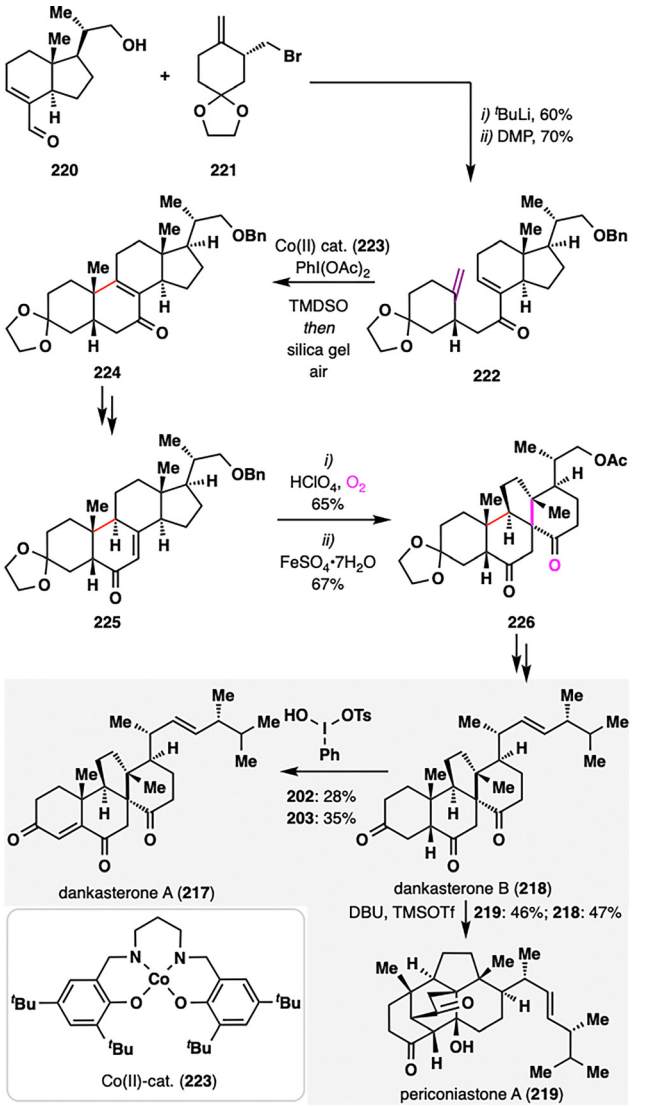

Scheme 26 Z. Ma's asymmetric total synthesis of dankasterones A and B (**217–218**), and periconiastone A (**219**).

including furan ring installation and oxidation-state adjustments, completed the total synthesis of viridin (**209**) and viridiol (**210**), showcasing a powerful new strategy for constructing oxygenated steroid frameworks using radical-based methodologies.

Dankasterones A (**217**) and B (**218**), and periconiastone A (**219**), isolated from marine sponges,[131–133] share an angularly fused tricyclic framework featuring two adjacent quaternary stereocenters—structural elements that present formidable challenges for chemical synthesis. Z. Ma and co-workers reported an enantioselective total synthesis of these complex terpenoids, employing a key MHAT-mediated radical cyclization to forge the *cis*-decalin core embedded within a 6/6/6/5 tetracyclic architecture (Scheme 26).[134] The requisite MHAT precursor **222** was assembled *via* a convergent strategy from aldehyde **220** and bromide **221**, followed by DMP oxidation. Upon exposure to an *in situ*-generated Co^{III}–H complex, a tertiary radical was generated at the terminal alkene, which then underwent intramolecular addition to the enone moiety. Subsequent $PhI(OAc)_2$-mediated oxidation furnished enone **224**. Remarkably, the MHAT cyclization proceeded with high diastereoselectivity, selectively delivering the desired *cis*-fused decalin framework. From the isomerized enone **225**, a radical rearrangement was employed: allylic oxidation generated a hydroperoxide intermediate,[135] which underwent Fe(II)-mediated reductive rearrangement to furnish spirocyclic intermediate **226**. Final functional group manipulations enabled divergent elaboration to the target natural products—dankasterones A and B (**217–218**) and periconiastone A (**219**).

Ding and co-workers accomplished the first asymmetric total synthesis of (+)-davisinol (**227**),[136] a C11-oxygenated hetisine-type alkaloid isolated from *Delphinium davisii* Munz (Scheme 27).[137] A pivotal feature of this synthesis is a HAT-initiated transannular redox radical addition, in which a tertiary radical—generated from an electron-deficient enone—undergoes intramolecular coupling with an electron-rich alkene, followed by oxygen trapping. The synthesis began with the construction of diketone **233**, accessed *via* a highly diastereoselective (d.r. > 32:1) oxidative dearomatization/intramolecular Diels–Alder (IMDA) cascade from intermediate **232**, which was in turn derived from **229** through a sequence of transformations, including a key acylative kinetic resolution.[138] Crucially, The MHAT-mediated transannular redox cyclization was made possible by the favorable spatial orientation of the olefinic carbons at C9 and C10 in **233**. Under optimized conditions, the desired polycyclic product **235** was obtained in 83% yield as a single diastereomer through radical transformation shown in **234**. Notably, fine-tuning the oxidation state at specific positions proved essential for downstream diversification toward

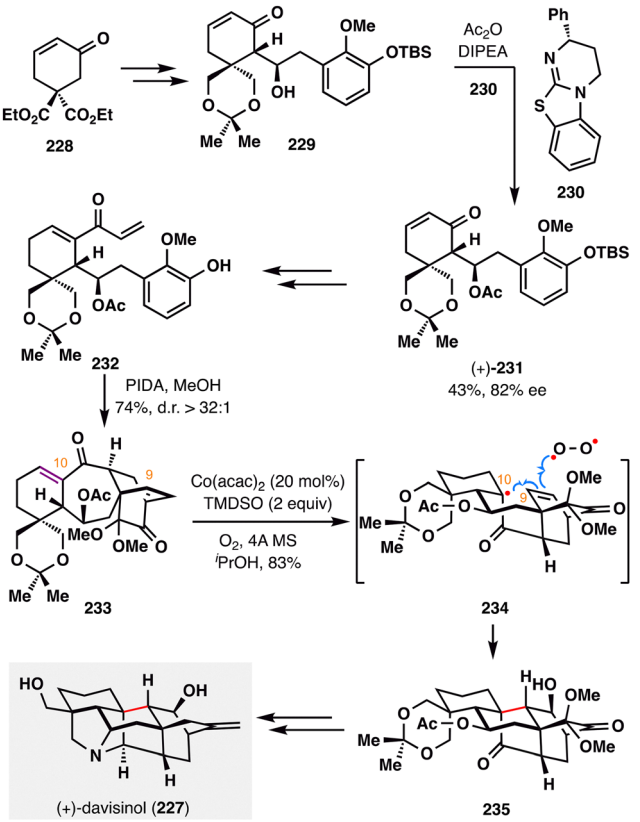

Scheme 27 Ding's total synthesis of (+)-davisinol (**227**).

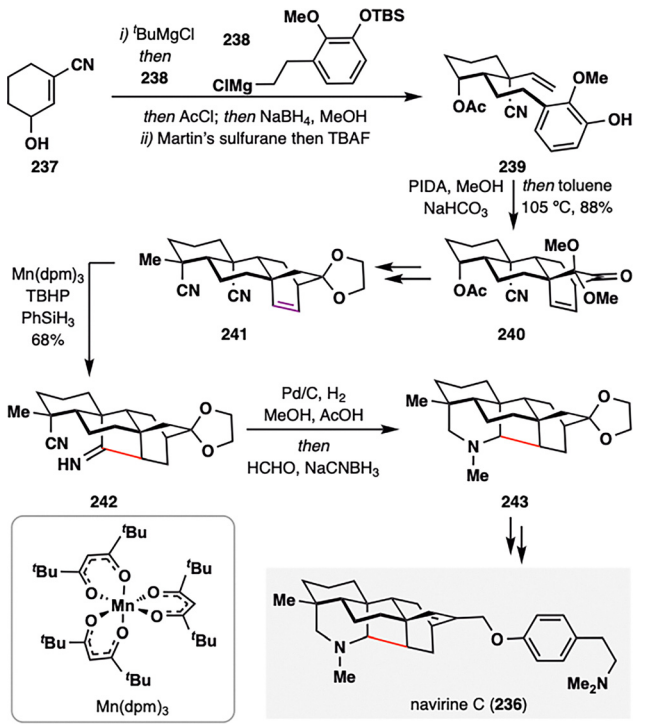

Scheme 28 Total synthesis of the proposed structure of navirine C (**236**) by D. Ma and co-workers.

other hetisine alkaloids, underscoring the broad utility of MHAT-based redox cyclizations in accessing this architecturally complex family. Final oxidation-state adjustments completed the total synthesis of the natural product (+)-davisinol (**227**).

Navirine C (**236**), a hetidine-type alkaloid isolated from *Aconitum naviculare*,[139] was synthesized by D. Ma and co-workers through a concise and efficient route that leveraged a Mn-catalyzed alkene–nitrile MHAT radical cyclization to establish the core framework for subsequent nitrogen heterocycle construction (Scheme 28).[140] The synthesis began with the preparation of phenol **239**, in which a chelation-controlled conjugate addition between nitrile **237** and Grignard reagent **238** was employed—marking the first use of this strategy in natural product synthesis.[141] Subsequent elaboration of **239**, including oxidative dearomatization and an intramolecular Diels–Alder cascade, furnished tetracyclic intermediate **240**. This was further converted to dinitrile **241**, strategically positioned to serve as the radical acceptor in the key MHAT cyclization. Upon treatment with Shenvi's MHAT conditions [$Mn(dpm)_3$, $PhSiH_3$, TBHP],[142] an intramolecular alkene–nitrile coupling occurred wherein the alkyl radical, derived from the terminal olefin, added to the cyano group to form an imine, thereby forging the complex pentacyclic framework **242** in 68% yield. The resulting imine intermediate was then subjected to Pd/C-catalyzed hydrogenation, followed by a one-pot Mannich reaction, delivering tertiary amine **243**. Final functional group manipulations completed the synthesis of navirine C (**236**), highlighting the power of alkene–nitrile MHAT radical cyclization as a strategic tool for efficiently assembling nitrogen-containing alkaloid scaffolds.

Despite the broad utility of MHAT cyclizations, achieving efficient radical closure onto *trans*-fused 6/5 ring systems remains a formidable synthetic challenge. Liu and co-workers addressed this issue in their asymmetric total synthesis of euphane triterpenoids (**245–247**),[143] a structurally diverse family of natural products characterized by a 6/6/6/5 tetracyclic core derived from six isoprene units (Scheme 29).[144] Their approach explored how substrate architecture and catalytic conditions govern MHAT reactivity and selectivity in the formation of such complex frameworks. The synthesis began with the preparation of key MHAT precursors **251**, constructed *via* a Liebeskind stannane–thioester coupling between organotin reagent **248** and thioester derivative **249**,[145] followed by DIBAL-H reduction to afford alcohol **250** as a single detectable diastereomer. Acetylation of the hydroxyl groups furnished the fully protected MHAT substrate **251**. Under Mn-catalyzed MHAT conditions (Shenvi's protocol),[142] **251** underwent smooth radical cyclization, delivering pentacycle **252** in 78% yield with excellent diastereoselectivity (d.r. = 10:1). This Mn-mediated cyclization represents a previously unreported transformation in the synthesis of this structural motif, as similar outcomes had only been achieved under cobalt catalysis. In contrast, modifying the protecting groups to pivaloyl esters and switching the catalyst system to Fe(III)/Fe(II)/$PhSiH_3$ conditions triggered a mechanistically distinct cyclization-elimination pathway, furnishing the product **254** in an impressive 93% brsm yield. Subsequent functional group manipulations of core intermediates **252** and

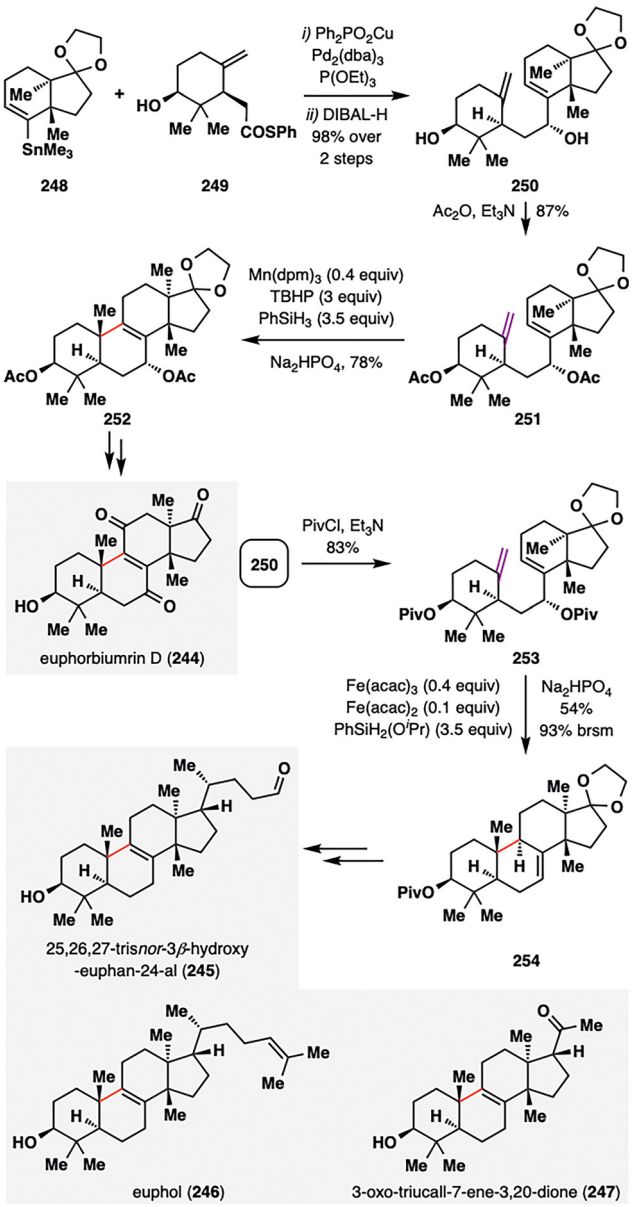

Scheme 29 Total synthesis of euphane triterpenoids (**245–247**) by B. Liu and co-workers.

254 enabled access to the natural products **245–247**, showcasing how fine-tuning catalytic systems and protecting-group strategies can expand the synthetic reach of MHAT cyclizations to encompass even topologically challenging *trans*-fused ring systems.

2.1.2. MHAT-radical-polar crossover cascade. Radical-polar crossover (RPCO) cascades are a powerful class of tandem reactions that couple radical and ionic steps into one sequence.[146–149] In a typical RPCO cascade, a carbon-centered radical is generated (for example *via* photoredox catalysis, HAT, or traditional radical initiators) and usually adds to an olefin or other π-system. These resulting radical intermediates are then converted into an ionic species—either by single-electron oxidation to give a carbocation or by single-electron reduction to give a carbanion—which immediately undergoes a polar bond-forming reaction (such as intramolecular nucleophilic addition, aldol or Michael addition, *etc.*). Because the radical addition and polar transformation occur in one pot without isolating intermediates, RPCO cascades can construct multiple bonds and ring systems in a single operation. By merging radical reactivity (which tolerates steric congestion and diverse functionality) with classic polar chemistry, these cascades enable dramatic increases in molecular complexity in an efficient way.

Meroterpenes derived from dimethylorsellinic acid (DMOA) and farnesyl pyrophosphate (FPP) have long captivated biosynthetic chemists due to their intricate polycyclic frameworks and intriguing biosynthetic origins.[89] Only recently, however, have these structures been synthetically realized.[150–155] Maimone, Newhouse, and co-workers accomplished the first bio-inspired total synthesis of andrastin- and terretonin-type meroterpenes (**255–258**) by leveraging a MHAT-initiated radical cyclization/radical fragmentation/oxidative RPCO cascade, which closely mimics the proposed biosynthetic transformations (Scheme 30).[156] Their synthesis began with the protoaustinoid-derived bicyclo[3.3.1]-nonane core **259**, which, under modified Shigehisa conditions [Co cat. (**266**), $PhSiH_3$, and *N*-fluoropyridinium salt (F^+)],[157] underwent a radical cascade to furnish the trisubstituted alkene **260**. Interestingly, substituting F^+ with TsCl led instead to the formation of the less substituted alkene **261**, a thermodynamically less favored isomer. Both divergent pathways proceeded through a common tertiary radical intermediate **262**, generated *via* HAT from a Co(III)–H species to the terminal alkene. This radical rapidly engaged in a 3-*exo*-trig cyclization onto the adjacent enone, followed by β-fragmentation to yield **264**. In the oxidative pathway (F^+), the resulting radical was oxidized to a carbocation that underwent β-elimination to furnish **260**. In contrast, under non-oxidative conditions (TsCl), radical quenching *via* HAT occurred preferentially at the less hindered methyl site, leading to **261**. This oxidation-state-dependent bifurcation elegantly illustrates how the MHAT-RPCO cascade can emulate biosynthetic logic and selectively guide divergent molecular outcomes from a common intermediate. Final elaboration of both intermediates enabled the convergent total synthesis of the meroterpenoid natural products andrastins and terretonins (**255–258**), highlighting the strategic power of RPCO logic in complex terpene synthesis.

Building upon the success of bioinspired MHAT-RPCO cascades in meroterpene synthesis, Vanderwal and co-workers extended this strategy to address a long-standing challenge: achieving polycyclization in highly oxidized contexts, a hallmark of abietane diterpenoids.[158–160] The poor compatibility of traditional acid-catalyzed carbocationic cyclizations with oxygen-rich substrates has historically impeded synthetic access to such densely functionalized frameworks. To overcome this limitation, Vanderwal and co-workers devised an RPCO-based approach that exhibited exceptional tolerance to multiple oxidation states and delivered high stereocontrol—even on substrates functionalized at nearly every position. As outlined in Scheme 31, a family of abietane diterpenoids (**267–270**) was accessed by tuning the oxidation patterns on the radical precursors. The cyclization sequence began with a Co(III)–H-mediated HAT to the terminal alkene of diene **271**, generating

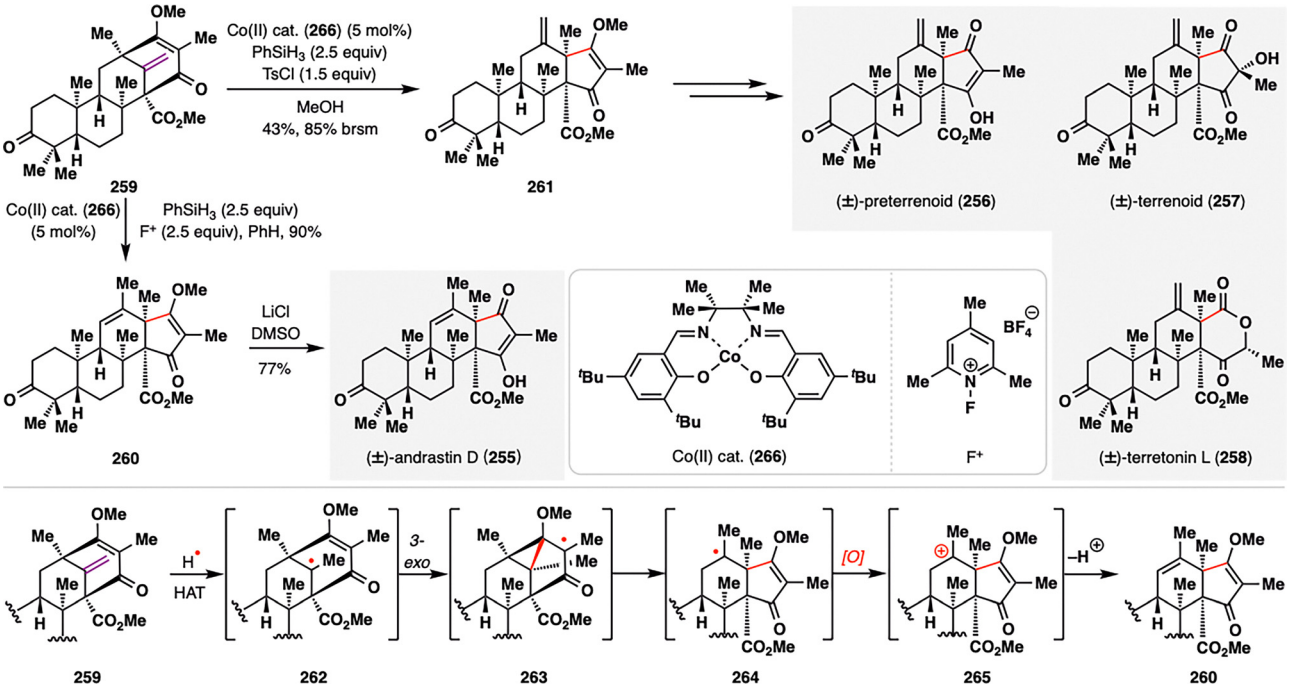

Scheme 30 Total synthesis of andrastin and terretonin meroterpenes (**255–258**) by Newhouse, Maimone, and co-workers.

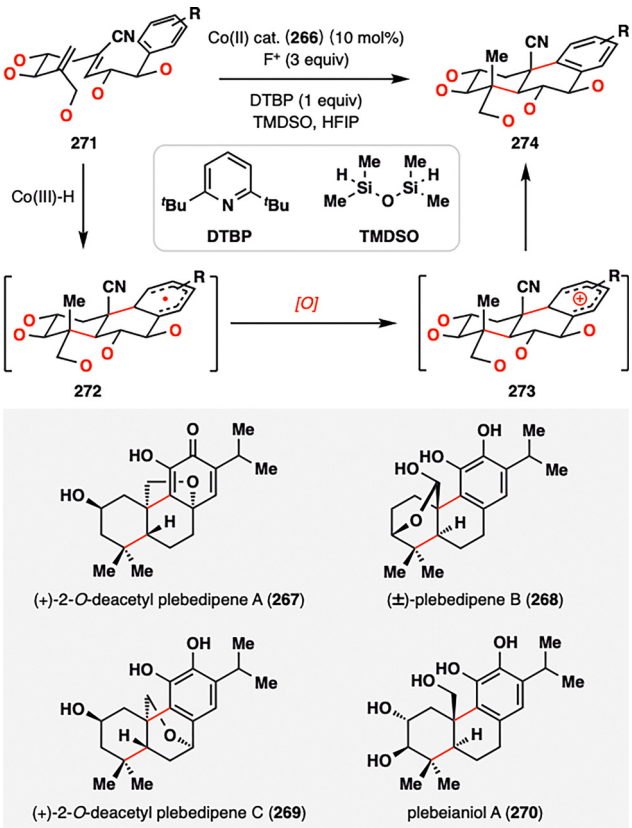

Scheme 31 Total synthesis of abietane diterpenoids (**267–270**) by Vanderwal and co-workers.

a tertiary radical that cyclized onto a proximal electron-deficient olefin. The resulting α-cyano radical then engaged in a second radical addition to the adjacent aromatic ring, forming a transient cyclohexadienyl σ-complex radical **272**. Upon oxidation and rearomatization, the tricyclic product **274** was furnished, forming two carbon–carbon bonds and three stereocenters, including two sterically demanding quaternary centers, in a single transformation. This elegant example underscores the strategic potential of MHAT-RPCO chemistry to invert the traditional sequence of cyclization followed by oxidation, enabling direct cyclization of highly oxidized substrates—a capability rarely achievable by conventional ionic approaches. It thus expands the synthetic logic for constructing complex polyoxygenated diterpenoid architectures.

Ding and co-workers further disclosed an elegant HAT-initiated Dowd–Beckwith rearrangement/radical-polar crossover cascade in the collective total synthesis of (−)-crinipellins (**275–282**).[161] As shown in Scheme 32, the key rearrangement precursor, ketone **286**, was efficiently assembled through a sequence involving an oxidative dearomatization-induced (ODI) [5+2] cycloaddition followed by a pinacol rearrangement from substrate **283.** To enable the critical rearrangement, the authors extensively screened conditions and identified two optimal Co(II)-catalyzed systems—one employing TBHP, and the other using *N*-fluoropyridinium salt (F^+) as oxidant—both affording the desired rearranged tetracycle **289** in excellent yields (98% and 90%, respectively). Interestingly, while both conditions proceeded *via* similar MHAT-initiated radical intermediates, they diverged mechanistically in the termination step: the TBHP pathway favored β-hydrogen elimination to regenerate the Co(III)–H catalyst, whereas the F^+ system facilitated a RPCO event, oxidizing the intermediate radical to a carbocation.

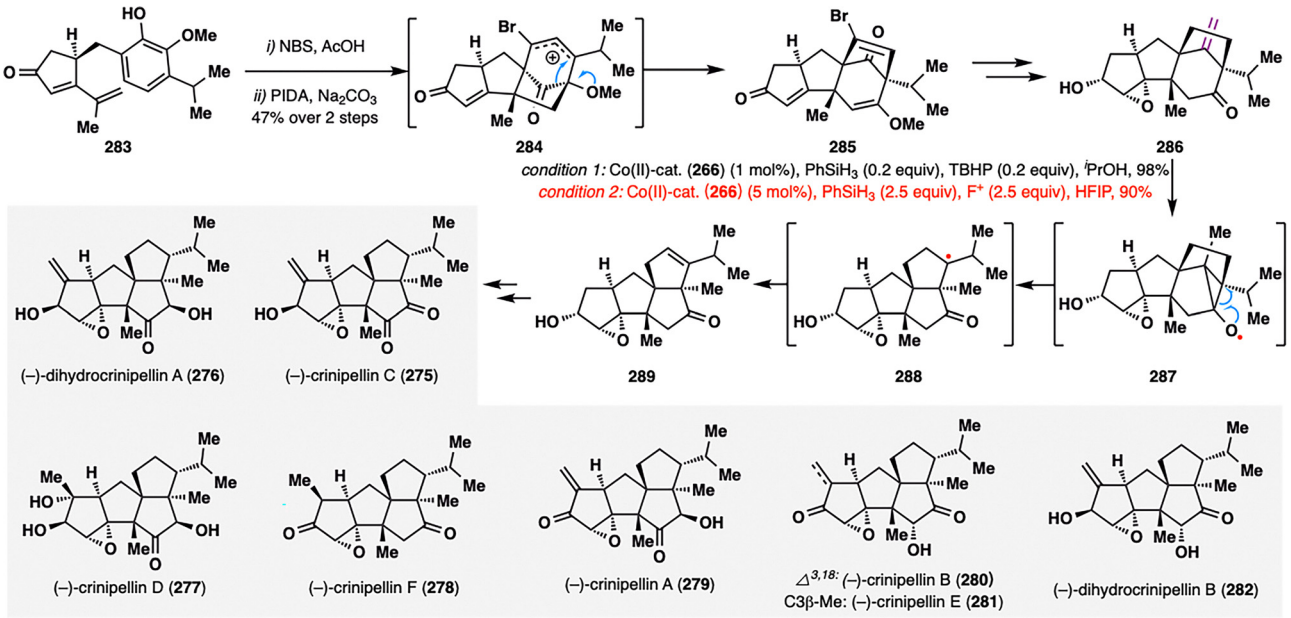

Scheme 32 Divergent total synthesis of (−)-crinipellins (**275–282**) by Ding, Xie, and co-workers.

This MHAT-enabled Dowd–Beckwith rearrangement not only provided an elegant solution for assembling the compact tetraquinane core but also established a platform for modular late-stage diversification. Through further functional group elaboration, the team successfully accessed the full series of (−)-crinipellins (**275–282**), underscoring the rearrangement's strategic utility in natural product synthesis.

In Vincent's total synthesis of dactyloquinone A (**290**), a pivotal transformation involved an MHAT-initiated RPCO event proceeding *via* an intramolecular redox process—remarkably achieved without the use of external oxidants (Scheme 33).[162] The radical coupling partners were constructed through a convergent sequence from **291** and **292** comprising intermolecular substitution and oxidative dearomatization, ultimately affording tricyclic quinone **295**. Upon treatment with $Fe(acac)_3$ and $PhSiH_3$, a tertiary radical was generated at the trisubstituted olefin. Rather than undergoing conventional carbon–oxygen radical coupling, the radical was more likely to engage in intramolecular single-electron oxidation *via* the pathway illustrated in **296**, forming a zwitterionic intermediate **297**. This process effectively completed the RPCO event, furnishing the polycyclic intermediate **290** in a synthetically satisfying 50% yield from **295**. A subsequent Wittig olefination, followed by ceric ammonium nitrate (CAN)-mediated oxidation, delivered dactyloquinone A (**290**) in 71% yield, thus completing the total synthesis in a concise and mechanistically elegant fashion.

In contrast to the previously described oxidative MHAT-RPCO transformations, the Pronin group pioneered a reductive variant of the MHAT-RPCO cascade for the rapid construction of complex terpenoid architectures.[23,163] Their strategy centered on MHAT-initiated BROC additions followed by intramolecular aldol condensations, offering a direct and convergent approach for forming multiple carbon–carbon bonds and stereocenters

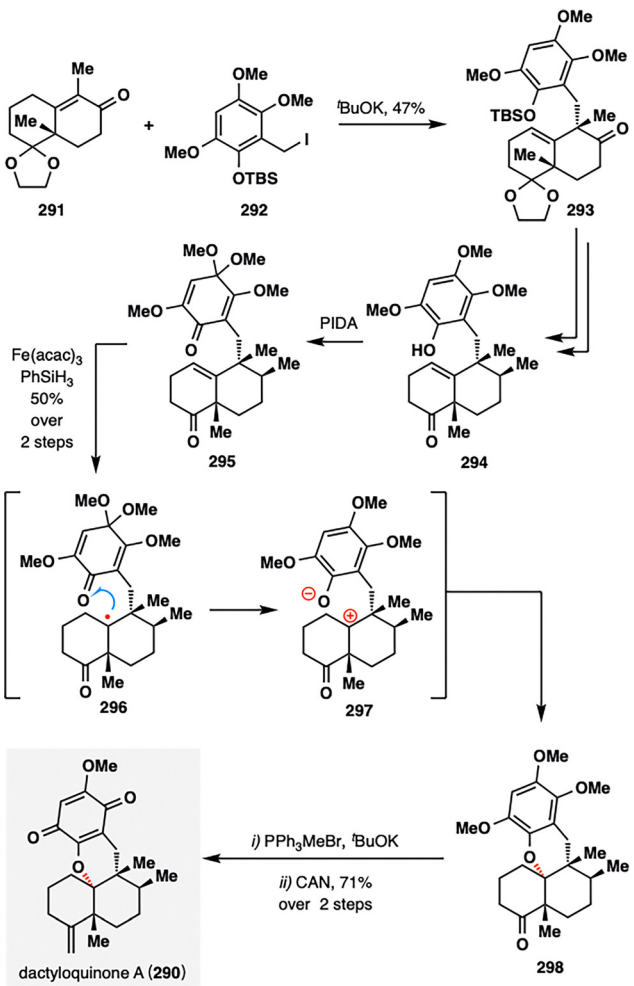

Scheme 33 Total synthesis of dactyloquinone A (**290**) by Vincent and co-workers.

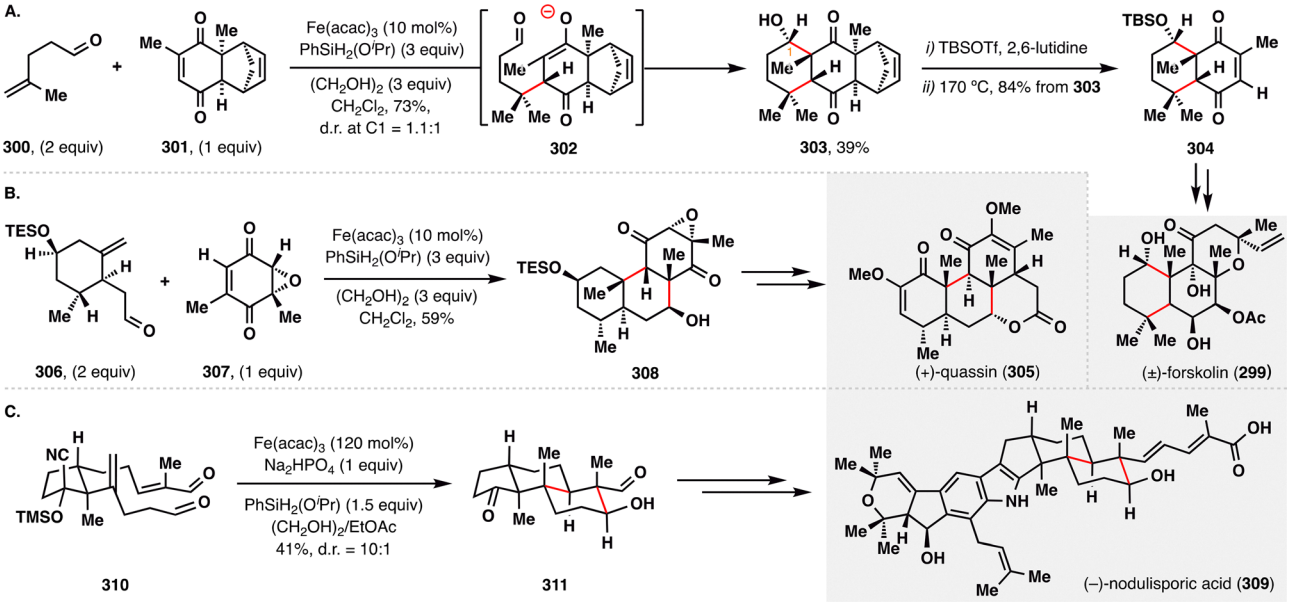

Scheme 34 Pronin's reductive radical-polar crossover in the total synthesis of forskolin (**299**), quassin (**305**), and nodulisporic acid (**309**).

under mild conditions. In their total synthesis of (±)-forskolin (**299**) and (+)-quassin (**305**) (Schemes 34(A) and (B)),[164,165] the MHAT-RPCO cascade was strategically employed to unite two advanced fragments while concurrently forging ring systems, efficiently delivering polycyclic intermediates **303** and **308**, respectively. These transformations proceeded *via* Fe(III)–H-initiated intramolecular radical addition to an enone, generating a stabilized radical intermediate that was subsequently reduced to an enolate anion. The resulting anion underwent intramolecular aldol condensation, forming two new C–C bonds and establishing three to four contiguous stereocenters in a single synthetic operation—dramatically enhancing molecular complexity.

In contrast, the total synthesis of (−)-nodulisporic acid (**309**) featured an intramolecular application of the MHAT-RPCO cascade (Scheme 34(C)).[166] Here, dialdehyde **310** underwent efficient cyclization to afford fused bicyclic intermediate **311** with excellent diastereoselectivity (d.r. = 10:1), guided by a stereogenic methyl substituent that favored *trans*-decalin formation. With the core polycyclic scaffolds efficiently assembled *via* these elegant reductive cascades, subsequent functional group elaborations enabled streamlined access to the complex natural product nodulisporic acid (**309**).

The power of reductive MHAT-RPCO chemistry was further exemplified by Liu, Fu, and co-workers in their total synthesis of rumphellclovane E (**312**),[167] a clovane-type sesquiterpenoid isolated from the gorgonian coral *Rumphella antipathies*.[168] As illustrated in Scheme 35, the authors employed a MHAT-mediated intramolecular reductive aldol strategy to construct the tricyclic core of the molecule. Following Fe(III)-mediated MHAT activation, a tertiary radical intermediate **314** was generated, which underwent a RPCO to form the corresponding enolate **315**. This enolate then participated in a highly diastereoselective intramolecular aldol cyclization, furnishing tricyclic product **316**. This concise cascade not only efficiently assembled the core ring system but

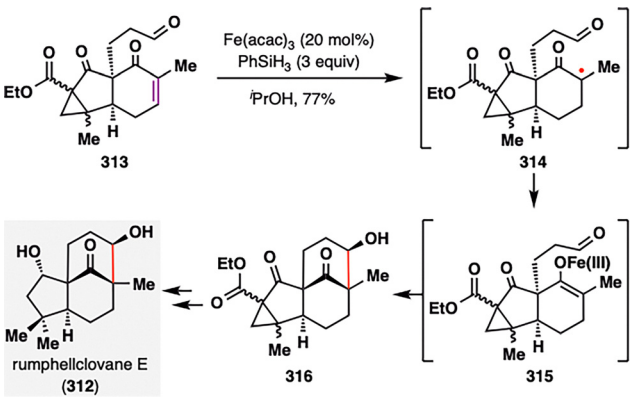

Scheme 35 Total synthesis of rumphellclovane E (**312**) by Liu, Fu, and co-workers.

also established two contiguous stereocenters—including a challenging all-carbon quaternary center—with excellent stereocontrol.

2.1.3. MHAT-S_H2 homolytic substitution. Beyond conventional radical additions and rearrangements, MHAT chemistry has recently been extended to homolytic substitution (S_H2) pathways,[63,69,169] in which a nucleophilic radical displaces a leaving group *via* a concerted bimolecular mechanism. These MHAT-S_H2 reactions offer a powerful strategy for constructing sterically congested C–C bonds at quaternary centers—transformations that are often inaccessible *via* classical two-electron disconnections. This single-electron substitution approach complements traditional radical addition chemistry by enabling C–C bond formation at sp^3-hybridized centers, typically under mild and redox-neutral conditions.

In a pioneering study, Shenvi and co-workers applied MHAT-S_H2 chemistry in the total synthesis of (−)-eugenial C (**317**),[169] a densely functionalized meroterpenoid isolated from the fruit of *Eugenia umbelliflora* (Scheme 36).[170] The synthesis culminated

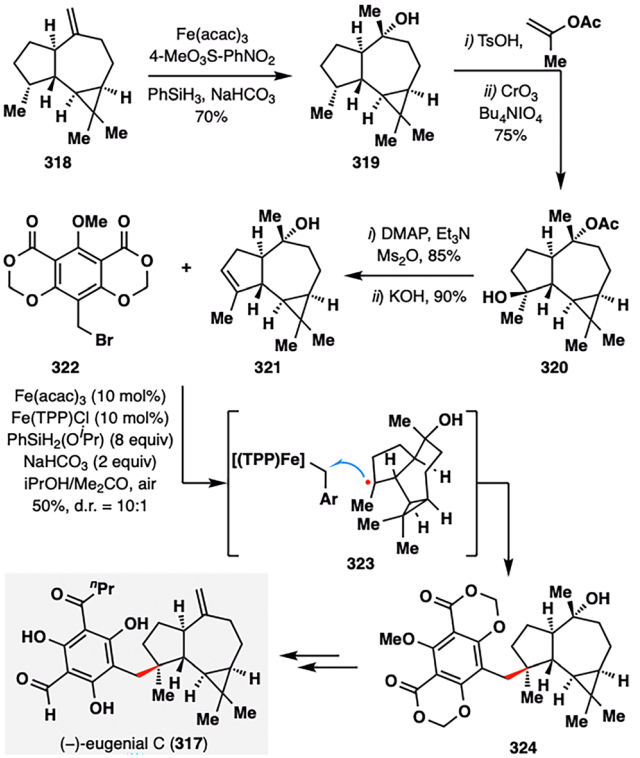

Scheme 36 Shenvi's total synthesis of (–)-eugenial C (**317**).

in an iron-catalyzed hydrobenzylation between alkene **321** and benzyl bromide **322**, forging the quaternary center with high diastereocontrol (d.r. = 10:1) and delivering the coupled product **324** in 50% yield. The alkene fragment **321** was constructed from **318** *via* a sequence involving MHAT-mediated hydration, acylation, site-selective C–H oxidation, and elimination of a tertiary alcohol. Under the optimized $Fe(acac)_3/PhSiH_3$ conditions, MHAT generated a tertiary radical from **321**, which then reacted with a benzyl–Fe(TPP) species *via* homolytic S_H2 substitution (illustrated in **323**), stereoselectively installing the quaternary center. The final elaboration of the coupling product **324** delivered (–)-eugenial C (**317**) in just four steps.

2.1.4. MHAT-fragmentations cascade. In a typical MHAT event an early transition metal Fe, Co or Mn catalyst (often in combination with a silane) delivers hydrogen atom to an unactivated alkene, generating a carbon-centered radical under very mild, functional-group tolerant conditions. Once formed, the alkyl radical can trigger ring opening of highly-strained rings through β-scission of an adjacent C–C bond. This β-scission effectively cleaves an adjacent C–C bond and "stitches" the remaining fragments into a new skeleton (Scheme 37). In other words, a single MHAT event can trigger a radical–fragmentation cascade that reorganizes an entire polycyclic framework. Such MHAT-triggered cascades are prized for their high chemoselectivity and "chemofidelity", and have been used extensively for skeletal rearrangements in terpenoid total synthesis.

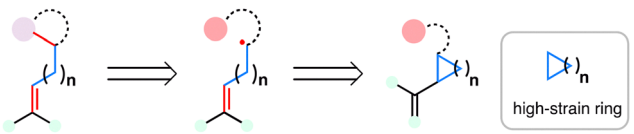

Scheme 37 Radical retrosynthesis employing the MHAT-fragmentation cascade.

Extending the scope of MHAT chemistry beyond bond formation, Shenvi and co-workers demonstrated its unique potential for skeletal rearrangement through a MHAT-fragmentation cascade—a transformation first disclosed in 2014 during their investigation of catalytic, chemoselective olefin isomerization.[171] In this foundational study, catalytic amounts of $Co(Sal^{tBu,tBu})Cl$ in the presence of catalytic amounts organosilanes were found not only to mediate positional isomerization of alkenes, but also to enable cycloisomerization of dienes and retrocycloisomerization of strained ring systems under mild conditions. This work highlighted the versatility of MHAT catalysis in promoting radical-induced skeletal editing processes.

Building on these insights, Shenvi's group remained at the forefront of leveraging MHAT-fragmentation logic in terpenoid synthesis. A notable example is the transformation of (–)-caryophyllene oxide (**326**) into (–)-humulene oxide II (**325**), a naturally occurring sesquiterpene commonly found in essential oils. As illustrated in Scheme 38, a single-step MHAT-induced retrocycloisomerization efficiently remodeled the bicyclic framework of **326** into the uncommon eleven-membered macro ring system in an impressive 95% yield. Mechanistically, the reaction was initiated by Co(III)–H-mediated HAT at the terminal alkene, generating tertiary radical intermediate **327**. This species underwent β-scission *via* cleavage of the adjacent cyclobutane ring to yield intermediate **328**, which then underwent β-hydrogen elimination to complete the ring expansion. This pioneering application of MHAT-fragmentation not only underscores the synthetic power of radical-based skeletal editing, but also continues to inspire novel strategies for terpenoid diversification and complexity generation.

Inspired by Shenvi's pioneering work on HAT-induced retrocycloisomerization, Sarlah and co-workers adopted a similar strategy in the synthesis of monobistropolones (**329–331**)—natural products isolated from *Phoma sp.* cultures that share a characteristic 11-membered humulene-derived core bearing pendent

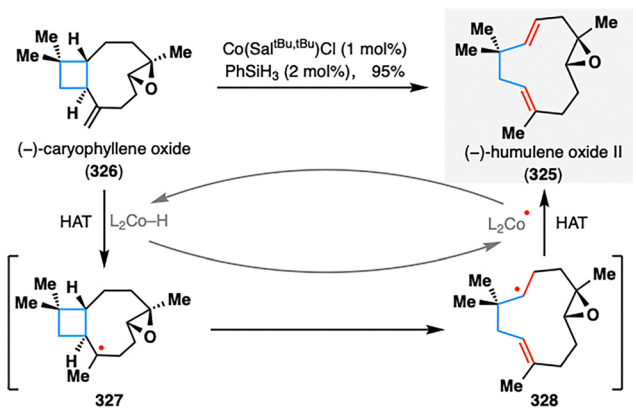

Scheme 38 Shenvi's synthesis of (–)-humulene oxide II (**325**) by HAT isomerization.

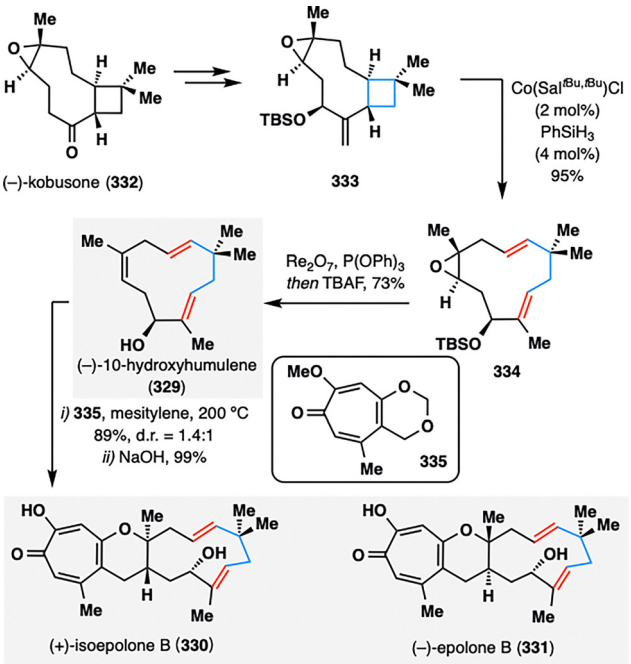

Scheme 39 Total synthesis of monobistropolones (**329–331**) by Sarlah and co-workers.

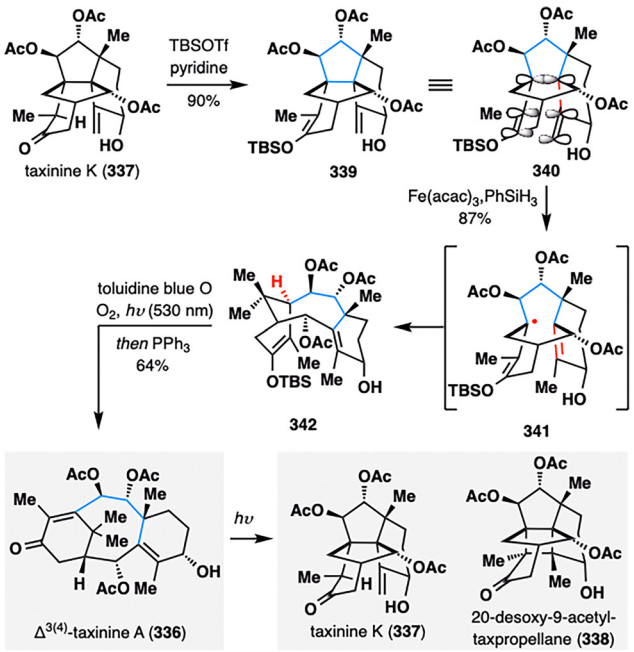

Scheme 40 Collective total synthesis of taxane diterpenes (**336–338**) by Gaich, Pan, and co-workers.

tropolone motifs (Scheme 39).[172,173] The fragmentation precursor **333** was assembled from readily available chiral pool material (−)-kobusone (**332**). Upon treatment of **333** with Shenvi's retrocycloisomerization conditions, the hydroxylated caryophyllene oxide derivative **333** underwent efficient ring-opening rearrangement, delivering the desired eleven-membered macrocyclic framework **334**. Subsequent epoxide reduction and TBS deprotection furnished (−)-10-hydroxyhumulene (**329**) in a concise and efficient sequence, setting the stage for further elaboration into the target monobistropolone natural products **330** and **331**.

To further expand the skeletal editing capabilities of MHAT-initiated retrocycloisomerization, Gaich and co-workers strategically employed an Fe(III)/$PhSiH_3$-catalyzed system within the context of the complex taxane scaffold (Scheme 40).[174] This transformation enabled the conversion of cyclotaxane **337** into the canonical taxane core **336**, thereby significantly broadening synthetic access to this pharmaceutically important diterpene family. Remarkably, the fragmentation proceeded only in the presence of an enol ether moiety, which enforced a stereoelectronic alignment between the exocyclic methylene and enol ether π-systems with the σ-bond undergoing cleavage (illustrated in **340**). This alignment, together with the formation of a stabilized allylic radical, provided the necessary thermodynamic driving force for the rearrangement. Following MHAT-triggered retrocycloisomerization, chemoselective oxidation of the enol ether with singlet oxygen delivered taxinine A (**336**), illustrating the utility of MHAT-radical fragmentation for late-stage skeletal remodeling of complex terpenoid frameworks. Notably, irradiation of **336** at 254 nm led to the formation of a [2+2] photocycloaddition product **338** after, along with taxinine K (**337**), proposed to arise *via* a 1,5-HAT process.

Analogous to MHAT-mediated radical fragmentations, Yang and co-workers developed a notable photocatalytic thiyl radical-initiated fragmentation–intramolecular annulation cascade.[175,176] As illustrated in Scheme 41, this strategy was harnessed to construct the intricate tetracyclic core of (−)-pavidolide B (**343**), a bioactive metabolite isolated from the marine soft coral *Sinularia pavida*.[177] The radical precursor **346** was obtained in 74% yield *via* a Mitsunobu coupling between enone **344** and vinylcyclopropane (VCP) **345**. Upon irradiation with blue LEDs in the presence of an Ir-based photocatalyst (**88**), a phenylthiyl radical was generated and selectively added to the electron-rich alkene, triggering β-scission of the adjacent cyclopropane ring. The resulting α-ester radical **347** underwent a 5-*exo*-trig cyclization onto the enone from the top face, yielding α-ketone radical **348**, which subsequently cyclized onto the allyl phenyl thioether moiety. Elimination of the thiyl radical then delivered tricyclic intermediate **349**. Notably, the regio- and stereoselectivity of the entire cascade were governed by the tethered ester group, which directed the facial selectivity of cyclization and relayed chirality from C14 to both the newly formed stereocenter at C13 and the challenging quaternary center at C4. This highly orchestrated radical sequence established all key stereocenters of the C-ring in a single step, enabling a streamlined completion of (−)-pavidolide B (**343**) through minimal downstream elaboration.

By marrying MHAT's chemofidelity with programmable coupling partners, modern synthesis achieves unprecedented brevity in constructing terpenoid skeletons—a testament to the synergy of radical reactivity and strategic disconnection.

2.2. Dealkenylative fragmentation

Dealkenative fragmentation has emerged as a powerful tool in synthetic chemistry for the selective remodeling of molecular

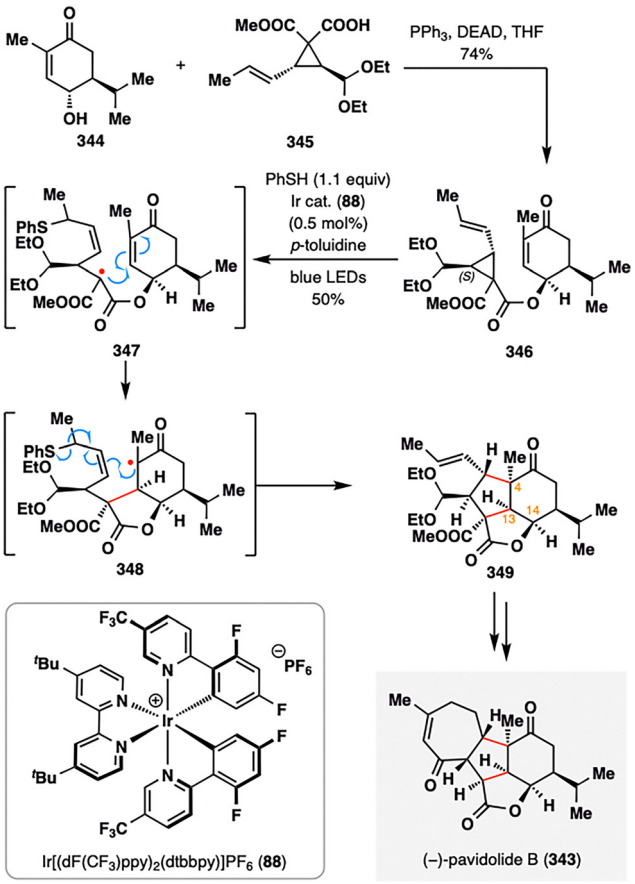

Scheme 41 Total synthesis of (–)-pavidolide B (**343**) by Yang and co-workers.

frameworks through radical-mediated cleavage of alkenes. Pioneering work by Kwon and co-workers has substantially expanded the scope of this strategy,[178,179] enabling its integration with a wide array of transformations—including hydrogenation,[180] thiylation,[181] hydroxylation,[182,183] alkenylation,[184] and alkynylation.[185] In recent years, dealkenative fragmentation, particularly the hydrodealkenylation, has gained increasing traction in the total synthesis of complex natural products, providing access to frameworks that are otherwise challenging to construct using classical disconnections. Mechanistically, the hydrodealkenylation process is initiated by ozonolysis (Scheme 42), which results in the elimination of formaldehyde and the formation of a

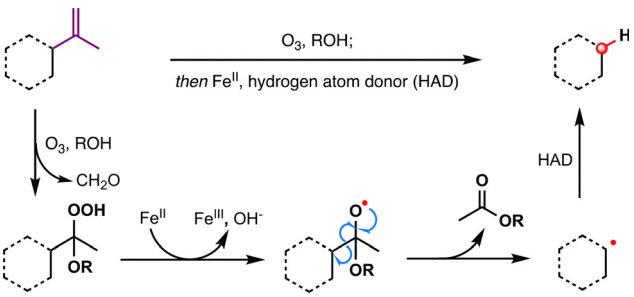

Scheme 42 General mechanism of hydrodealkenylation.

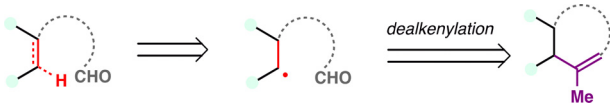

Scheme 43 Radical retrosynthesis employing the hydrodealkenylation.

hydroperoxide intermediate. Upon reduction by Fe(II), the resulting alkoxy radical undergoes β-scission to cleave the adjacent C–C bond, generating an alkyl radical. This radical subsequently undergoes HAT with a suitable hydrogen atom donor (HAD) to afford the hydrodealkenylated product.

From a retrosynthetic standpoint, Kwon's dealkenylative alkylation represents a compelling strategic disconnection by enabling selective cleavage of $C(sp^3)$–$C(sp^2)$ bonds in alkenes to reveal synthetically valuable alkyl radical fragments. This approach inverts conventional logic, shifting from forward alkene functionalization to a deconstructive paradigm in which complexity is introduced through fragmentation. In retrosynthesis, complex alkyl-substituted motifs can be traced back to terminal or internal alkenes, which function as latent radical precursors (Scheme 43). The strategic power of this method lies in its ability to cleave unactivated C–C bonds, a longstanding challenge in traditional polar disconnection-based strategies.

Notably, hydrodealkenylation was first applied in total synthesis by Newhouse and co-workers in their construction of the complex indole diterpenoid shearilicine (**350**), a natural product featuring a highly oxidized right-hand ring (Scheme 44).[186] The synthesis began with the chiral pool compound (*R*)-carvone

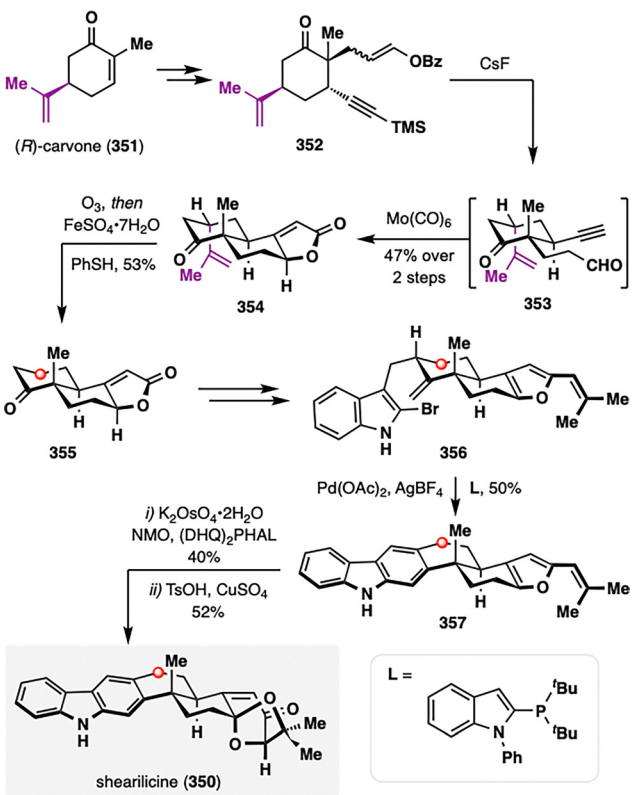

Scheme 44 Newhouse's total synthesis of (+)-shearilicine (**350**).

(**351**), enabling diastereoselective conjugate addition to yield **352**, which then underwent CsF-mediated desilylation and hydrolysis to afford **353**, followed by a Pauson–Khand reaction to furnish tricyclic intermediate **354** with excellent stereocontrol. While the isopropylidene motif in carvone proved invaluable for asymmetric induction, it is absent in the native natural product. To resolve this structural incongruity, the authors employed a reductive dealkenylation strategy: ozonolysis of **354** followed by treatment with Fe(II) as a reductant and benzenethiol as a hydrogen atom donor delivered the dealkenylated product **355** in 53% yield.[180] This transformation not only capitalized on the stereochemical utility of the carvone scaffold in early-stage synthesis but also enabled its strategic removal to match the substitution pattern of shearilicine. A final late-stage convergent coupling with the indole fragment completed the total synthesis of shearilicine (**350**).

Building upon the strategic precedent established by Newhouse, Ito and co-workers similarly leveraged the asymmetric potential of (*S*)-carvone (**53**) as a native chiral pool in their total synthesis of (−)-lemnalemnane A (**358**) and (+)-lemnardosinane A (**363**)—two sesquiterpenoids isolated from marine soft corals of the *Lemnalia* genus (Scheme 45).[187–189] The isopropylidene group in carvone served as a highly effective stereocontrol element, enabling the diastereoselective installation of two stereocenters in intermediate **360** from (*S*)-carvone (**53**) in 99% yield with excellent diastereoselectivity (d.r. = 30:1). To remove this now-superfluous functionality, Kwon's hydrodealkenylation protocol was applied to **360**, delivering the dealkenylated product **361** in 71% yield. In a variant of this strategy used *en route* to (+)-lemnardosinane A (**358**), the same isopropylidene moiety was excised from a related intermediate to furnish enone **365**. In this case, the radical intermediate was intercepted by Cu(II) and underwent β-elimination,[190] directly installing the oxidized enone motif. Through subsequent elaborations of these intermediates, both (−)-lemnalemnane A (**358**) and (+)-lemnardosinane A (**363**) were accessed in asymmetric fashion, further highlighting the strategic utility of chiral-pool-based hydrodealkenylation in natural product synthesis.

Unlike previous studies that focused on terminal alkene cleavage to achieve traceless stereocontrol, Qin and co-workers uniquely applied the hydrodealkenylation strategy to a trisubstituted internal alkene in their total synthesis of viloracanitine (**367**),[191] a C19-diterpenoid alkaloid isolated from medicinal plants of the *Aconitum* genus.[192] This natural product features a highly congested heptacyclic framework, including a rigid cyclopropane unit. Notably, this strategy allowed the resulting fragment to remain embedded within the molecular framework, facilitating not only precise control over N-heterocycle construction but also streamlined oxidation-state management in downstream transformations. As shown in Scheme 46, phenol derivative **368** underwent an IMDA cascade to furnish tricyclic scaffold **369** bearing an extraneous alkene moiety on the bridged ring system. To address this, hydrodealkenylative fragmentation was applied to oxidatively cleave the alkene in **370**, generating an aldehyde group in **371**, thereby enabling a subsequent Mannich-type annulation to construct the N-heterocycle **372** *en route* to the intricate viloracanitine skeleton. Following a series of elaborations—including a Robinson

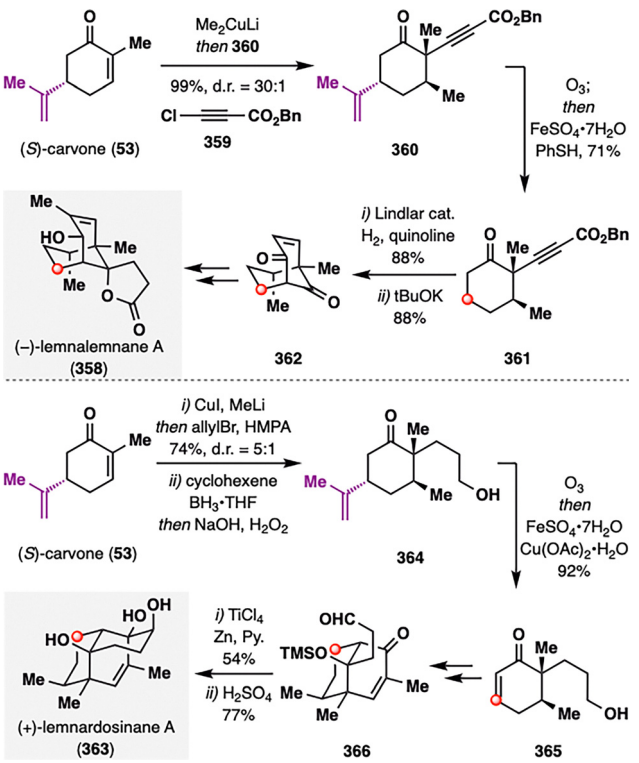

Scheme 45 Ito's asymmetric synthesis of (−)-lemnalemnane A (**358**) and (+)-lemnardosinane (**363**).

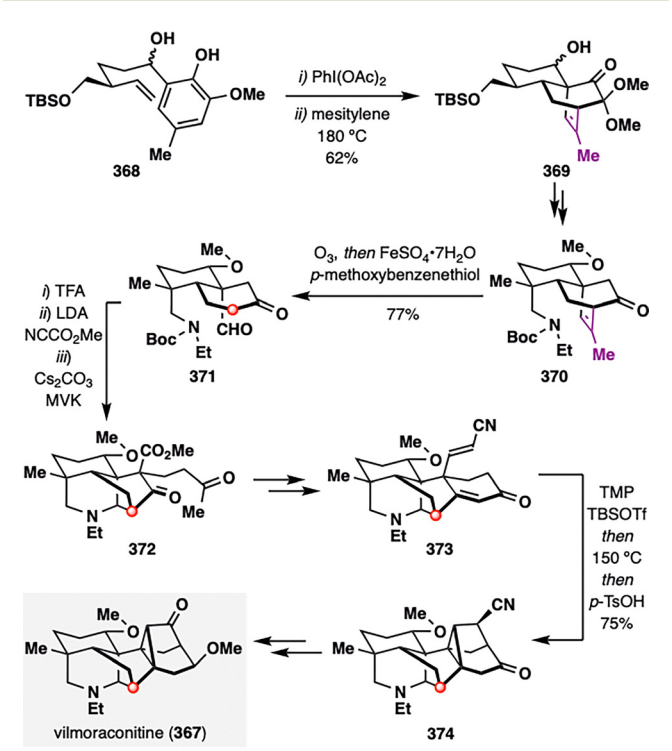

Scheme 46 Total synthesis of vilmoraconitine (**367**) by Qin, Liu, and co-workers.

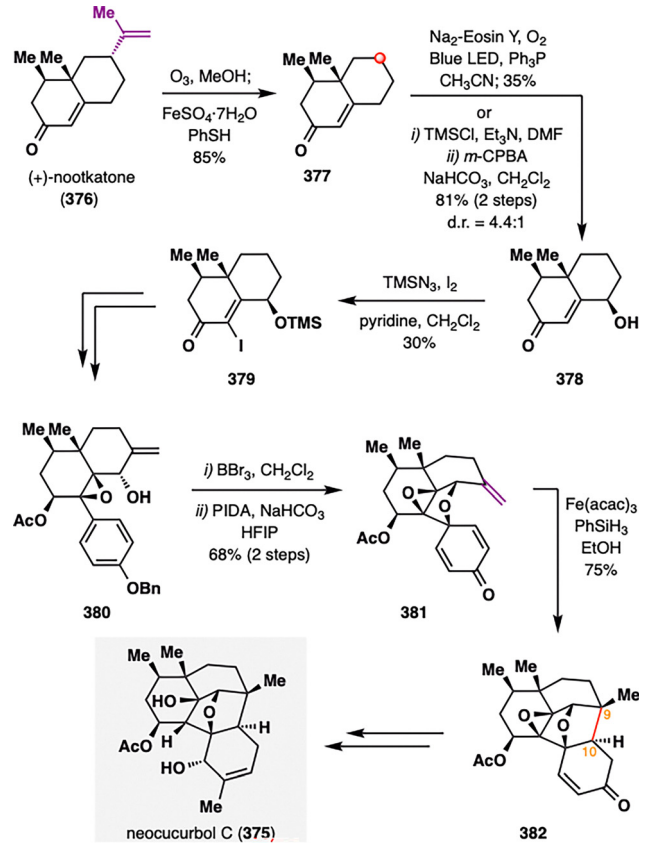

Scheme 47 Dai's total synthesis of neocucurbol C (**375**).

annulation and a second IMDA reaction—the desired natural product viloraconitine (**367**), featuring a rigid cyclopropane motif, was successfully assembled.

Dai and co-workers showcased the utility of hydrodealkenylation at the outset of their total synthesis of neocucurbol C (**375**),[193] a structurally intricate natural product isolated from *Neocucurbitaria unguis-hominis* FS685,[194] thereby demonstrating that this transformation can be performed on large scale. As depicted in Scheme 47, the synthesis commenced with Kwon's hydrodealkenylative fragmentation of commercially available (+)-nootkatone (**376**), delivering intermediate **377** on a gram scale and underscoring the expanded utility of chiral pool terpenoids in complex molecule synthesis. Subsequent site-selective C–H hydroxylation of **377** and $TMSN_3$-promoted α-iodination of **378** furnished intermediate **379**. Benzyl deprotection of **380** then unveiled a phenol primed for dearomatization. Owing to its inherent instability—attributed to *para*-quinone methide formation—this phenol was directly subjected to oxidative dearomatization with PIDA in HFIP to give cyclized intermediate **381**. Treatment of **381** with $Fe(acac)_3$ and $PhSiH_3$ initiated a pivotal BROC radical cyclization, delivering **382** in 75% yield. This sequential oxidative dearomatization/BROC radical cyclization forged the challenging C9–C10 bond, thereby completing the unprecedented 6/6/5/5/6 fused polycyclic skeleton while simultaneously establishing two contiguous stereocenters at C9 and C10. With the neocucurbol core in hand, subsequent functional group manipulations enabled completion of the first total synthesis of neocucurbol C (**375**) in 24 steps.

3. Carboxylic acids as radical precursors: versatile handles for terpenoid assembly

The strategic utilization of carboxylic acids as radical precursors has evolved from classical Barton decarboxylation into a cornerstone of modern terpenoid synthesis. Over the past decade, innovations such as photoredox-mediated decarboxylative couplings,[9,195] Et_3B-driven decarbonylation of α-alkoxyacyl tellurides,[196,197] and reductive decarboxylation of redox-active esters [RAEs, *e.g.*, *N*-(acyloxy)phthalimide esters] have revolutionized the field.[198] These methods transform abundant carboxylic acids into modular radical sources under mild conditions. By enabling direct C–C and C–heteroatom bond formations—critical for constructing quaternary carbons, polycyclic cores, and oxygenated side chains—decarboxylative strategies now offer unparalleled efficiency in assembling sterically congested terpenoid architectures. From taxane diterpenes to meroterpenoids, these advances exemplify how radical reactivity bridges the gap between feedstock simplicity and molecular complexity, redefining ideality in natural product synthesis.

From a radical retrosynthetic perspective, the disconnection of key bonds in terpenoid skeletons into carbon radicals and their coupling partners has been revolutionized over the past decade by three principal carboxylate-derived precursors (Scheme 48): (1) RAEs, which undergo single-electron reduction to liberate alkyl radicals;[198–200] (2) carboxylate anions, which undergo single-electron oxidation followed by decarboxylation (*e.g.*, photoredox-mediated processes);[195] and (3) α-alkoxyacyl tellurides, activated *via* Et_3B-mediated decarbonylation to generate stabilized alkoxy radicals.[197] Each precursor class offers distinct advantages in chemoselectivity and functional group tolerance, with RAEs emerging as the most versatile due to their mild reaction conditions. The coupling partners for these radicals—ranging from electron-deficient olefins and alkenyl/aryl zinc reagents (Ni/Fe-catalyzed cross-couplings) to vinyl

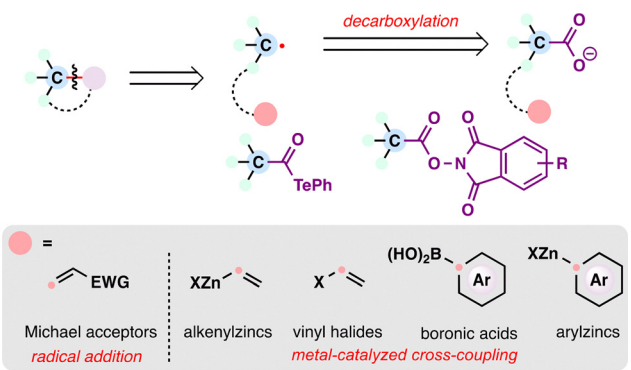

Scheme 48 Advanced radical retrosynthesis of C–C bonds employing the decarboxylative reactions.

halides and arylboronic acids—form a versatile toolkit for forging critical bonds in terpenoid synthesis. While these partners have been widely employed over the past decade, emerging strategies such as alkynyl reagents for C(sp)–C(sp^3) bond formation remain underexplored in terpenoid contexts.[201,202]

The choice of carboxylate precursor and coupling partner is dictated by the target bond type [*e.g.*, C(sp^3)–C(sp^2) and C(sp^3)–C(sp^3)]. In the following sections, we analyze the application of decarboxylative radical chemistry in terpenoid synthesis through the lens of bond formation types, including decarboxylative C(sp^3)–C(sp^3) bond formation and decarboxylative C(sp^2)–C(sp^3) bond formation.

3.1. Decarboxylative C(sp^3)–C(sp^3) bond formation

Over the past decade, decarboxylative radical addition to electron-deficient alkenes has appeared as a transformative strategy for stereoselective construction of C(sp^3)–C(sp^3) bonds.[203] This approach leverages carboxylate-derived precursors to generate carbon radicals, which engage in conjugate additions to α,β-unsaturated carbonyl systems or related electrophilic partners. By bypassing classical ionic pathways prone to steric hindrance and regiochemical limitations, these radical-mediated reactions enable efficient access to sterically congested architectures. Given the extensive application of decarboxylative C(sp^3)–C(sp^3) bond formation in terpenoid synthesis, we herein categorize advancements in this field based on three pivotal carboxylate precursors: (1) RAEs,[204,205] (2) carboxylate anions,[206] and (3) α-alkoxyacyl tellurides—each offering distinct practical advantages.[197]

3.1.1. Decarboxylation from RAEs. In 2012, Overman and co-workers introduced a pioneering strategy for the total synthesis of (−)-aplyviolene (**383**),[207] leveraging Okada's decarboxylative radical addition to generate tertiary radicals *via* visible light-mediated fragmentation of RAEs.[208] This work marked the first application of such mild radical precursors in natural product synthesis, enabling the diastereoselective construction of sterically congested quaternary carbon centers under mild photoredox conditions. Notably, according to Overman's study, the reaction mechanism may involve multiple, potentially competing pathways;[204] nevertheless, it delivers impressive efficiency and selectivity.

As shown in Scheme 49(A), the quaternary stereocenter at C8 of (−)-aplyviolene (**383**)—a rearranged spongian diterpenoid bearing a *cis*-perhydroazulene core and a fused 6-acetoxy-2,7-dioxabicyclo[3.2.1]octan-3-one fragment—was constructed *via* a photoredox-catalyzed decarboxylative coupling. The requisite RAE **387** was prepared from inexpensive (+)-fenchone (**385**) *via* a Beckmann fragmentation to yield tertiary nitrile **386**, followed by formation of a seven-membered ring and subsequent functional group interconversions. Irradiation of a mixture of **387**, enone **388**, $Ru(bpy)_3(BF_4)_2$, Hantzsch ester, and DIPEA in CH_2Cl_2 provided the coupled product **389** in 61% yield as a single diastereomer. This transformation replaced the two-electron Michael addition previously used to construct the same bond in their earlier synthesis,[209] thereby enabling completion of (−)-aplyviolene (**383**) by following the established downstream sequence. This revision not only streamlined the construction of the C8–C14 quaternary–tertiary junction but also reduced the number of isolated intermediates by five relative to the polar pathway, highlighting the strategic efficiency of radical disconnections in complex settings.

Building on this success, Overman and co-workers extended their radical-based approach to the synthesis of cheloviolene A (**384**),[210] another rearranged spongian diterpenoid. The same RAE **387** was employed in a decarboxylative coupling with enone **390**. Interestingly, the same product **391** could also be accessed using MacMillan's Ir(III)-catalyzed oxidative photoredox conditions *via* direct coupling of carboxylic acid **392** with enone **390** (Scheme 49(B)).[210] This alternative approach improved the coupling efficiency, raising the yield from 30% to 44%, and further underscored the utility and adaptability of photoredox-enabled decarboxylative strategies.

In 2015, Overman's group reported a concise and enantioselective synthesis of *trans*-clerodane diterpenoids using a similar radical strategy (Scheme 49(C)).[211] The *trans*-decalin RAE **397** was constructed from chloroalkyne **394** *via* a nickel-catalyzed regioselective hydroalumination, followed by an enantioselective conjugate addition to 3-methylcyclohex-2-en-1-one (**395**) catalyzed by a silver–NHC complex developed by Hoveyda.[212] The pivotal 1,6-addition of a tertiary radical derived from RAE **397** to β-vinylbutenolide **399** stereoselectively forged the key C9 quaternary center. This was the first demonstration of tertiary radical 1,6-addition to electron-deficient dienes, broadening the reactivity landscape of decarboxylative radical chemistry.

The power of this platform was further illustrated in the total synthesis of (−)-chromodorolide B (**400**),[213] a highly complex member of the rearranged spongian diterpenoid family (Scheme 49(D)). The tertiary RAE **405** was synthesized from methyl ester **404**, which was itself prepared *via* a modified NHK coupling between iodide **402** and aldehyde **403**.[214] The final radical cascade—an intermolecular decarboxylative addition/cyclization/fragmentation (ACF) sequence—was initiated under photoredox conditions with a Hantzsch ester in the absence of DIPEA, which improved the reaction efficiency. This cascade formed two C–C bonds and established four contiguous stereocenters, furnishing tetracyclic intermediate **407** in a single operation. This work showcased the unique ability of radical cascades to rapidly generate complexity.

Building on the conceptual framework established by Overman, Yoshimitsu and co-workers developed a decarboxylation-initiated radical addition/cyclization/oxidative aromatization cascade to construct the tetralin motif of (±)-hamigeran B (**408**),[215] a tricyclic natural product isolated from the marine sponge *Hamigera tarangaensis* (Scheme 50).[216] In this transformation, a novel Zn(II)–porphyrin photocatalyst (**411**) was employed in place of conventional Ru(II)-based systems, significantly improving the yield of tetralin product **413** from 52% to 82%. Upon irradiation, photoexcited **411** facilitated single-electron reduction of RAE **409** in the presence of DIPEA, generating a tertiary carbon radical that underwent addition to an acrylate acceptor **410**, forming an α-ester radical. This intermediate then cyclized onto the aromatic ring, and the resulting dearomatized species was oxidized *via* SET by the

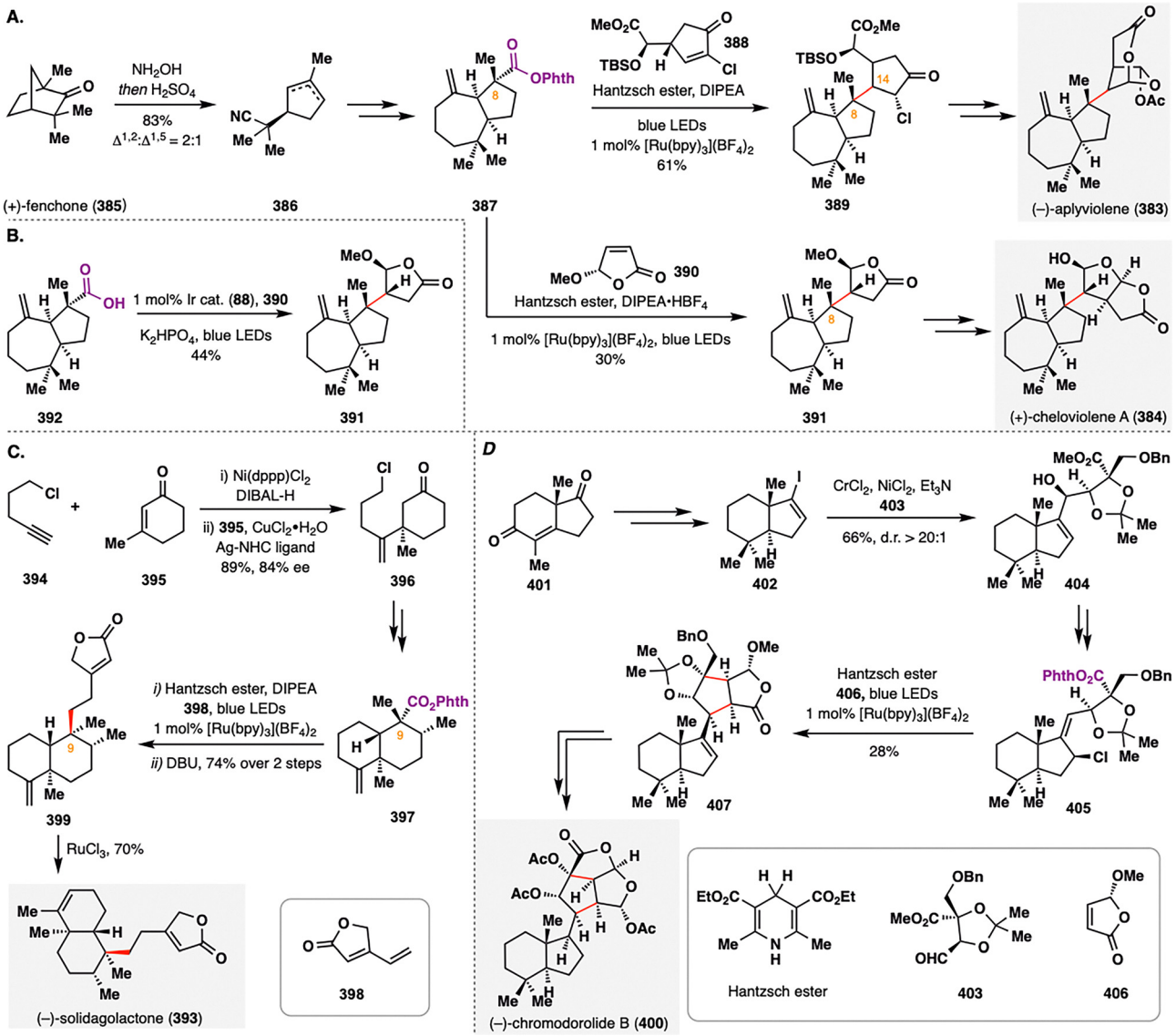

Scheme 49 Overman's total synthesis of spongian (**383–384**), clerodane (**393**), chromodorolide (**400**) diterpenoids.

photocatalyst to regenerate aromaticity—completing the radical annulation sequence. Notably, the reduced by-product **412** could be converted to **413** in 93% yield *via* DDQ-mediated oxidation, further highlighting the efficiency and robustness of this decarboxylative cascade. Subsequent elaboration of **413** provided access to (±)-hamigeran B (**408**) in a concise fashion.

While prior studies have predominantly employed photocatalysts to mediate decarboxylation, Wu and co-workers developed a photocatalyst-free, photoinduced decarboxylative allylation based on a donor–acceptor (EDA) complex strategy to achieve side-chain elaboration in the total synthesis of (25*S*)-Δ^4-dafachronic acids (**415–417**),[217] a class of steroidal hormones identified in nematodes (Scheme 51). In the key transformation, the EDA complex **420**—formed between the Hantzsch ester (donor) and the RAE **419**—underwent visible-light excitation to enable single-electron transfer, generating an alkyl radical. This radical engaged allyl sulfone **421** in a radical addition followed by β-scission, furnishing ester **422** in 69% yield under optimized conditions. Subsequent transformations enabled a divergent route to (25*S*)-Δ^4-dafachronic acid (**415**). Notably, the same EDA-mediated strategy was also applied to the synthesis of (25*S*)-Δ^7-dafachronic acid (**416**) and desulfated boophiline (**417**),[218] further demonstrating the generality and utility of this mild, catalyst-free radical methodology in complex steroidal frameworks.

Recently, our group demonstrated the synthetic utility of reductive, metal-mediated decarboxylative coupling in the enantioselective total synthesis of (−)-macrocalyxoformins A (**423**) and B (**424**), as well as (−)-ludongnin C (**425**)—three highly oxygenated enmein-type *ent*-kauranoids (Scheme 52).[219] The first key transformation involved the construction of tetrahydrofuran fragment **428** *via* a cascade comprising reductive decarboxylative cyclization, RPCO, and subsequent carboxylation. Initiated by Ni(II)/Zn-mediated reduction of a RAE embedded in enone **426**, the resulting radical underwent intramolecular conjugate addition

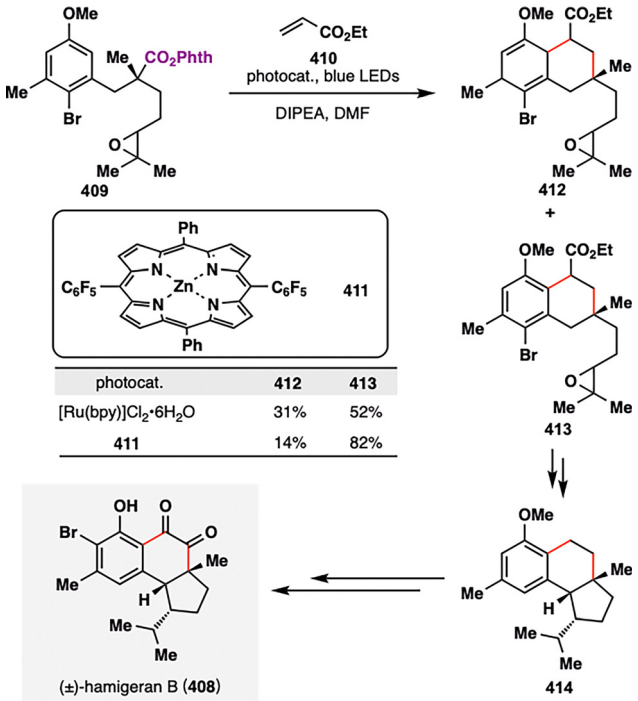

Scheme 50 Yoshimitsu's formal synthesis of hamigeran B (**408**).

to form radical intermediate **429**. This intermediate was then reduced to enolate **430**, which intercepted CO_2—either from the decarboxylation event or released during the following esterification step with Boc_2O—to afford carboxylate **431**. In the presence of Boc_2O, **431** was converted into the *tert*-butyl ester **428**. Notably, the dual role of CO_2—as both a byproduct and a reactive species—was confirmed by isotopic labeling experiments conducted by our team. After installation of a hydroxymethyl substituent at C10, a Suárez-type radical cyclization furnished the second tetrahydrofuran ring, yielding intermediate **433**. This was then converted into RAE **434**, which underwent a second Ni(II)/Zn-mediated decarboxylative coupling—this time with 2,2,2-trifluoroethyl acrylate—stereoselectively constructing the C10 all-carbon quaternary center in **435**.[205] Final elaboration of the C/D-ring system ultimately delivered (−)-macrocalyxoformins A (**423**) and B (**424**), as well as (−)-ludongnin C (**425**), underscoring the strategic value of sequential decarboxylative radical disconnections in the synthesis of architecturally complex natural products.

3.1.2. Decarboxylation from carboxylate anions. While the conversion of carboxylic acids to RAEs, as outlined in Section 3.1.1, enables radical generation under mild single-electron reduction conditions, this strategy necessitates an additional step to derivatize the native carboxyl group. In contrast, direct single-electron oxidation of carboxylate anions offers superior step economy by bypassing prefunctionalization, directly transforming abundant carboxylic acids into carbon radicals.[220] This approach, exemplified by photoredox-mediated decarboxylative radical addition pioneered by Macmillan and colleagues, relies on oxidizing agents (*e.g.*, visible-light-excited photocatalyst Ir^{III}) to abstract an electron from the carboxylate, triggering decarboxylation and radical formation (Scheme 53).[206] However, it is noteworthy that the practical utility of this method hinges on substrate compatibility with oxidative conditions. The high oxidation potentials required to activate carboxylates may limit applicability to oxidation-sensitive substrates.

Reisman and co-workers achieved the total synthesis of the cyclobutane-containing meroterpenoid (+)-rumphellaone A (**436**) by employing enantioenriched cyclobutene derivatives as chiral starting materials, leveraging C–H arylation and oxidative decarboxylative radical addition as key steps (Scheme 54).[221] A directed C–H arylation of **437** with **438**, facilitated by an 8-aminoquinolinamide auxiliary (8AQ), furnished *cis*-arylated cyclobutene **439** in excellent yield (90%). Hydrolysis of **439** triggered epimerization at the carboxyl center, delivering the thermodynamically favored *trans*-diastereomer **440**. Subsequent oxidation, methylation, and hydrogenation of **440** delivered lactone **441**, which was then subjected to oxidative decarboxylative radical addition. In the presence of K_2HPO_4, photoexcited Ir(III)* catalyzed a direct decarboxylative Giese reaction with methyl vinyl ketone (MVK), providing (+)-rumphellaone A (**436**) in good yield. This concise sequence underscores the strategic value of oxidative radical disconnections for the stereocontrolled assembly of highly substituted cyclobutane frameworks.

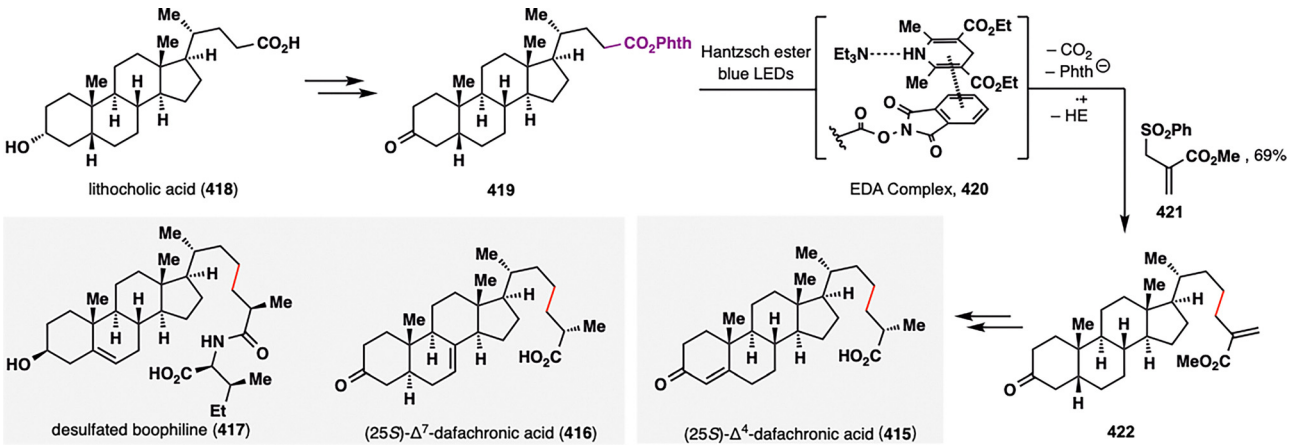

Scheme 51 Wu's synthesis of (25*S*)-Δ^4-dafachronic acid (**415**), (25*S*)-Δ^7-dafachronic acid (**416**), and desulfated boophiline (**417**).

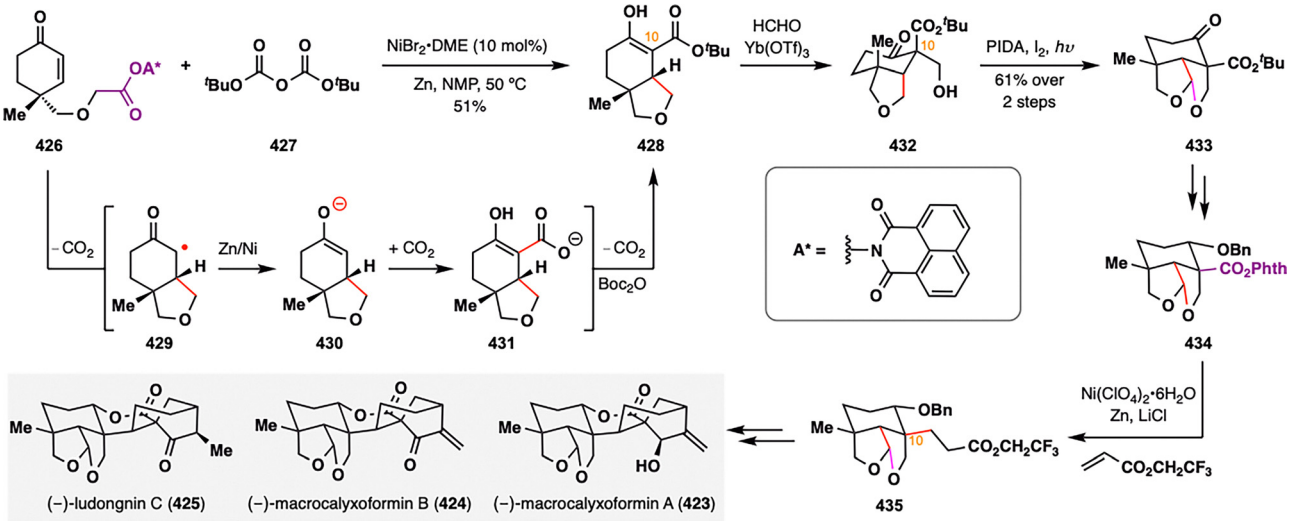

Scheme 52 Li's total synthesis of (−)-macrocalyxoformins A (**423**) and B (**424**), and (−)-ludongnin C (**425**).

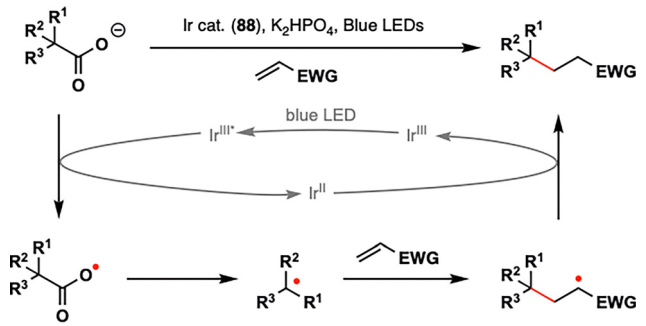

Scheme 53 Macmillan's pioneered study on direct decarboxylative Giese reaction.

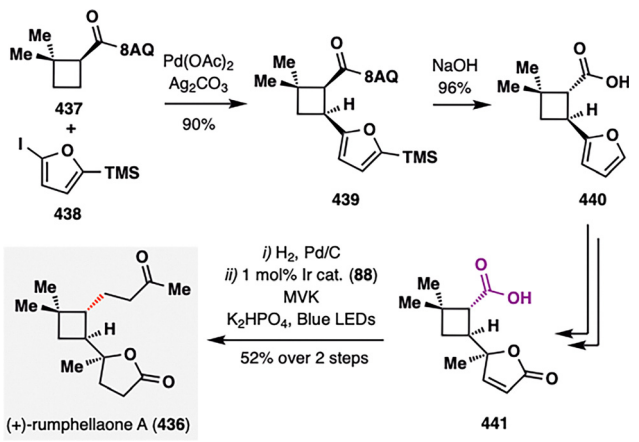

Scheme 54 Reisman's total synthesis of meroterpenoid (+)-rumphellaone A (**436**).

Inoue and co-workers strategically employed an oxidative decarboxylative radical cyclization to achieve a pivotal 7-*endo*-trig ring closure in their total synthesis of resiniferatoxin (**442**),[222] a highly oxygenated daphnane diterpenoid isolated from *Euphorbia resinifera* (Scheme 55).[223] The key cyclopentanone intermediate

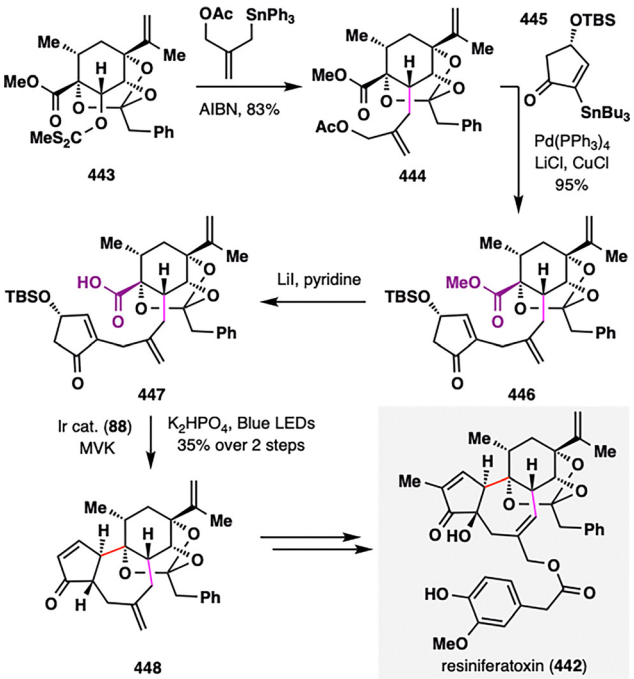

Scheme 55 Inoue's total synthesis of resiniferatoxin (**442**).

446 was constructed through a Barton dehydroxylative allylation of **443** followed by a Trost-type cross-coupling between fragments **444** and **445**. Upon hydrolysis and base-promoted deprotonation, the resulting carboxylate underwent single-electron oxidation by photoexcited Ir(III)*, generating a conformationally rigid bridgehead radical *via* CO_2 extrusion.[206] This radical then engaged in a stereocontrolled intramolecular 7-*endo*-trig addition. Crucially, a pre-installed OTBS group served as a steric control element, enforcing radical approach from the opposite face; simultaneously, β-elimination of the OTBS group delivered tricyclic scaffold **448**. Subsequent side-chain elaboration furnished resiniferatoxin (**442**), highlighting the utility of radical-based ring

closures for constructing densely functionalized diterpenoid frameworks.

While most previous examples of oxidative decarboxylation rely on base-mediated deprotonation to generate carboxylate anions, Inoue and co-workers developed a base-free decarboxylative coupling protocol in their total synthesis of taxol (**449**)—a structurally intricate taxane diterpenoid with well-established anticancer activity—thereby substantially broadening the substrate scope and functional group compatibility of this strategy (Scheme 56).[224] The key carboxylic acid precursor **451** was prepared enantioselectively from 2,2-dimethylcyclohexane-1,3-dione (**450**). The decarboxylative coupling was accomplished under neutral conditions using a Pt-doped TiO_2 photocatalyst (MPT-623) and violet LED irradiation in ethyl acetate,[225] effecting a direct union of acid **451** with enone **452**. A subsequent one-pot DDQ oxidation furnished enone **453** in 45% overall yield, with full preservation of stereochemical integrity. Unlike conventional Ir(III)-based photoredox methods—which typically require basic conditions to generate the carboxylate—this neutral protocol avoids the use of external bases, rendering it particularly advantageous for substrates bearing base-sensitive functional groups. The mild conditions significantly enhance chemoselectivity and broaden the functional group tolerance. With this complex enone **453** in hand, a series of intramolecular cyclizations and late-stage elaborations ultimately enabled completion of the total synthesis of taxol (**449**).

Following their successful application of base-free decarboxylative cross-coupling in the total synthesis of taxol (**449**), Inoue and co-workers extended this strategy to achieve the first total synthesis of euphorbialoid A (**456**),[226] a highly oxygenated member of the rare premyrsinane diterpenoid family characterized by a 5/7/6/3-membered tetracyclic framework (Scheme 57). Initial attempts employing Ir(III)-based photocatalysis under basic conditions

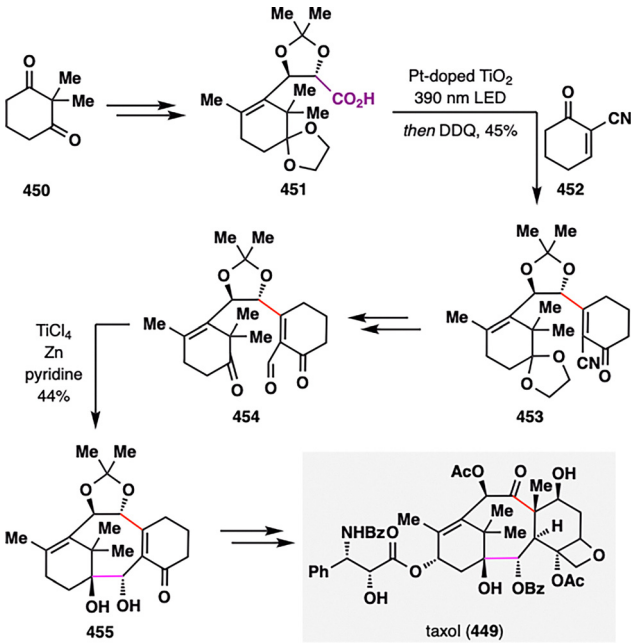

Scheme 56 Inoue's total synthesis of taxol (**449**).

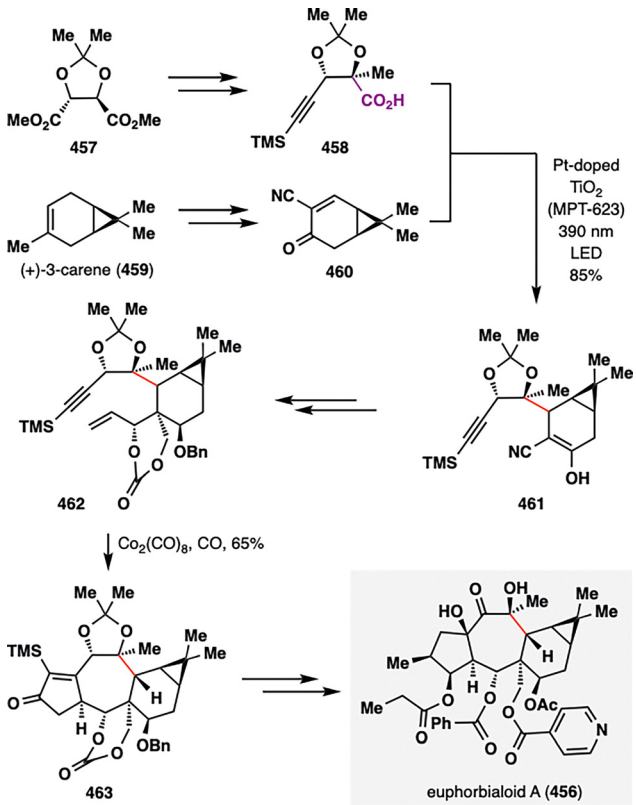

Scheme 57 Inoue's total synthesis of euphorbialoid A (**456**).

resulted in substantial substrate decomposition. To circumvent this limitation, they turned again to their previously developed Pt-doped TiO_2 (MPT-623) photocatalyst,[225] which enabled efficient coupling of carboxylic acid **458** with enone **460** under neutral conditions. Remarkably, the decarboxylative radical addition proceeded with high stereoselectivity, delivering a single diastereomer and forging a sterically congested quaternary center. The diastereoselectivity was rationalized by the steric shielding imparted by the TMS-alkyne on the bottom face of fragment **458** and the dimethylcyclopropane moiety on the top face of fragment **460**, directing the radical addition to the least hindered trajectory. This transformation efficiently installed two contiguous stereocenters and markedly increased molecular complexity in a single operation. A late-stage Pauson–Khand reaction then forged the 5/7/6/3 fused carbocyclic core **463**, setting the stage for final oxidation-state adjustments to furnish euphorbialoid A (**456**).

3.1.3. Decarboxylation from α-alkoxyacyl tellurides. While the strategies detailed in Sections 3.1.1 and 3.1.2 exploit single-electron reduction of RAEs or single-electron oxidation of carboxylate anions to access carbon radicals, the Et_3B/O_2-mediated decarbonylation of α-alkoxyacyl tellurides, pioneered by Inoue and coworkers in 2015,[197] introduces a mechanistically distinct yet synergistic approach to decarboxylative $C(sp^3)$–$C(sp^3)$ bond formation. Although divergent in radical initiation, this methodology remains rooted in the decarboxylative paradigm, as its α-alkoxyacyl telluride precursors are directly derived from carboxylic acids. Central to this strategy is the

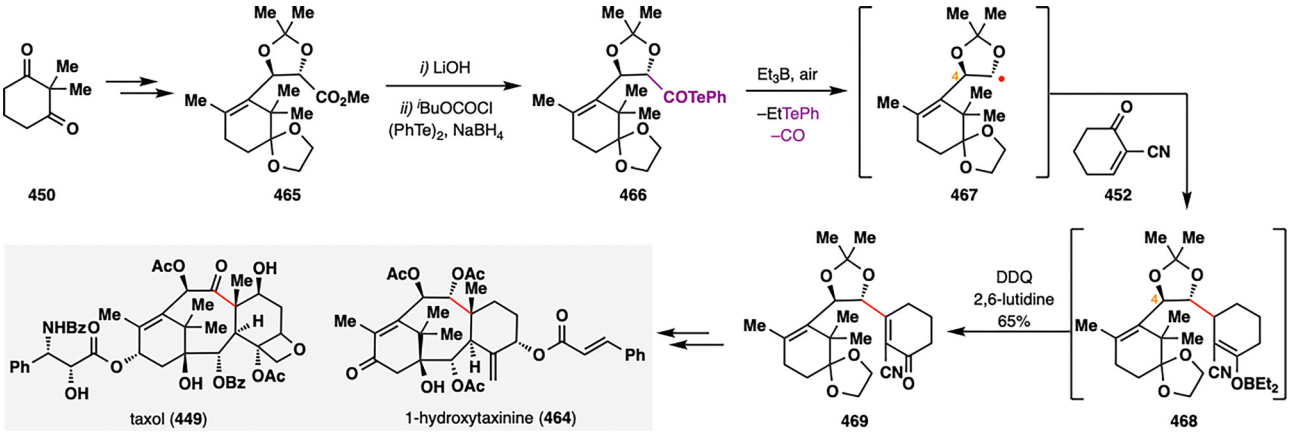

Scheme 58 Inoue's total synthesis of 1-hydroxytaxinine (**464**) and taxol (**449**).

homolytic cleavage of the C–Te bond under mild Et_3B/O_2 conditions, which triggers rapid decarbonylation to generate stabilized α-alkoxy carbon radicals. These intermediates exhibit remarkable reactivity and stereochemical fidelity, engaging in stereoselective conjugate additions to electron-deficient alkenes or orchestrating multi-component couplings. Notably, the reaction proceeds under ambient conditions—eschewing light, heat, or stringent deoxygenation—while enabling the single-step construction of densely oxygenated carboskeletons, a defining feature of architecturally complex terpenoid natural products.

Inoue and co-workers resourcefully employed their developed Et_3B/O_2-mediated decarbonylation of α-alkoxyacyl tellurides as a key transformation in their total synthesis of 1-hydroxytaxinine (**464**),[227] particularly for constructing sterically hindered C–C bonds within highly oxygenated frameworks (Scheme 58). This strategy effectively demonstrated excellent functional group compatibility under mild radical conditions. Mechanistically, homolytic cleavage of the C–Te bond, initiated by Et_3B/O_2, generated a ketyl radical that underwent spontaneous decarbonylation to afford α-alkoxy radical **467**. Importantly, while this step erased the original stereochemistry at the radical center, the subsequent radical addition to an enone **452** re-established stereocontrol, as the coupling partner selectively approached from the face opposite to the bulky C4 substituent. The resulting radical intermediate was then trapped by Et_3B to generate a boron enolate **468**, which upon oxidation furnished enone **469** as a single diastereomer in 65% yield. Inoue further demonstrated the synthetic utility of this radical-based approach in their synthesis of taxol (**449**),[224] using it as an alternative to MPT-623 photocatalysis for stereocontrolled decarboxylative coupling—thereby underscoring the versatility of radical-mediated strategies in the construction of complex taxane architectures.

Building on the success of their earlier taxane synthesis, Inoue and co-workers further refined their approach in 2023 by unveiling a streamlined route to taxol (**449**) that shortened the overall sequence by six steps while preserving the key Et_3B/O_2-mediated decarbonylation of α-alkoxyacyl tellurides as a pivotal transformation (Scheme 59).[228] Specifically, guided by theoretical calculations, they envisioned that bicycle **475**'s 6–H/Br/CN

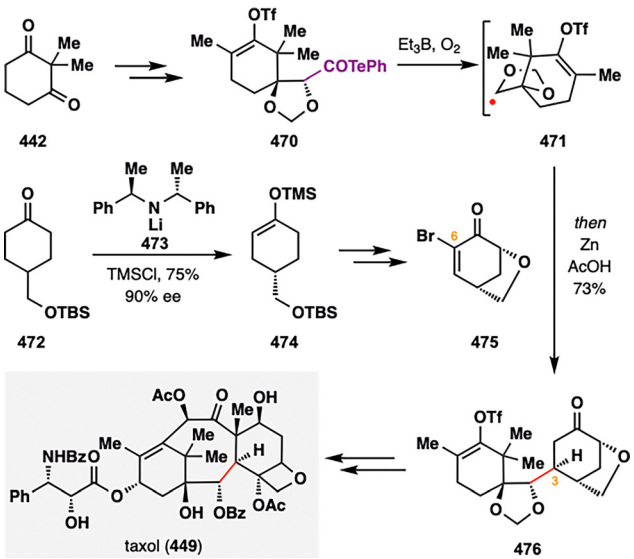

Scheme 59 Inoue's total synthesis of taxol (**449**).

would all deliver C3-stereoselectivity, and the radical accepting propensities was expected to be 6–CN > 6–Br > 6–H, based on their respective LUMO energies. Upon experimental validation, 6–Br emerged as the optimal coupling partner, serving as electron-acceptor with α-alkoxyketyl radical through radical addition. The observed stereoselectivity was attributed to the steric shielding imposed by the proximal dimethyl group in intermediate **470** and the ether bridge within **475**, which collectively blocked the bottom face and directed radical addition to the less-hindered top face. Following the coupling event, the bromide was reductively removed under Zn/AcOH conditions, enabling downstream elaboration toward the complex taxol (**449**) with minimal functional group manipulations.

Continuing their pioneering application of α-alkoxyacyl tellluride couplings, Inoue and co-workers accomplished a formal total synthesis of batrachotoxin (**477**),[229,230] a potent steroidal alkaloid originally isolated from a Colombian poison-dart frog,[231] featuring a densely functionalized 6/6/6/5-membered carbocyclic framework (Scheme 60). A central element of this

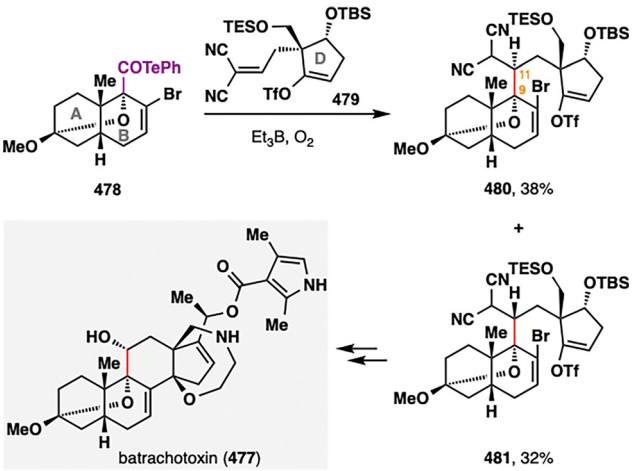

Scheme 60 Inoue's formal total synthesis of batrachotoxin (**477**).

strategy was the Et_3B/O_2-mediated decarbonylation of an α-alkoxyacyl telluride, which enabled the union of the A/B ring system **478** and the D-ring fragment **479** with stereospecific establishment of a quaternary center. Notably, the decarbonylative transformation proceeded with high chemoselectivity: selective homolytic cleavage of the C–Te bond in **478** occurred without perturbing the adjacent C–Br bond, a distinction attributed to the activating influence of the neighboring oxygen substituent. This process generated a bridgehead α-alkoxy radical with fixed stereochemistry, which underwent a radical addition to the electron-deficient alkene of **479**. While the radical coupling afforded two diastereomers (**480** and **481**) at C11 without significant stereoselectivity, both intermediates could be funneled toward the desired diastereomer through subsequent elaborations.

3.2. Decarboxylative C(sp^2)–C(sp^3) bond formation

The construction of C(sp^2)–C(sp^3) bonds, particularly through alkenylation, is indispensable in constructing terpenoid frameworks. Building on Baran's pioneering work in 2016, which established the viability of Ni-catalyzed cross-coupling of RAEs with aryl zinc reagents,[232] subsequent advancements have expanded this paradigm to alkenyl systems—encompassing alkenylzinc reagents,[233] vinyl halides,[234,235] and related electrophiles.[236,237] These methodological innovations have profoundly streamlined terpenoid synthesis, offering unparalleled efficiency in forging their complex architectures. Notably, all reported decarboxylative C(sp^2)–C(sp^3) bond formations in terpenoid synthesis exclusively utilize RAEs as radical precursors, underscoring their unique combination of practicality, stability, and chemoselectivity. The defining feature of RAEs lies in their ability to undergo single-electron reduction under transition metal catalysis (*e.g.*, Ni, Ir, Cu), generating alkyl radicals that engage alkenyl or aryl coupling partners. This radical-mediated pathway circumvents the electronic limitations inherent to classical ionic mechanisms, thereby enabling the convergent assembly of sterically congested terpenoid skeletons with precision.

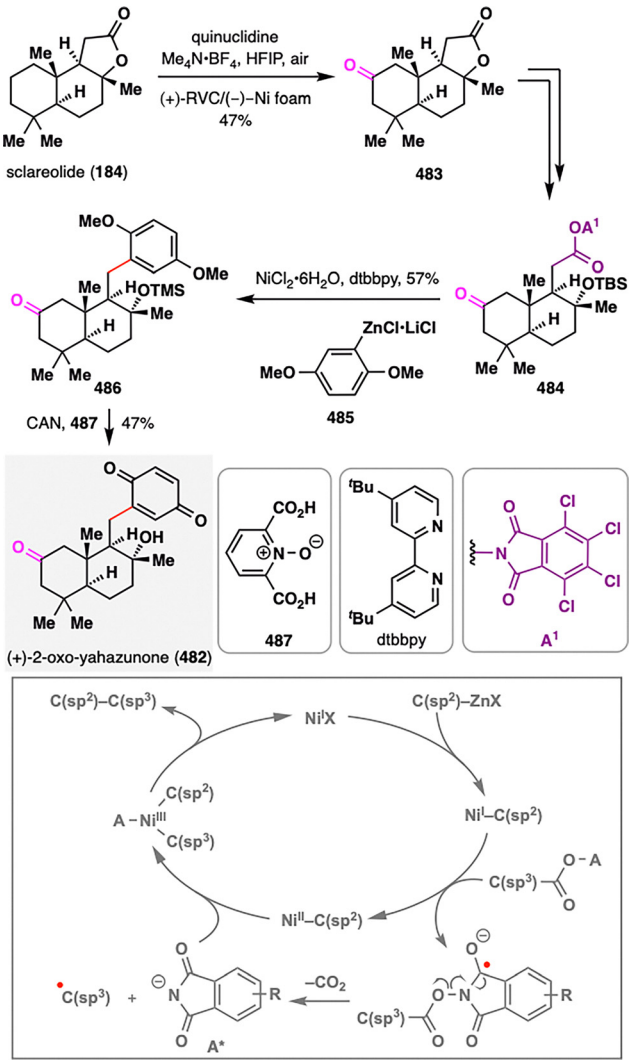

Scheme 61 Baran's synthesis of (+)-2-oxo-yahazunone (**482**).

Following Baran's pioneering 2016 work on RAEs,[232] the strength of this methodology was swiftly illustrated in Baran's synthesis of (+)-2-oxo-yahazunone (**482**) using a decarboxylative arylation.[238] As detailed in Scheme 61, electrochemical C–H oxidation of sclareolide (**184**) at a 50 g scale delivered ketone **483**, which was subsequently converted to RAE **484** and coupled *via* Ni-catalyzed decarboxylative cross-coupling to form the critical C–C bond,[232] culminating in the efficient synthesis of **486**. Followed by CAN-mediated oxidative dearomatization, (+)-2-oxo-yahazunone (**482**) was obtained in high efficiency. This seamless integration of electrochemical oxidation and RAE-based decarboxylative coupling exemplifies the transformative potential of these methodologies in streamlining complex natural product assembly.

Regarding the Ni-catalyzed cross-coupling of RAEs with aryl zinc reagents, a plausible mechanism is outlined in Scheme 61.[232] The catalytic cycle is proposed to initiate with transmetalation between a Ni^I complex and the aryl zinc reagent, furnishing an aryl–Ni^I intermediate. This species then undergoes single-electron reduction of the NHPI ester, generating an alkyl radical—following

decarboxylation—and an aryl–Ni(II) complex. Subsequent radical capture by the aryl–Ni(II) species delivers a key aryl–Ni(III)–alkyl intermediate, which undergoes reductive elimination to provide the desired $C(sp^2)$–$C(sp^3)$ cross-coupled product. Notably, the same mechanistic paradigm can be extended to the following decarboxylative alkenylation reactions.

Building upon their earlier work on decarboxylative arylation in 2016,[232] Baran and co-workers subsequently disclosed an efficient decarboxylative alkenylation strategy,[233] enabling the construction of $C(sp^2)$–$C(sp^3)$ bonds across a broad substrate scope—including mono- to fully substituted olefins and a wide range of carboxylic acids, from primary to tertiary (Scheme 62(A)). The decarboxylative alkenylation, which proceeded between RAEs and organozinc reagents in the presence of inexpensive Ni(II) catalysts, had proven exceptionally efficient for the streamlined synthesis of diterpenes and steroids, as illustrated in Scheme 62(B).[233] Utilizing carboxylic acid **495** as a common intermediate, Baran and co-workers demonstrated a divergent approach to access three clerodane diterpenes (**492**–**494**) *via* the above alkenylation sequence, significantly reducing the total synthesis of (−)-kolavenol (**492**) from 21 steps to just 9 steps with excellent stereoselectivity ($E:Z > 20:1$), in particular. Similarly, employing carboxylic acid **497** as the decarboxylative precursor, α-tocotrienol (**496**) was efficiently assembled in only two steps—substantially improving upon the previously reported seven-step sequence.

As shown in Scheme 62(C)–(E), Baran and co-workers further expanded the scope of their decarboxylative alkenylation platform by applying it to the divergent total synthesis of several structurally distinct pyrone diterpenoids,[239] all derived from a common *trans*-decalin intermediate (**501**). As outlined in Scheme 62(C), the *trans*-decalin scaffold was efficiently assembled *via* an electrochemically assisted, Mn-catalyzed oxidative radical polycyclization of **499** to furnish intermediate **500**, followed by a Tsuji allylation to deliver **501**. Conversion of the C4 *exo*-methylene into a carboxylic acid, along with construction of the right-hand tetrahydrofuran ring, afforded carboxylic acid **502**. Under the group's previously developed reductive decarboxylative radical addition conditions,[205] **502** underwent coupling with methyl acrylate to furnish ester **503**. Oxidation of the C12 hydroxymethyl group then generated a carboxylic acid, which was subjected to nickel-catalyzed decarboxylative alkenylation to install an isopropenyl substituent at C12 with high diastereoselectivity. Notably, this radical-based approach was particularly advantageous in this context, as traditional α-oxy radical precursors such as halides are inherently unstable at this position. Subsequent olefination at C3 yielded olefin **505**, a versatile intermediate that could be converted to subglutinol B (**498**) following Hong's reported protocol.[240]

Leveraging insights from the synthesis of subglutinol B (**498**), the team next achieved the total synthesis of higginsianin A (**506**)—another architecturally complex member of the pyrone diterpenoid family—by reversing the order of the decarboxylative transformations (Scheme 62(D)). Specifically, decarboxylative radical addition at C4 was carried out after the nickel-catalyzed alkenylation at C12. This sequence inversion preserved high stereoselectivity at both sites but led to an opposite diastereoselectivity at C12, thereby enabling access to the stereochemical configuration required for higginsianin A (**506**). The resulting intermediate **510** was further elaborated to complete the first total synthesis of higginsianin A (**506**). Remarkably, the decarboxylative alkenylation proceeded smoothly even in the presence of an unprotected primary alcohol, underscoring the functional group tolerance of the method. The same modular strategy was extended to the synthesis of sesquicillin A (**511**) (Scheme 62(E)), where the radical-based disconnections effectively addressed stereochemical challenges that had previously defied solution using traditional two-electron disconnections. These studies collectively highlight the synthetic power of radical cross-coupling in constructing highly oxidized and stereochemically complex terpenoid architectures.

Advancing their decarboxylative alkenylation platform, Baran and co-workers developed an electrochemical reductive decarboxylative $C(sp^2)$–$C(sp^3)$ cross-coupling strategy between RAEs and alkenyl halides (Scheme 63(A)).[235] This method provided a powerful and modular approach to terpene synthesis (Scheme 63(B)–(F)), obviating the need for preformed alkenylzinc reagents and minimizing functional group manipulations, protecting group interconversions, and redox fluctuations. A key mechanistic insight emerged from their studies: although pure silver electrodes were ineffective, silver ions proved indispensable. Under electrochemical conditions, Ag-based nanoparticles formed *in situ* on the cathode surface, playing a crucial role in promoting the cross-coupling.

To demonstrate the utility of this approach in complex molecule synthesis, the group streamlined the preparation of a polyene cyclization precursor *en route* to progesterone (**521**) (Scheme 63(B)). Conventional retrosynthetic disconnections toward this intermediate were both non-intuitive and inefficient. In contrast, their electrocatalytic decarboxylative strategy enabled direct forging of a pivotal $C(sp^2)$–$C(sp^3)$ bond between well-defined building blocks, thereby simplifying the overall synthetic route. Through sequential electrocatalytic couplings of geometrically defined fragments, they accessed the key polyene intermediate in a modular and convergent fashion, ultimately enabling an efficient total synthesis of progesterone (**521**).

Applying a similar strategy, Baran's group efficiently synthesized two additional polyene precursors *en route* to structurally complex terpenoids: isosteviol (**530**) and celastrol (**536**) (Scheme 63(C) and (D)), using their electrochemical decarboxylative alkenylation twice in each case. These examples further highlight the robustness of the method, which exhibited broad functional group tolerance—including epoxides, alkynes, unprotected alcohols, and carboxylic acids.

To assess the generality of this strategy, the group extended its application to a wider range of terpenoid targets. In particular, they accomplished the first chemical synthesis of ambliol A (**542**), a natural product originally isolated from the sponge *Dysidea amblia*, by cross-coupling an epoxy acid **543** with alkenyl iodide **544**, followed by reductive epoxide opening (Scheme 63(E)). Further examples—including the synthesis of polyene terpenoids **546**–**552** (Scheme 63(F))—demonstrate the remarkable flexibility of this electrocatalytic decarboxylative

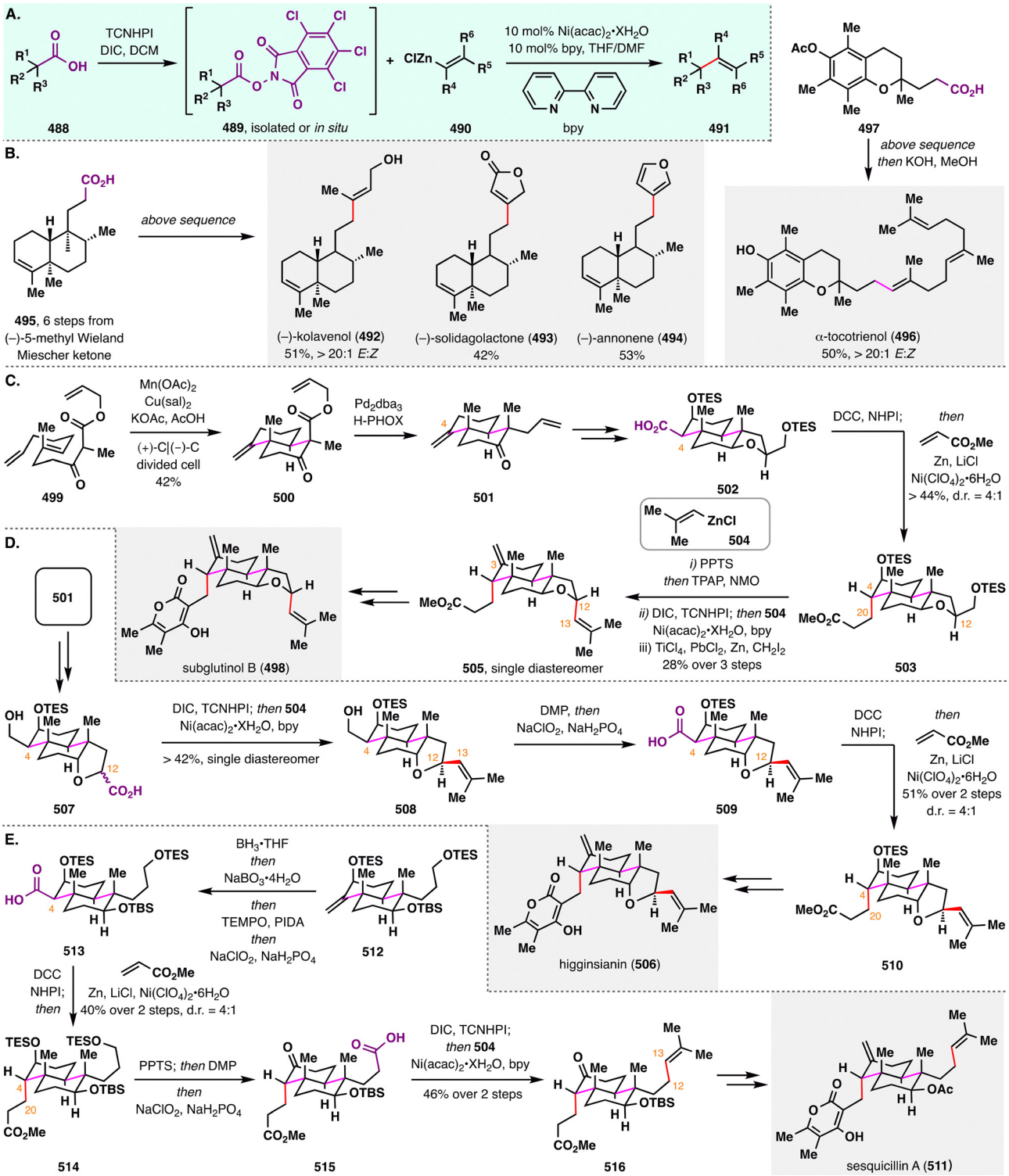

Scheme 62 Baran's decarboxylative alkenylation and their applications in terpenoid synthesis.

platform for the modular construction of complex terpenoid scaffolds.

Building on the success of their electrocatalytic decarboxylative platform for modular terpene synthesis, Baran and co-workers expanded its application to a more synthetically demanding target—(+)-calcipotriol (**553**),[241] a clinically relevant secosteroid and structural analog of vitamin D. This class of molecules, widely recognized for their broad-spectrum biological activities, has long served as a privileged framework in therapeutic development.[242] Guided by their radical-based retrosynthetic logic, the team designed a route that strategically combined electrochemical reductive alkenylation with an intramolecular BROC radical

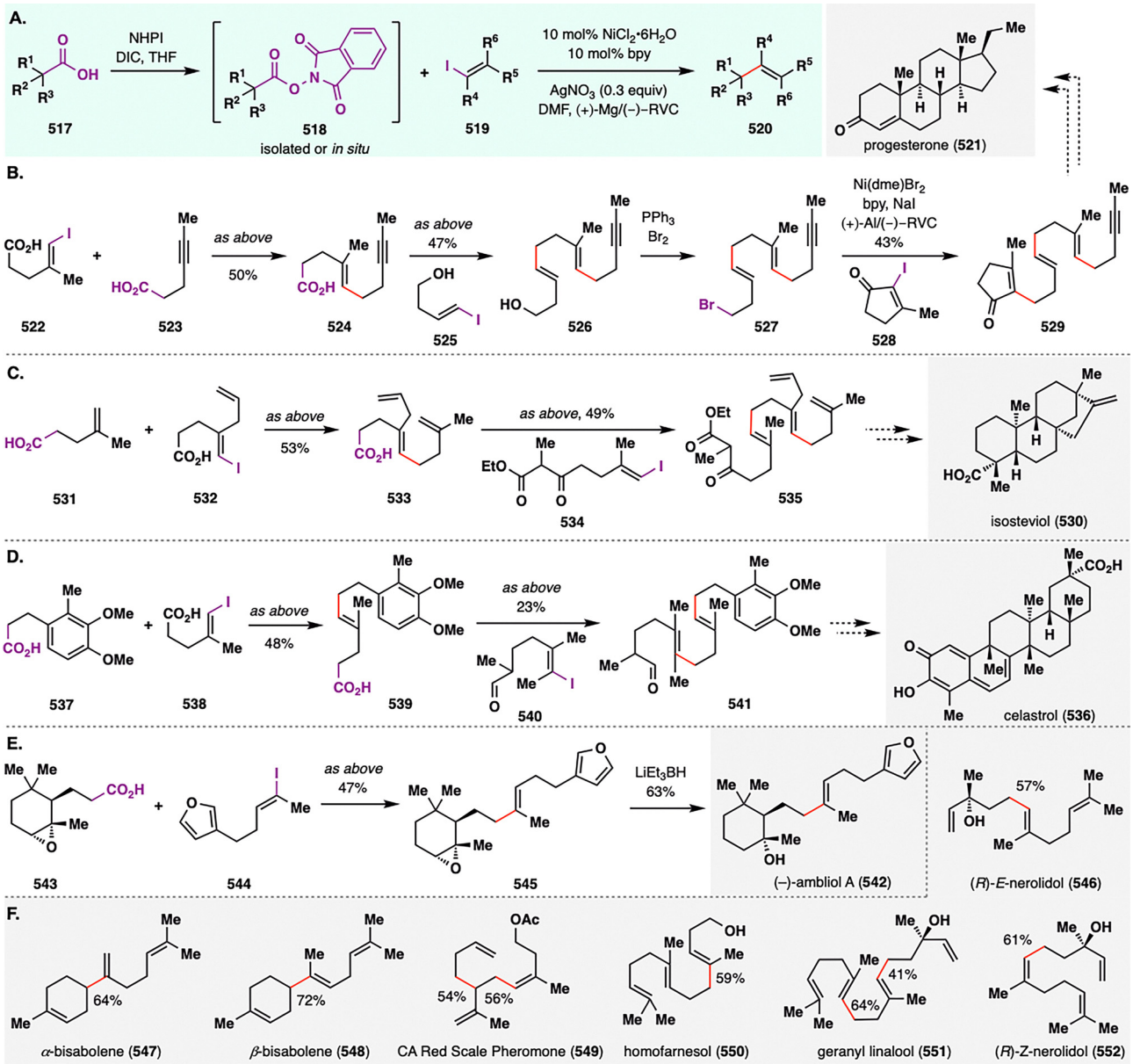

Scheme 63 Baran's modular terpene synthesis.

cyclization. As illustrated in Scheme 64, the key carboxylic acid **555** was synthesized from readily available cyclohexenone (**554**) and subjected to their electrocatalytic decarboxylative alkenylation with alkenyl iodide **556**.[235] This transformation efficiently forged a critical C(sp^2)–C(sp^3) bond, installing an α,β-unsaturated ester motif and furnishing intermediate **557** in 63% yield—while simultaneously embedding the radical handle for the forthcoming BROC radical cyclization.

The thermodynamically disfavored *trans*-6/5 ring system **559** was then constructed through a BROC reaction followed by a semipinacol rearrangement. Coupling **559** with alkyne **560** and converting the C20 ester into a RAE set the stage for a second decarboxylative alkenylation with **562** to afford **563**. Although this transformation exhibited modest diastereoselectivity (d.r. = 1:1), subsequent hydrogenation of the alkyne and global deprotection of the TBS group successfully delivered (+)-calcipotriol (**553**). This synthesis exemplifies the power of integrating sequential decarboxylative radical couplings with innovative radical cyclization strategies to streamline access to architecturally complex and pharmacologically relevant secosteroids.

Building upon the demonstrated versatility of their electrocatalytic reductive decarboxylative platform, Baran and coworkers further highlighted its synthetic utility in the concise total synthesis of the marine diterpenoid (−)-bipinnatin J (**564**),[243] employing sequential decarboxylative couplings using succinate as a linchpin for modular C–C bond formation (Scheme 65). A central feature of this synthesis was the strategic use of a succinate unit as a two-carbon ethylene bridge to unite sp^2-hybridized fragments with high efficiency. The sequence began with commercially available monomethyl succinate (**565**),

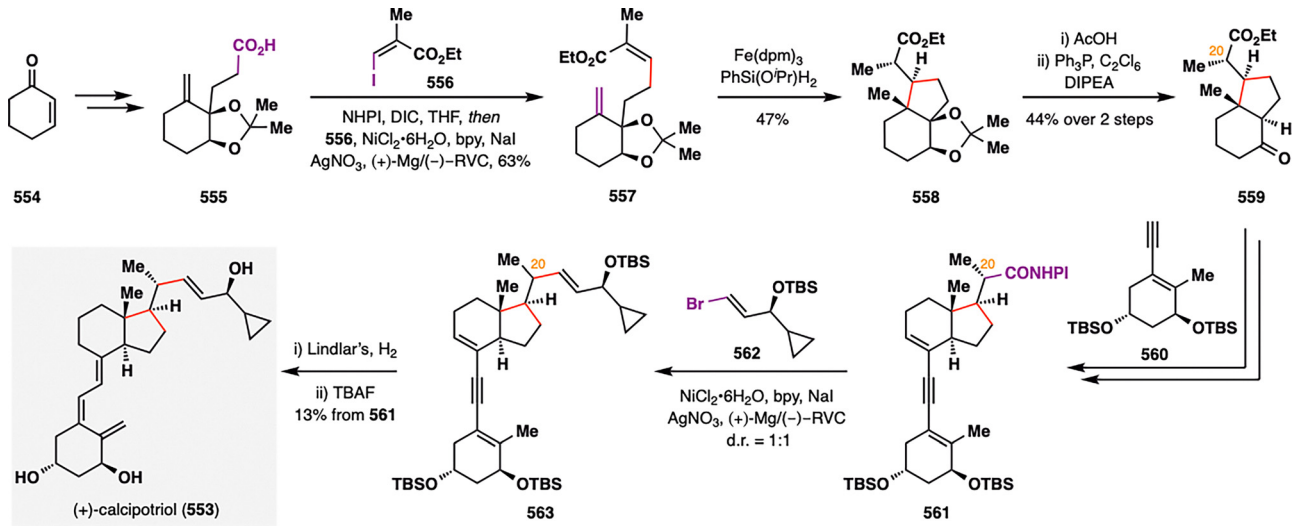

Scheme 64 Baran's total synthesis of (+)-calcipotriol (**553**).

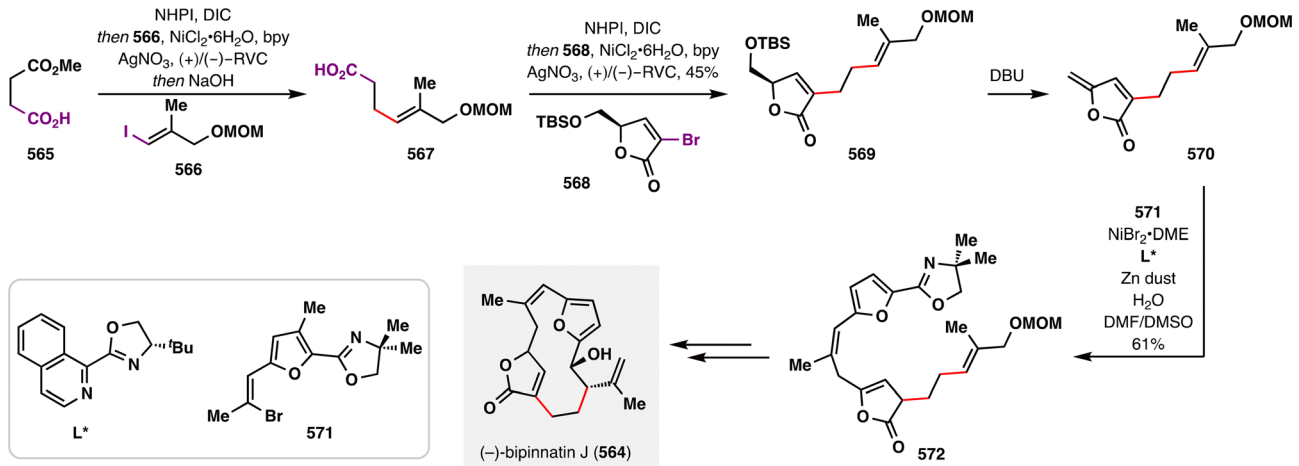

Scheme 65 Baran's total synthesis of (−)-bipinnatin J (**564**).

which underwent electrochemical decarboxylative alkenylation with alkenyl iodide **566**. Subsequent hydrolysis delivered carboxylic acid **567**. A second decarboxylative coupling—this time with alkenyl bromide **568**—furnished butanolide intermediate **569**, effectively stitching together the two alkenyl fragments through the succinate-derived ethylene linker. Finally, a Ni(II)/Zn-mediated 1,6-conjugate addition using J. Zhou's protocol introduced the furan unit in a convergent fashion,[244] enabling late-stage elaboration to the natural product (−)-bipinnatin J (**564**).

Recently, the Tomanik group accomplished a convergent and stereoselective total synthesis of the nominal structure of (+)-talaromyolide D (Scheme 66).[245] Their strategy pivoted on a stereoretentive, nickel-catalyzed electrochemical decarboxylative cross-coupling between sp^2 and sp^3 carbons, complemented by strategic C–H functionalizations. The synthesis commenced with the preparation of the *cis*-substituted cyclobutane building block **575** from (−)-verbenone in three steps: oxidative cleavage of the alkene followed by Baeyer–Villiger oxidation with *m*-CPBA furnished the key intermediate, whose derived carboxylic acid was subsequently converted to the redox-active NHPI ester **575**. A pivotal decarboxylative cross-coupling between **575** and vinyl iodide **576**, under Baran's nickel–electrocatalytic conditions using silver nanoparticle-modified electrodes, afforded the **577** in 85% yield with 11:1 dr. An aromatic moiety was then installed at C14 *via* an oxime-directed C(sp^3)–H arylation; subsequent removal of the directing group and Wittig olefination delivered alkene **578**. This alkene underwent diastereoselective iron-catalyzed Mukaiyama-type hydration, and the resulting tertiary alcohol participated in an intramolecular S_NAr reaction with a pendant aryl fluoride to construct the C-ring, yielding **579** in 80% over two steps. Finally, two late-stage carboxylic-acid-directed C(sp^2)–H oxidations installed the isocoumarin lactone, thereby completing the synthesis of talaromyolide D.

While previous C(sp^2)–C(sp^3) decarboxylative coupling strategies have primarily relied on organozinc reagents or alkenyl halides as coupling partners, Gui and co-workers expanded the scope of this methodology by employing organoboron reagents—originally

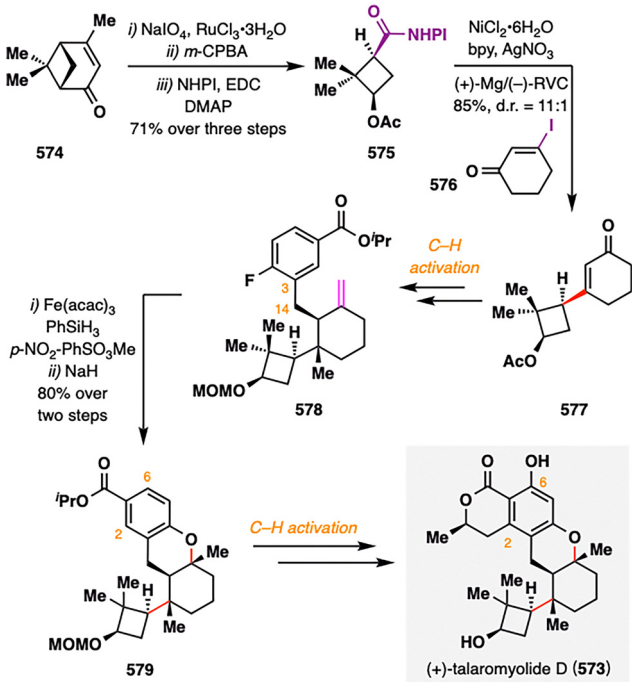

Scheme 66 Tomanik's total synthesis of talaromyolide D (**573**).

developed for such transformations by the Baran group—in the first total synthesis of myrmenaphthol A (**580**),[246,247] a structurally unique phenolic steroid featuring a naphthyl-fused A/B ring system (Scheme 67). The synthesis began with sitolactone (**581**), which was converted into the corresponding carboxylic acid *via* a one-pot lactone hydrolysis followed by Jones oxidation. Subsequent condensation with *N*-hydroxytetrachlorophthalimide furnished RAE **582**, setting the stage for a Baran's Ni-catalyzed decarboxylative cross-coupling with boronic acid **583**. This strategy again demonstrated its efficacy for constructing C(sp^2)–C(sp^3) bonds, affording tricyclic intermediate **584** in 60% yield. A sequence of downstream elaborations—including a key Friedel–Crafts cyclization/olefin isomerization/oxidative aromatization cascade—culminated in a concise 10-step total synthesis of myrmenaphthol A (**580**).

Inspired by Baran's pioneering work on decarboxylative alkenylation, our group developed a tandem decarboxylative

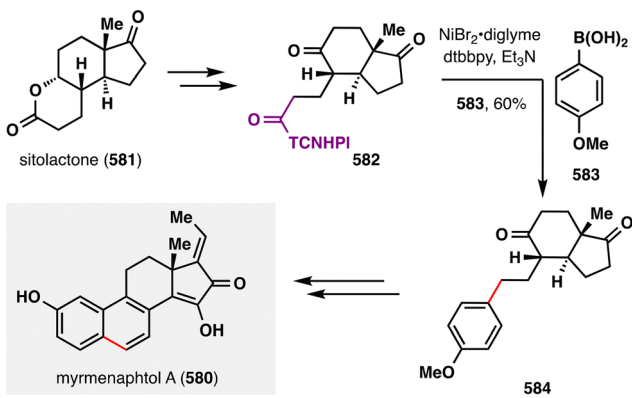

Scheme 67 Gui's total synthesis of myrmenaphthol A (**580**).

cyclization/alkenylation strategy that enabled the divergent total synthesis of (+)-effusin (**585**), (+)-longirabdolactone (**586**), and (+)-longirabdiol (**587**), three highly oxygenated spiro-lactone type *ent*-kauranoids (Scheme 68).[248] Notably, we employed a modified decarboxylative cross-coupling protocol originally developed by Weix and Reisman,[249,250] utilizing RAEs and C(sp^2)-haloalkenes as coupling partners. In contrast to Baran's approach, which employed alkenylzinc reagents and often led to undesired direct alkenylation at C6 due to the high reactivity of the organozinc species,[233] our protocol minimized such side reactions and improved site-selectivity. Key to the success of this transformation was the use of $CuCl_2$ as the catalyst, Davephos as ligand, and 2-bromopropionic acid as an additive, which significantly enhanced the coupling efficiency. Under these conditions, the desired vicinal alkene **590** was obtained as a diastereomeric mixture (d.r. = 4.2:1) in 60% yield. Subsequent elaboration furnished monocyclic carboxylic acid **591**, which then underwent a reductive decarboxylative Giese-type radical addition with an acrylate, installing the all-carbon quaternary stereocenter at C10. This transformation set the stage for divergent synthesis of the spiro-lactone *ent*-kauranoid core, culminating in the successful preparation of (+)-effusin (**585**), (+)-longirabdolactone (**586**), and (+)-longirabdiol (**587**).

In contrast to the previously discussed Ni-catalyzed decarboxylative cross-coupling strategies involving RAEs and alkenylzinc, alkenyl halide, or boronic acid coupling partners, Magauer and co-workers developed a tandem photochemical decarboxylation/Friedel–Crafts cyclization that elegantly incorporates a RPCO event for the efficient construction of the tetralone scaffold in lingzhiol (**593**)—a meroterpenoid natural product isolated from *Ganoderma* fungi, distinguished by its 1,2,4-trisubstituted aromatic ring and polycyclic terpenoid core (Scheme 69).[251,252]

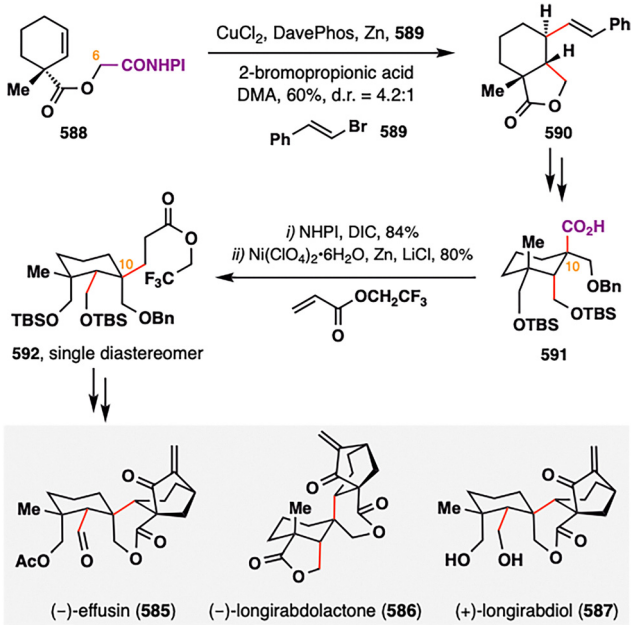

Scheme 68 C. Li's total synthesis of (+)-effusin (**585**), (+)-longirabdolactone (**586**), and (+)-longirabdiol (**587**).

In this transformation, RAE **596** underwent a photoinduced single-electron reduction by an excited-state Ir(III)* complex, generating stabilized tertiary radical **598** after extruding CO_2. Subsequent single-electron oxidation by Ir(IV) produced the corresponding tertiary carbocation **599**—thereby completing the RPCO sequence. This carbocation was then rapidly trapped by a tethered electron-rich arene *via* an intramolecular Friedel–Crafts cyclization, furnishing tetralone intermediate **600**. A critical aspect of this strategy involved strategic protection of phenolic hydroxyl groups to prevent undesired overoxidation of the electron-rich aromatic ring during the RPCO step. Final global deprotection of **600** delivered lingzhiol (**593**) in a concise and convergent fashion, highlighting the utility of RPCO-based radical strategies in the efficient assembly of complex meroterpenoid architectures.

4. Organohalides as radical precursors: versatile handles for terpenoid assembly

The utilization of organohalides as radical precursors embodies a classically rooted yet dynamically evolving strategy in synthetic organic chemistry. The homolytic cleavage of carbon–halogen bonds, a foundational mechanism for generating carbon-centered radicals, has historically underpinned diverse bond-forming reactions through its operational simplicity and broad applicability. Over the past decade, methodological breakthroughs—spanning metal-catalyzed systems,[253] photoredox platforms,[9,254] and catalyst-free protocols[255]—have substantially augmented the functional group compatibility, regioselectivity, and environmental sustainability of dehalogenative transformations. These advances have reinvigorated the strategic value of organohalide-derived radicals in addressing synthetic challenges posed by structurally intricate molecules. Within the framework of terpenoid natural product synthesis,three organohalide-enabled radical strategies have garnered significant attention in contemporary methodologies: dehalogenative XEC,[10,256] visible-light-induced dehalogenative radical addition,[9] and dehalogenative cross-coupling.[257]

From a retrosynthetic perspective (Scheme 70), the construction of a $C(sp^3)$–$C(sp^2)$ bond can be traced to its precursors *via* dehalogenative XEC reactions, disconnecting to an alkyl halide and an aryl or vinyl halide. Alternatively, this bond formation may be retrosynthetically envisioned through dehalogenative cross-coupling, derived from an alkyl halide (serving as the radical precursor) and an organometallic coupling partner (such as organotin reagents). Similarly, the formation of a $C(sp^3)$–$C(sp^2)$ bond can be retrosynthetically analyzed through radical addition pathways, retracing to an alkyl halide and an alkene (typically an electron-deficient olefin). Note that this retrosynthetic analysis is grounded in the current application of organohalides as radical precursors within the context of reported terpenoid natural product synthesis. We anticipate that the recent emerging novel synthetic methodologies leveraging organohalides as radical sources, particularly the asymmetric

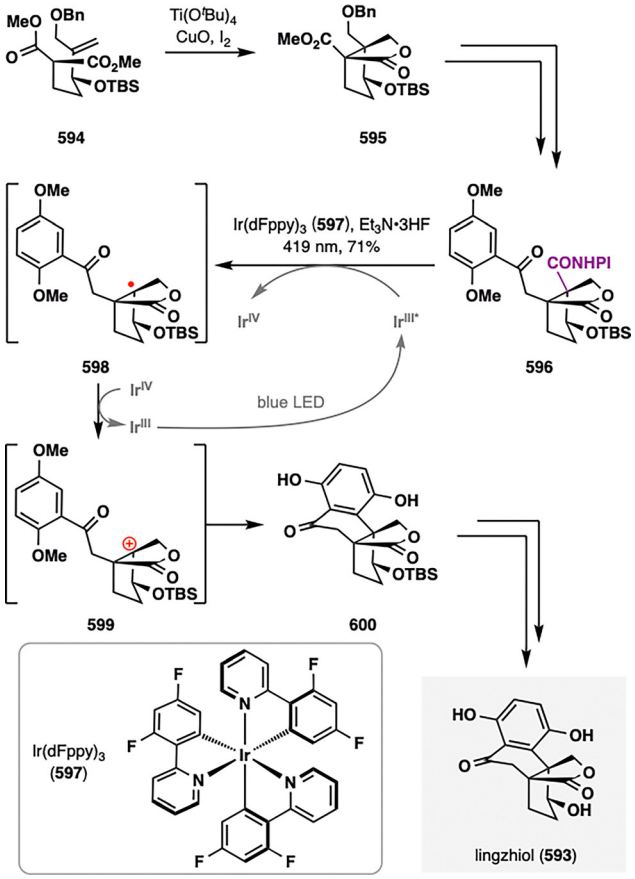

Scheme 69 Magauer's total synthesis of lingzhiol (**593**).

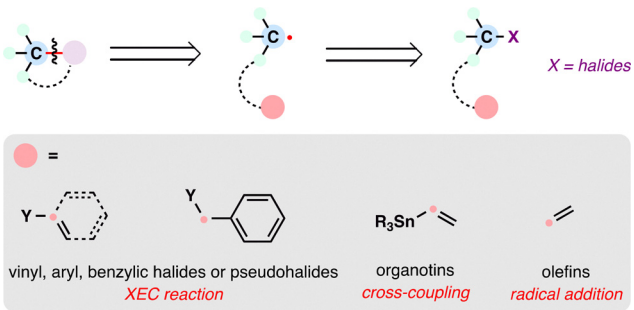

Scheme 70 Modern radical retrosynthesis of C–C bonds from organohalides.

dehalogenative cross-couping,[257] will find increasingly fruitful applications in the efficient construction of complex terpenoid architectures.

4.1. Dehalogenative cross-electrophile coupling (XEC)

Dehalogenative XEC—a strategy enabling the direct union of two electrophiles through single electron transfer (SET) pathways—has redefined $C(sp^2)$–$C(sp^3)$ bond construction in complex molecule synthesis.[10] Pioneered by Périchon in the 1990s *via* electrochemical reductive cross-couplings,[258] this methodology was later advanced by Weix,[259] Gong,[260] Reisman[261] *et al.* through transition-metal catalysis (*e.g.*, Ni, Co), which bypasses the need

for preparing organometallic reagents. XEC facilitates the direct coupling of two electrophilic components *via* SET pathways, exhibiting unparalleled tolerance toward diverse functional groups, including alcohols and carbonyls—features that are indispensable for manipulating multifunctional terpenoid intermediates. By leveraging the innate reactivity of organohalides and avoiding stoichiometric metal reagents, XEC achieves streamlined synthetic workflows and enhanced step economy, making it particularly suited for forging polycyclic terpenoid frameworks. In current total synthesis of terpenoid natural products, XEC has been predominantly employed to forge $C(sp^2)$–$C(sp^3)$ bonds with exceptional functional group tolerance.[10]

Christmann and co-workers exemplified the synthetic power of XEC by achieving the first protecting-group-free total synthesis of the cytotoxic diterpenoid alkaloids vitepyrroloids A (**601**, IC_{50} = 8.7 μM) and B (**602**),[262] isolated from the dried leaves of *Vitex trifolia L.*[263] As shown in Scheme 71, the key transformation was a Ni(II)/Zn-mediated dehalogenative XEC between alkyl iodide **603**—readily prepared from sclareolide (**184**)—and pyrrole bromide **604**. Mechanistically, the process is proposed initiated by the reduction of Ni(II) to low-valent Ni(0) by zinc. The alkyl iodide **603** undergoes SET with Ni(0) to generate a carbon-centered radical, while the aryl halide **604** undergoes oxidative addition to Ni(0), forming an aryl–Ni(II) complex. Radical capture by this aryl–Ni(II) species forms a high-valent Ni(III) intermediate, which undergoes reductive elimination to forge the $C(sp^3)$–$C(sp^2)$ bond, thereby delivering vitepyrroloid A (**601**). Importantly, the inclusion of NaI was found to effectively suppress undesired homocoupling side products by modulating the halide speciation. It is worth noting that multiple mechanistic pathways have been proposed for XEC reactions, and the exact mechanism may vary depending on the nature of the substrates and ligands involved.[10] From this intermediate, vitepyrroloid B (**602**) was obtained in 79% yield *via* a straightforward S_N2 displacement with a brominated ester, completing the efficient and concise synthesis of both natural products.

Similarly, Burtoloso and co-workers harnessed a dehalogenative XEC strategy to achieve concise total synthesis of the icetaxane diterpenoids (±)-brussonol (**605**) and (±)-komaroviquinone (**606**),[264] featuring a densely functionalized fused 6/7/6 tricyclic scaffold, in only six and eight steps, respectively (Scheme 72). A key aspect of their approach was the *in situ* generation of alkyl iodide **609** through NaI-mediated epoxide opening of **607**, enabling the subsequent XEC with arylbromide **608**. This approach exhibited excellent functional group tolerance—including compatibility with sensitive aldehyde moieties—and enabled the convergent union of two complex fragments to forge bycyclic **610**, setting stage for further manipulations to furnish (±)-brussonol (**605**) and (±)-komaroviquinone (**606**).

As previously discussed in Section 2.1.1 (Scheme 7), Renata and co-workers employed a strategically designed sequence combining chemoenzymatic oxidation with BROC to construct the key tricyclic intermediate **50**, which served as a versatile branching point *en route* to taondiol (**43**), and chevalone A (**44**).[90] As shown in Scheme 73, the team subsequently adopted a nickel-catalyzed dehalogenative XEC to forge the critical $C(sp^2)$–$C(sp^3)$ bonds. This strategic pivot was driven by the failure of decarboxylative couplings between C11 RAE and either alkenyl iodide **611** or aryl iodide **613**, prompting the use of the corresponding C11 iodide **50** as a more reliable radical precursor. Under Weix's Ni-catalyzed conditions,[259] the cross-couplings proceeded efficiently, delivering the coupled products in excellent yields of 85% and 76%, respectively. Subsequent acid-catalyzed cyclizations completed the formation of the dihydropyran rings, culminating in the total synthesis of taondiol (**43**) and chevalone A (**44**).

Li, Puno, and co-workers strategically employed a protecting-group-free dehalogenative XEC to install the side chain in their concise total synthesis of (−)-isoscopariusin A (**614**),[265] an enantioenriched immunosuppressive meroditerpenoid characterized by a sterically congested 6/6/4 tricyclic carbon framework

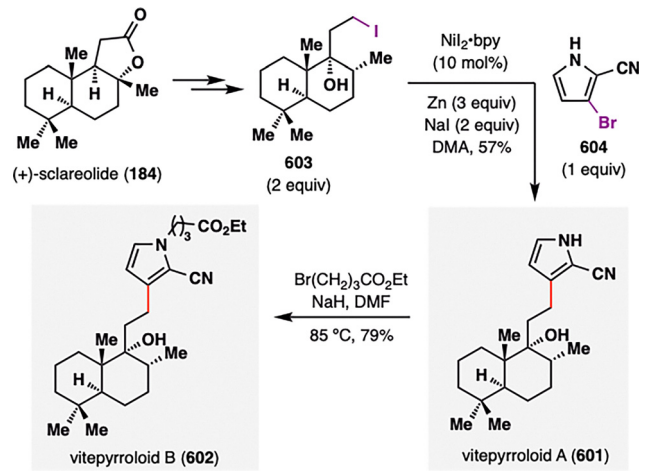

Scheme 71 Christmann's synthesis of (+)-vitepyrroloids A (**601**) and B (**602**).

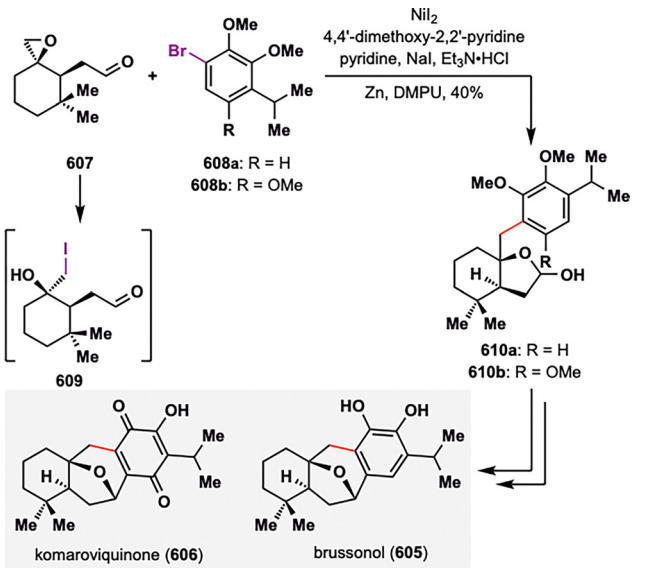

Scheme 72 Burtoloso's total synthesis of (±)-brussonol (**605**) and (±)-komaroviquinone (**606**).

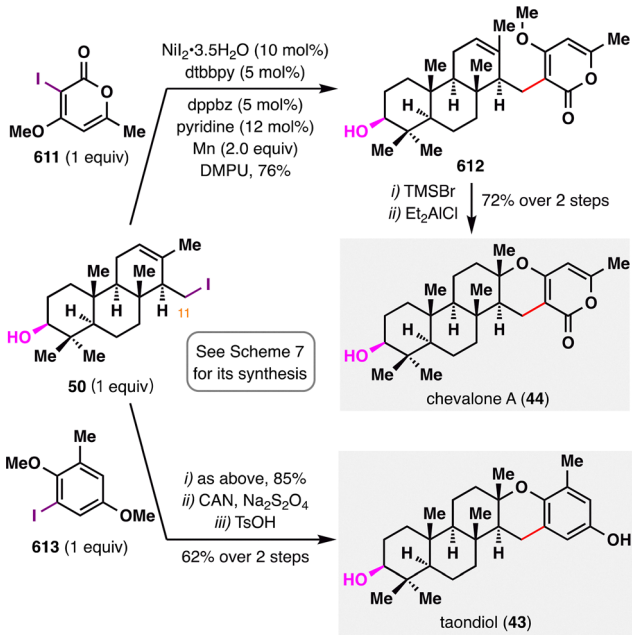

Scheme 73 Renata's synthesis of oxidized meroterpenoids taondiol (**43**) and chevalone A (**44**).

bearing seven contiguous stereocenters. As shown in Scheme 74, under Ni-catalyzed XEC conditions, functionalized alkyl bromide **615** coupled efficiently with (*E*)-3-bromobut-2-en-1-ol (**616**) under Weix's protocol,[266] enabling the regio- and stereoselective installation of the (*E*)-crotyl alcohol side chain in 68% yield. Notably, this XEC transformation exhibited excellent functional group tolerance, accommodating both free allylic alcohols and carboxylic acids without the need for protecting groups. Moreover, the reaction was readily scalable to gram quantities. Following this key cross-coupling event, a streamlined sequence of

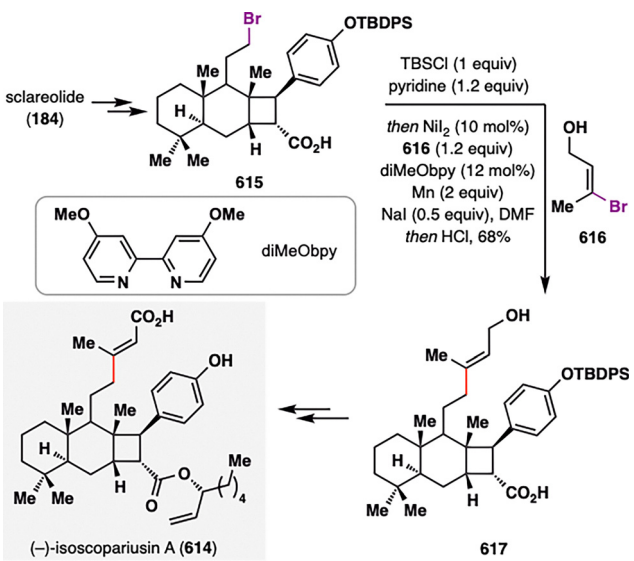

Scheme 74 Total synthesis of (–)-isoscopariusin (**614**) A by Li, Puno and co-workers.

elaborations culminated in the total synthesis of (–)-isoscopariusin A (**614**) in just 12 steps from commercially available (+)-sclareolide (**184**).

M. Yang and co-workers further showcased the remarkable utility of dehalogenative XEC in their terpenoid synthesis of *trans*-clerodanes and sesquiterpene (hydro)quinones to install different side chain with sterically hindered alkyl halides.[267] As illustrated in Scheme 75(A), a $NiBr_2$/Mn-catalyzed XEC under Shu's conditions successfully coupled sterically congested alkyl bromide **620** with oxalate ester **621** to forge a key $C(sp^3)$–$C(sp^3)$ bond,[268] yielding annonene (**618**). This terpenoid then underwent [4+2] addition with the singlet oxygen, furnishing PL3 (**619**) in 78% yield. In a related transformation (Scheme 75(B)), a XEC enabled the formation of a $C(sp^2)$–$C(sp^3)$ bond *via* coupling of alkyl iodide **624** with aryl bromide **625**, affording phenolic intermediates that were further oxidized to yield avarone-type natural products (**622–623**). The same dehalogenative arylation strategy was also employed in the synthesis of dysidavarones A–D (**627–629**, **634**), further showcasing the broad applicability of XEC for assembling diverse terpenoid and quinonoid frameworks under mild, functional-group-tolerant conditions.

Recently, Jia and co-workers stratagically combined the Ni(II)/Mn catalyzed dehalogenative XEC and Mn(III)-mediated radical tandem cyclization to achieve a protecting-group-free total synthesis of the diterpenoid (+)-aberrarone (**637**, Scheme 76),[269] a cyclohexane-angularly-fused triquinane natural product isolated from the West Indian gorgonian octocoral *Pseudopterogorgia elisabethae*.[270] Specifically, Ni-catalyzed XEC between alkyl iodide **638** and alkenyl iodide **639** proceeded efficiently in the presence of an unprotected hydroxyl group to deliver compound **640** in 68% yield. Oxidation of **640** with IBX, followed by ketone acylation, furnished enyne **641**. Then, a $Mn(OAc)_3$-mediated radical cascade cyclization forged three rings in a single operation,[271] delivering triquinane **642** in 40% yield. Further elaboration of this intermediate ultimately led to the completion of (+)-aberrarone (**637**).

Together, these studies highlight the growing impact of XEC in complex terpenoid synthesis, offering a robust and modular platform for constructing highly congested carbon frameworks under mild and operationally simple conditions, with broad compatibility for sensitive functional groups.

4.2. Visible-light-induced dehalogenative radical addition

Visible-light-induced dehalogenative radical addition represents a paradigm shift in radical-mediated bond formation, harnessing photoredox catalysis to generate carbon-centered radicals under spatiotemporally controlled and environmentally benign conditions.[9,254,272,273] Unlike traditional dehalogenative radical additions reliant on toxic initiators (*e.g.*, AIBN, $^nBu_3SnH$), Modern photoredox systems employ tunable visible-light irradiation to drive SET events, selectively reducing organohalides to radicals while bypassing hazardous byproducts.

From a retrosynthetic perspective, the bond disconnection logic for visible-light-induced dehalogenative radical addition aligns with classical dehalogenative radical addition strategies: target C–C bonds are traced to halogenated precursors and olefins. However, the photoredox platform sometimes exhibits

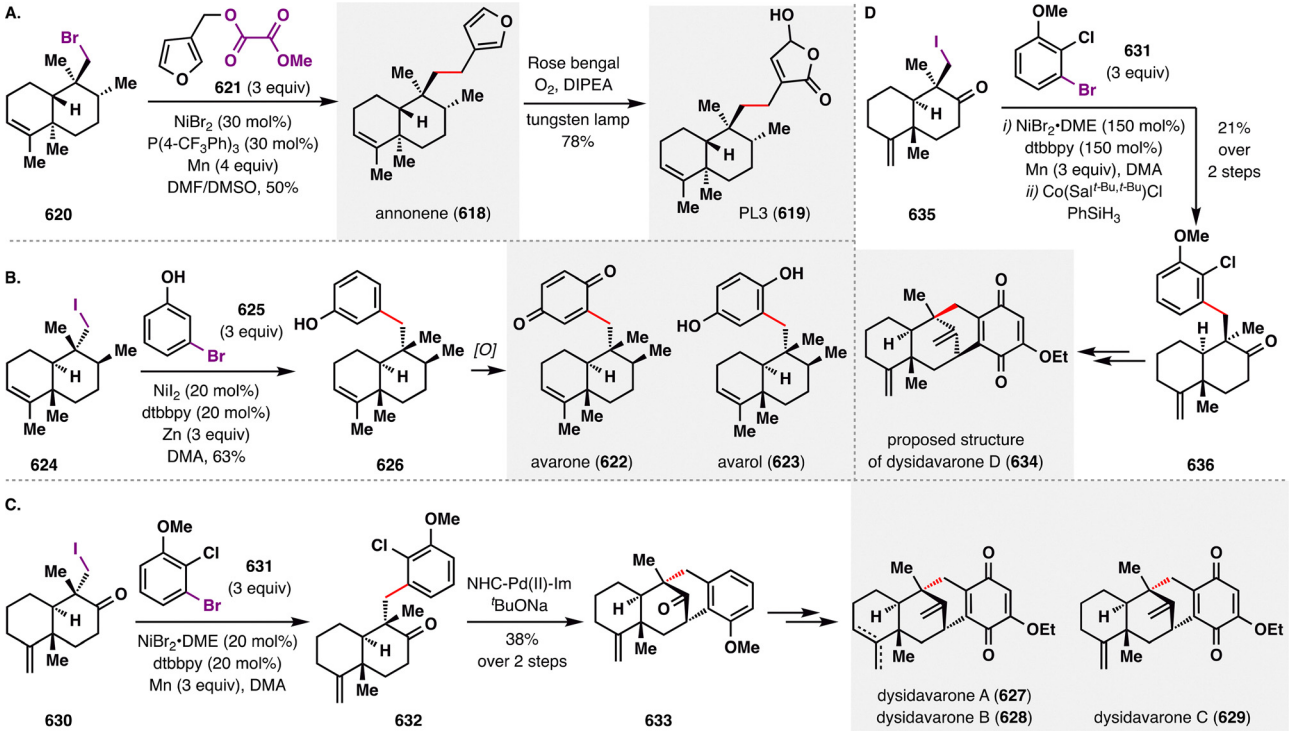

Scheme 75 Modular total synthesis of *trans*-clerodanes and sesquiterpene (hydro)quinones by Yang and co-workers.

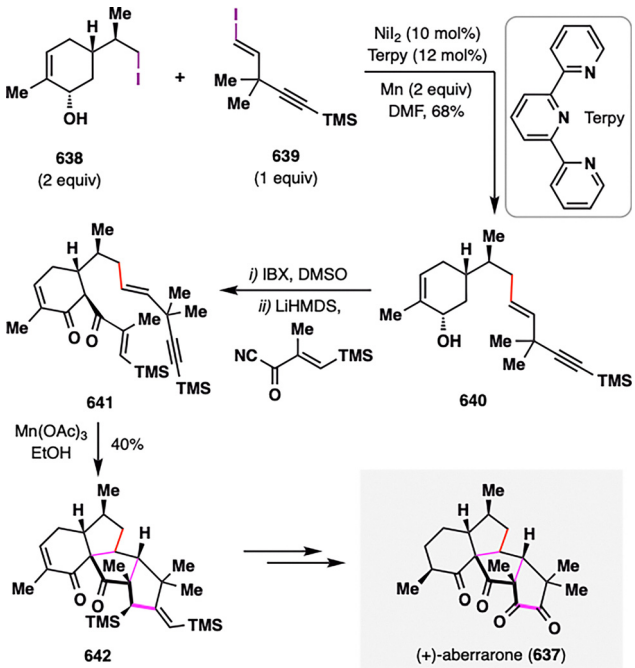

Scheme 76 Jia's total synthesis of (+)-aberrarone (**637**).

superior efficiency, as demonstrated in Yang's total synthesis of haperforin G (**643**) (Scheme 77).[274,275] Traditional methods employing azobis(isobutyronitrile) (AIBN)/^{n}Bu$_3$SnH-mediated coupling of enone **644** and alkyl iodide **645** generated the desired product in only 21–40% yield. By contrast, a photoredox system employing a catalytic iridium-based photocatalyst ([Ir(ppy)$_2$(dtbbpy)]PF$_6$ (**88**), 2.5 mol%) under blue LED irradiation, with Hantzsch ester as a mild reductant, enabled efficient activation of the unactivated C(sp^3)-hybridized iodide **645**. The generated alkyl radical underwent intermolecular stereoselective addition to enone **644**, delivering the adduct **646** as a single diastereoisomer in 64% yield. Subsequent intramolecular aldol condensation and dehydration then furnished haperforin G (**643**).

Notably, the redox-ambiphilic nature of photoredox catalysts enables unique mechanistic bifurcations. Following the initial single-electron reduction (SET) of the organohalide, the resulting carbon-centered radical may undergo a secondary SET oxidation by the now-oxidized photocatalyst—generating a carbocation and thereby opening pathways to radical-polar crossover (RPCO) transformations or tandem cationic cyclizations. This versatility significantly broadens the reactivity landscape of halogenated synthons, enabling sequential bond constructions within a single photocatalytic cycle—a powerful strategy for streamlining the assembly of structurally complex terpenoids.

As exemplified in the synthesis of norascyronone A (**647**) (Scheme 78),[276] Lou, Cheng, and co-workers developed a photoredox-mediated aryl radical addition/cyclization/oxidative RPCO/Friedel–Crafts cascade that efficiently constructs densely functionalized polycyclic frameworks using diaryliodonium salts as aryl radical precursors. Mechanistically, photoexcited Ru(bpy)$_3$Cl$_2$ reduced diaryliodonium salt **649** to generate an aryl radical, which underwent intermolecular addition to enone **648**, forming tertiary radical intermediate **650**. This intermediate cyclized intramolecularly onto the alkenyl side chain to form alkyl radical **651**, which was then oxidized by Ru(III) to generate carbocation **652**. A subsequent intramolecular Friedel–Crafts-type

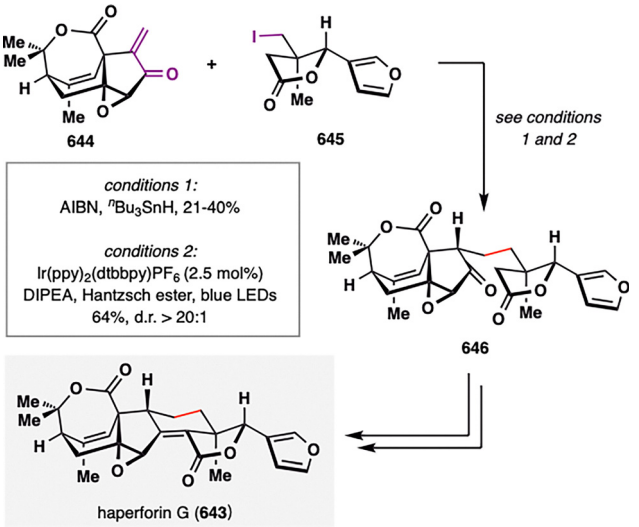

Scheme 77 Yang's total synthesis of (+)-haperforin G (**643**).

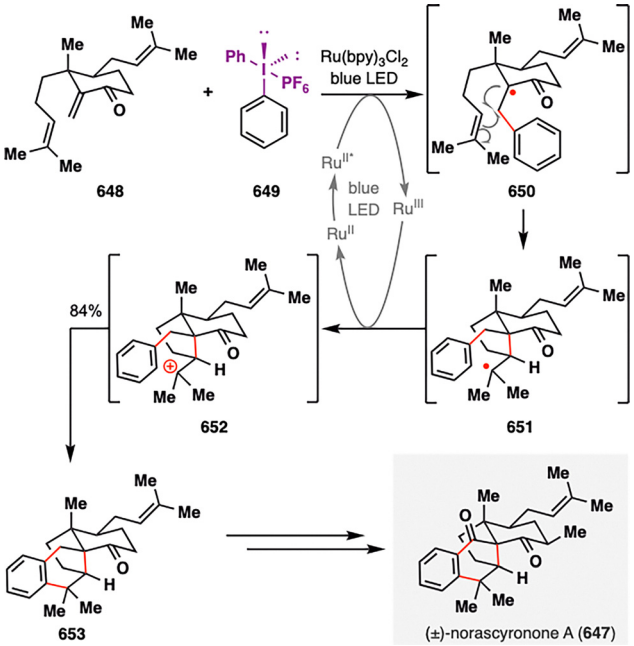

Scheme 78 Total synthesis of norascyronone A (**647**) by Lou, Cheng, and co-workers.

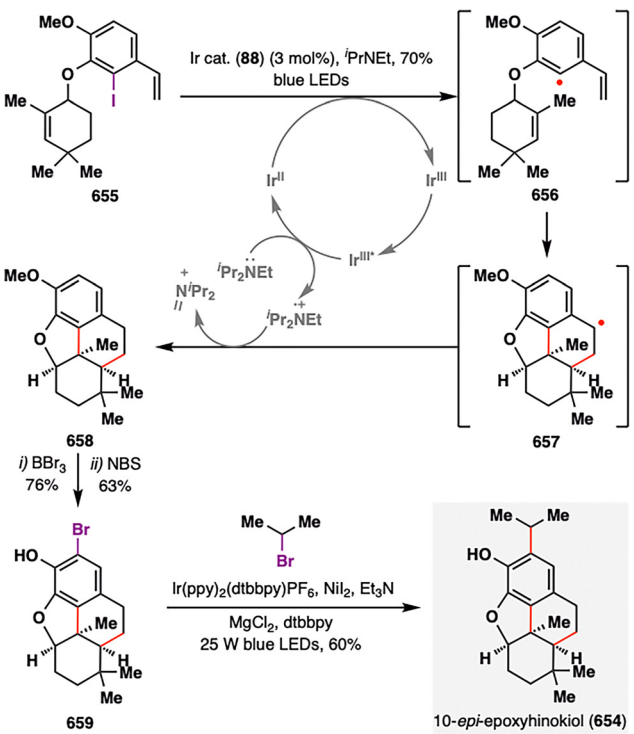

Scheme 79 Total synthesis of 10-*epi*-epoxyhinoliol (**654**) by Peng and co-workers.

reaction with a proximal arene furnished tetracyclic scaffold **653** in an optimized 84% yield. Final benzylic oxidation afforded the natural product norascyronone A (**647**).

While visible-light-induced dehalogenative radical additions are typically redox-neutral, Peng and co-workers developed a photocatalytic reductive radical cascade—employing DIPEA as a sacrificial electron donor—that features an unusual 5-*exo*-trig/6-*endo*-trig cyclization sequence (Scheme 79).[277] This transformation enabled the efficient and divergent construction of tricyclic diterpenoid frameworks, providing the first synthetic access to 10-*epi*-epoxyhinoliol (**654**), a structurally distinct abietane diterpenoid bearing a rare dihydrobenzofuran motif. The cascade was initiated by SET from Ir(II) to aryl iodide **655**, triggering C–I bond homolysis and generating aryl radical **656**. Note that Ir(II) was generated from the reduction of photoexcited Ir(III)* by DIPEA. This intermediate underwent sequential 5-*exo*-trig and 6-*endo*-trig cyclizations to form benzyl radical **657**, which was subsequently quenched by HAT from cationic radical of DIPEA. Deprotection and regioselective bromination of the aromatic ring yielded aryl bromide **659**, which then underwent a photoredox/nickel dual-catalyzed dehalogenative XEC with isopropyl bromide—using conditions developed by the MacMillan group—to deliver 10-*epi*-epoxyhinoliol (**654**) in 60% yield.

The emerging strategy of visible-light-induced dehalogenative radical addition not only overcomes long-standing challenges associated with C–C bond formation between two electrophilic partners but also enables the orchestration of cascade processes under mild and redox-economical conditions. Its growing integration into terpenoid synthesis underscores its potential as a versatile platform for forging densely functionalized carbon architectures.

4.3. Dehalogenative cross-coupling

While dehalogenative cross-coupling has yet to gain broad traction in terpenoid assembly, recent methodological advances in radical involved transition-metal-catalyzed nucleophilic substitutions—particularly those achieving enantioselective C–C bond formation *via* chiral ligand design—signal its growing relevance.[257] For instance, Ni-catalyzed asymmetric construction

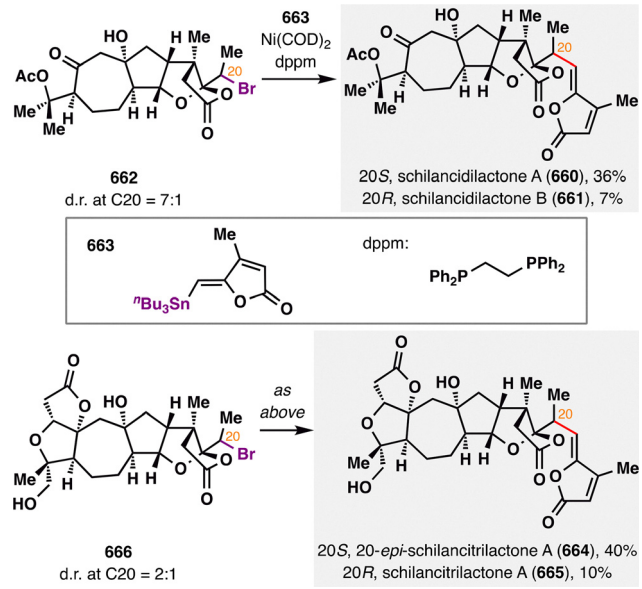

Scheme 80 Tang's total synthesis of schilancidilactones A and B (**660–661**), schilancitrilactone A (**664**), and 20-*epi*-schilancitrilactone (**665**).

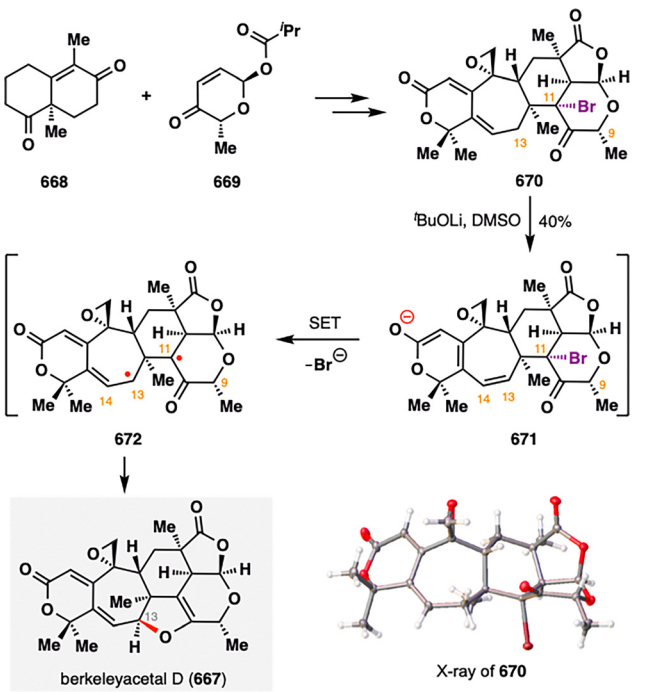

Scheme 81 C. Li's total synthesis of berkeleyacetal D (**667**).

of quaternary carbons now enable the programmed installation of chiral motifs in congested environments.[278–281] These developments, when adapted to terpenoid systems, will unlock novel disconnections for stereochemically dense terpenoids.

To date, the most illustrative application of dehalogenative cross-coupling is found in P. Tang's landmark total synthesis of schilancidilactones A (**660**) and B (**661**), 20-*epi*-schilancitrilactone (**664**), and schilancitrilactone A (**665**), as illustrated in Scheme 80.[282] At the final step, a Ni-catalyzed cross-coupling between alkyl bromide **662** and vinyl stannane **663** was employed to forge the sterically encumbered C(sp^2)–C(sp^3) bond in these schisandraceae triterpenoid architectures (**660–661**, **664–665**).[283] Notably, conventional radical conditions (AIBN and $^nBu_3SnH$) exclusively yielded hydrodebromination byproducts, underscoring the inefficacy of classical initiators in such demanding contexts. In contrast, the nickel-mediated system achieved good efficiency and exquisite functional group tolerance toward hydroxyl group and proximal acetal group, delivering the desired coupling products. This success underscores the strategy's unique capacity to access sterically hindered junctions in polyoxygenated terpenoid frameworks where traditional polar reactivity falters.

Transition-metal-catalyzed dehalogenative cross-coupling has witnessed significant advances in forging C–C bonds. Nonetheless, the development of milder, more economical, and transition-metal-free alternatives to achieve carbon–heteroatom bond constructions remains highly appealing. A striking example of such an approach emerged in our total synthesis of berkeleyacetal D (**667**)—a highly oxidized member of the DMOA-derived meroterpenoid family (Scheme 81).[284] Specifically, treatment of intermediate **670** with ^{t}BuOLi in DMSO directly furnished the key 2,3-dihydrofuran moiety of **667** in 40% yield, effectively bypassing multiple anticipated steps. Mechanistic studies propose that the transformation proceeds *via* an intramolecular SET from an *in situ*–generated trienolate **671** to the adjacent C–Br bond (highlighted in purple), a hypothesis supported by the observation of enhanced yields under photoirradiation. The resulting diradical intermediate **672** is proposed to undergo rapid intramolecular radical recombination, forging the strained dihydrofuran ring embedded within the berkeleyacetal D (**667**) framework.

5. Alcohol derivatives as radical precursors

The pervasive presence of hydroxyl functionalities across diverse molecular scaffolds makes alcohols as intrinsically appealing candidates for generating C(sp^3) radicals. However, the inherent stability conferred by the high bond dissociation energy (BDE) of the C–O bond, coupled with the poor leaving group propensity of the hydroxide (OH^-), typically precludes their direct utilization as alkylating agents in cross-coupling manifolds.[285,286] Consequently, strategic derivatization of the alcohol moiety is essential to convert this ubiquitous functional group into a viable radical precursor amenable to SET processes. Common activating groups enabling this transformation include tosylates,[287–290] mesylates,[291] oxalates,[292] and halides (this category having been discussed in the preceding section).

Among these activated species, oxalate-based derivatives have emerged as particularly prominent radical precursors in contemporary terpenoid total synthesis (Scheme 82). Their prominence arises from two distinct activation pathways utilizing different types of oxalate derivatives: (i) SET reduction of methyl oxalate esters (*e.g.*, R-OC(O)C(O)OCH_3) to generate nucleophilic alkyl radicals;[268,292] (ii) SET oxidation of oxalate salts (*e.g.*, cesium/potassium alkyl oxalates, R-OC(O)COO^-Cs^+/K^+) to yield electrophilic alkyl radicals.[293] The carbon-centered radicals generated *via*

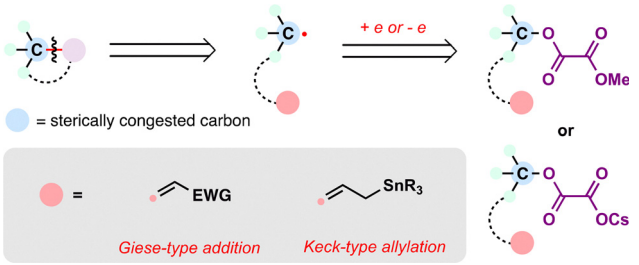

Scheme 82 Emerging radical retrosynthesis of C–C bonds employing the dehydroxylative reactions.

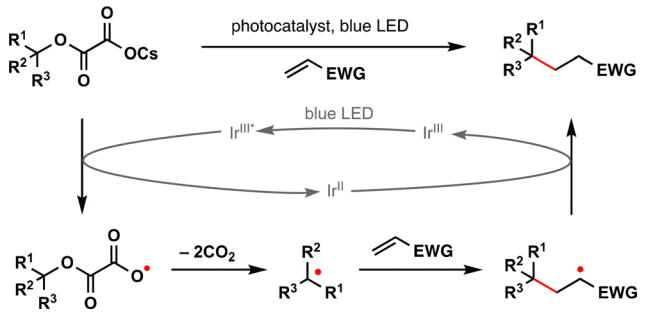

Scheme 83 Dehydroxylative Giese reaction through SET-oxidation of oxalate salts.

these pathways are efficiently captured in pivotal C–C bond-forming reactions, most notably Giese-type radical additions to electron-deficient alkenes and Keck-type radical allylations.

Critically, both reaction manifolds exhibit exceptional efficiency for constructing challenging quaternary carbon centers—a common structural motif in complex terpenoids. This synthetic prowess translates into powerful retrosynthetic disconnections: a quaternary carbon center within a target molecule can often be traced retrosynthetically to a tertiary alcohol precursor, transformed into its corresponding oxalate derivative (methyl ester or cesium/potassium salt, Scheme 82), and an appropriate coupling partner (*e.g.*, an electron-deficient alkene for the Giese pathway or an allylic acceptor for the Keck pathway). The strategic power of this approach lies in the accessibility of the tertiary alcohol precursor. Such alcohols are readily synthesized *via* nucleophilic addition to readily available ketones, significantly simplifying the retrosynthetic tree. By leveraging oxalate activation of tertiary alcohols and radical-based C–C bond formation, synthetic chemists gain a streamlined, convergent route to architecturally demanding terpenoid frameworks containing all-carbon quaternary stereocenters.

Soon after Overman, MacMillan, and co-workers introduced a redox-neutral dehydroxylative coupling strategy using alkyl oxalates as radical precursors in 2015,[293] Overman and co-workers extended this methodology to the synthesis of a diverse array of structurally complex diterpenoids (**384**, **673**, **677**, **682**, and **683** in Scheme 84). By developing stable *tert*-alkyl oxalate salts as radical progenitors, they addressed a longstanding challenge in radical chemistry—the effective utilization of tertiary alcohols in C–C bond formation—via a net redox-neutral process. Mechanistically, photoexcited Ir(III)* oxidizes the *tert*-alkyl oxalate salt, generating an alkyl oxalate radical (Scheme 83). This intermediate undergoes sequential extrusion of two molecules of CO_2 to furnish a stabilized tertiary carbon-centered radical. The resulting radical then engages in a Giese-type addition to an electron-deficient alkene, forming a new C–C bond. The resulting adduct radical is subsequently reduced by Ir(II), completing the catalytic cycle in a redox-neutral manner.

This methodological innovation enabled an enantioselective synthesis of *trans*-clerodane (**673**) *via* a highly diastereoselective photoredox-catalyzed coupling between a tertiary cesium alkyl oxalate (**675**) and an electron-deficient butenolide (**676**), simultaneously constructing the quaternary stereocenter with exceptional selectivity (d.r. > 20:1) (Scheme 84(A)).[293] The generality of the approach was further showcased in concise synthesis of (−)-macfarlandin C (**677**) and cheloviolenes A, B, and C (**384**, **682**, and **683**, Scheme 84(B) and (C)),[210,294,295] underscoring how the oxalate-based strategy, when paired with visible-light photocatalysis, offers a unified and efficient platform for accessing complex diterpenoid frameworks with high yield and stereocontrol---outcomes that were previously difficult to achieve using conventional methods.

During the peer-review process of our manuscript, Gui and co-workers reported a striking demonstration of radical retrosynthetic logic in their total synthesis of harziandione (**689**), a harziane diterpenoid isolated from *Trichoderma* species featuring a highly caged 6/5/7/4 tetracyclic framework and four contiguous stereocenters.[296,297] As illustrated in Scheme 85, the synthesis combined a BROC radical cyclization, a photocatalytic dehydroxylative Giese reaction, and an acyl radical cyclization to rapidly assemble the bridged [3.2.1] ring system and three of the four contiguous stereocenters. The sequence commenced with formation of the C13–C14 bond in **692** *via* an $Fe(acac)_3$/$Ph(^iPrO)SiH_2$-mediated BROC reaction, simultaneously establishing a prochiral quaternary center at C13 and a tertiary center at C14 in 83% yield. Installation of an oxalate group in **693** then set the stage for a photocatalytic dehydroxylative Giese reaction, which—through substrate-controlled stereocontrol (**694**)—furnished the C6 quaternary center in **695** as a single diastereomer in 54% yield. A subsequent desymmetrizing intramolecular aldol reaction under ^tBuOK established the remaining stereochemistry at C13 while constructing the strained bicyclo[5.2.0]nonene motif in **696**. This concise sequence enabled access to harziandione (**689**) in only 12 steps from commercially available intermediates **690**/**691**, underscoring the potential of radical retrosynthetic strategies for assembling complex bridged architectures.

Inspired by Gong's pioneering work on the single electron reduction of methyl oxalates,[292] our group employed a tertiary alkyl oxalate as a radical precursor to achieve the total synthesis of a series of *ent*-kaurane and beyerane-type diterpenoids (**698**–**707**),[298] featuring a strained and bridged bicyclo[3.2.1]octane core, *via* a dehydroxylative radical addition/annulation protocol (Scheme 86). This radical-based [3+2] annulation strategy enabled the efficient conversion of precursor **708** to the key intermediate **710** in synthetic useful yield. The reaction was facilitated by a $MgCl_2$/PBI/Zn reductive system, with TEMPO serving as a crucial

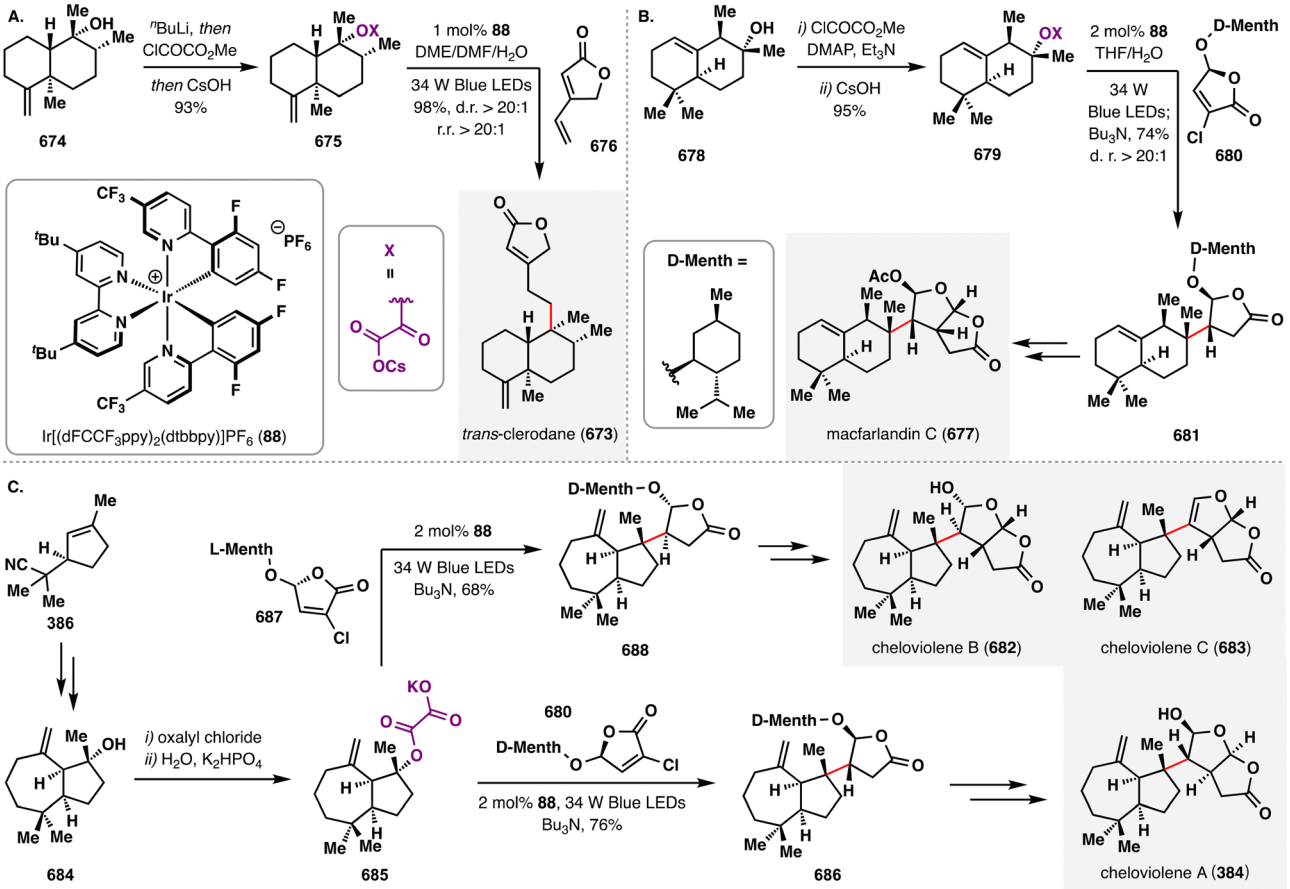

Scheme 84 Overman's total synthesis of *trans*-clerodane (**673**), macfarlandin C (**677**), and cheloviolenes (**384**, **682**, **683**).

additive; the *in situ* generation of TEMPO–H or $Zn(TEMPO)_2$ can selectively quench the secondary radical intermediate through a HAT or S_H2 process, thereby preventing uncontrolled radical addition of **713** to the acrylate. Because of the steric hindrance, the reaction of tertiary radical **712** with TEMPO–H or $Zn(TEMPO)_2$ is not favorable. With rapid access to the core skeleton secured, further elaborations enabled the divergent synthesis of both *ent*-kaurane and beyerane-type diterpenoids (**698–707**).

While previous studies have demonstrated the utility of tandem dehydroxylative Giese-type radical addition reactions, Baudoin and co-workers pursued an alternative strategy by employing a dehydroxylative Keck-type allylation to accomplish the total synthesis of (+)-randainin D (**716**) and (+)-barekoxide (**719**)—two architecturally complex diterpenoids bearing a *trans*-hydroazulenone core and a butenolide moiety (Scheme 87).[299] In their initial attempts, dehydroxylative radical addition of methyl oxalate **717** to electron-deficient olefins proved ineffective, leading primarily to undesired C8-hydrogenated by-products due to inefficient radical trapping.

To circumvent this limitation, the team adopted a Keck-type radical allylation using allylstannane **718** as the radical acceptor.[300,301] Upon single-electron reduction of **717** by photo-excited Ir(III)*, an α-ketone radical was generated. This radical was successfully intercepted by **718**, forging the sterically hindered C8 all-carbon quaternary center with high efficiency. Notably, the Ir(IV) species generated in the reduction step was reduced back to Ir(III) by the leaving group (a methyl oxalate salt), thereby completing the redox-neutral photocatalytic cycle. Following the radical allylation, DBU-mediated alkene isomerization and global deprotection with HF furnished (+)-randainin D (**716**). Encouraged by this success, the same photoredox-mediated allylation strategy was applied to install the side chain in the synthesis of (+)-barekoxide (**719**), further demonstrating the efficacy of organostannane-mediated radical allylation in constructing sterically congested quaternary stereocenters.

6. Aldehyde derivatives as radical precursors

The aldehyde functional group occupies a privileged position as a multifaceted radical precursor, enabling innovative and streamlined disconnections in complex molecule assembly. While the classical generation of nucleophilic ketyl radicals *via* single-electron reduction (most notably employing SmI_2) has found extensive historical application in total synthesis.[302–306] A major modern paradigm leverages the relatively weak aldehyde C(O)–H bond (BDE ≈ 88 kcal mol^{-1}) for direct generation of synthetically valuable ketyl radicals through efficient HAT using photoredox catalysis (*e.g.*, tetrabutylammonium decatungstate).[307,308] The

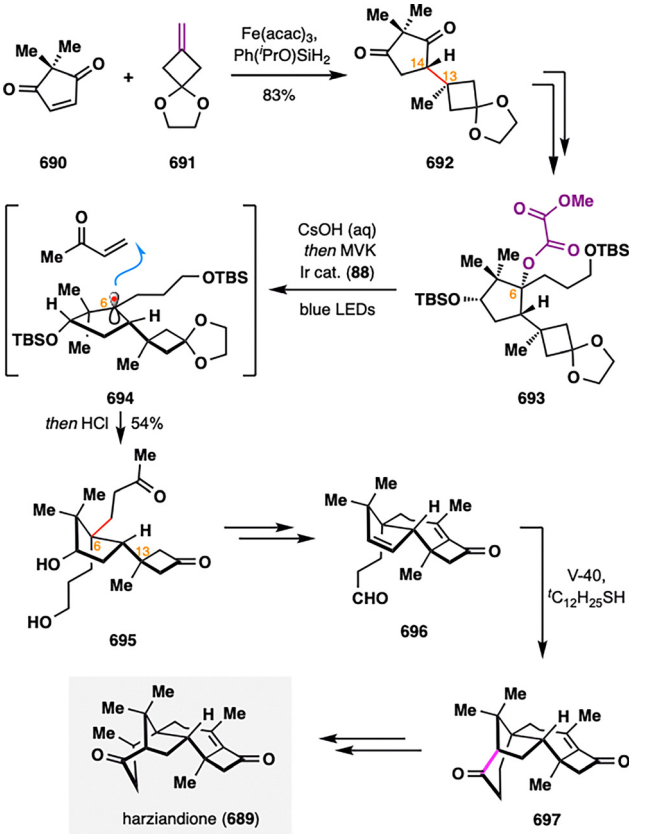

Scheme 85 Gui's total synthesis of harziandione (**689**).

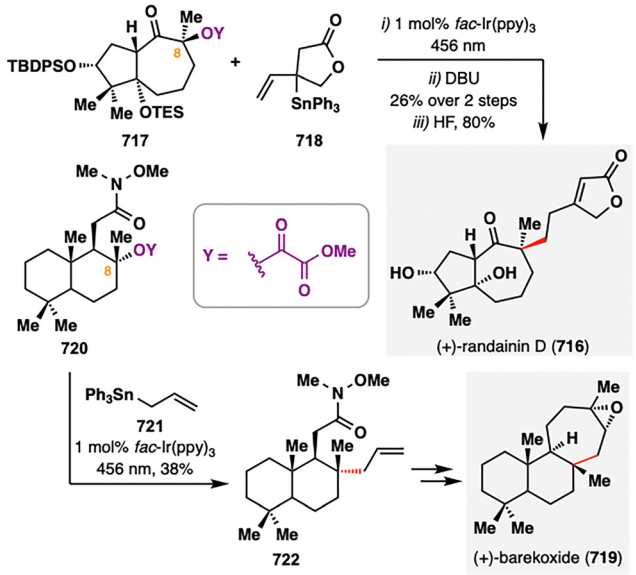

Scheme 87 Baudoin's total synthesis of (+)-randainin D (**716**) and (+)-barekoxide (**719**).

resulting ketyl radicals can be engaged in radical additions or be harnessed in metal-catalyzed cross-coupling reactions, enabling the formation of $C(sp^2)$–$C(sp^3)$ or $C(sp^2)$–$C(sp^2)$ bonds.

Complementing this approach, the strategic SOMO-activation of aldehydes represents another powerful modern tactic.[309–312] This method involves the condensation of aldehydes with secondary amines to form electron-rich enamines, which subsequently undergo single-electron oxidation—facilitated by chemical oxidants like CAN or photoredox catalysis—to generate electrophilic α-amino radical cations (SOMOphiles). These highly reactive species excel in intramolecular radical cyclizations with tethered alkenes. This reactivity provides efficient and often stereoselective routes to access challenging ring systems ubiquitous in polycyclic terpenoid

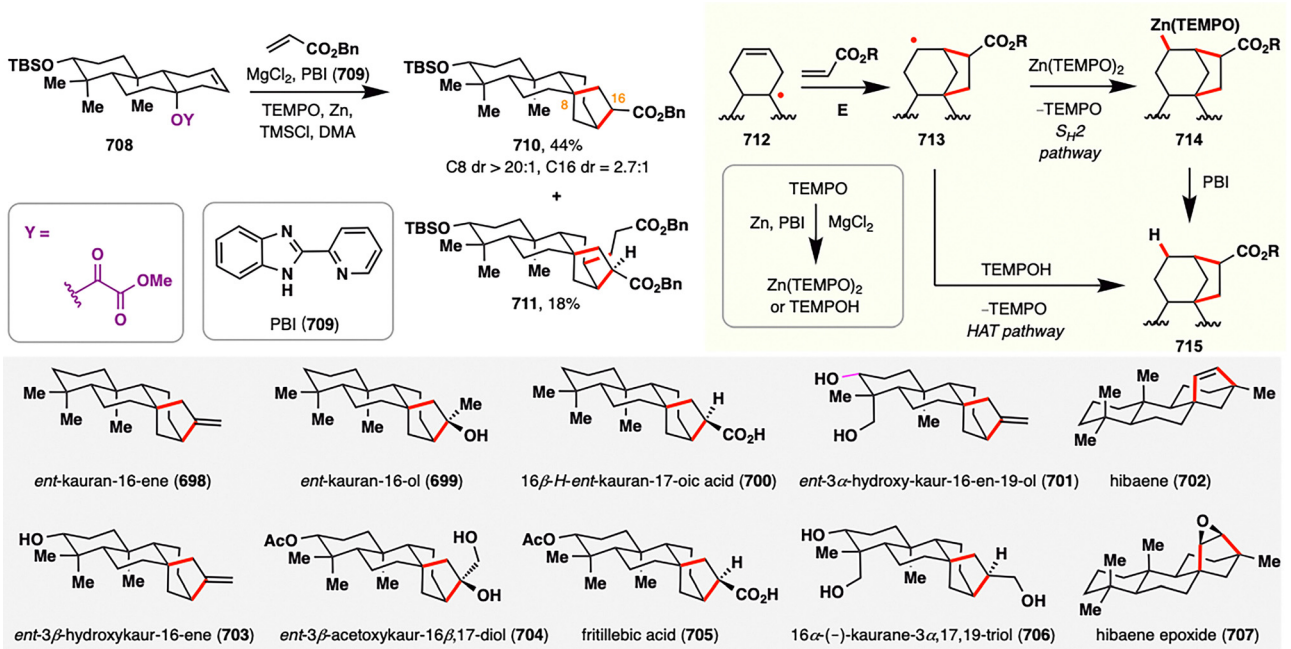

Scheme 86 C. Li's collective synthesis of tetracyclic *ent*-kauranoids (**698–707**) *via* [3+2] radical annulation.

frameworks. The development of enantioselective variants employing chiral catalysts further enhances the synthetic utility of this method for establishing critical stereocenters.

From a retrosynthetic perspective, the modern radical methodologies involving aldehydes enable powerful disconnections in terpenoid planning (Scheme 88). A ketone functionality within the target molecule can be strategically traced back to its precursors through an ketyl radical intermediate. This disconnection implies the convergent coupling of an aldehyde (serving as the ketyl radical precursor) with either an alkene (for radical addition) or an organohalide (for transition metal-catalyzed cross-coupling), effectively forging the new C–C bond *via* the pathways previously described. Furthermore, when the carbon atom α to an aldehyde group resides within a ring system—a common feature in polycyclic terpenoids—the SOMO-activation strategy offers a unique disconnection opportunity. Here, the critical insight is to cleave the C–C bond between the α and β carbons (Cα–Cβ) relative to the aldehyde. This retrosynthetic step effectively deconstructs the cyclic framework, revealing a synthetically accessible, linear or acyclic aldehyde precursor bearing a tethered alkene. The superiority of this approach depends on its power to utilize the aldehyde both as the radical precursor (*via* enamine formation and oxidation) and as the anchor point for the intramolecular radical cyclization that rebuilds the ring during the forward synthesis. This represents a particularly elegant application of radical chemistry for simplifying the synthesis of complex carbocyclic structures prevalent in terpenoid natural products.

Cross-dehydrogenative coupling (CDC) reactions have proven to be powerful tools for constructing C–C bonds directly from C–H bonds.[313] However, intermolecular CDC reactions between aldehydes and electron-deficient alkenes remain relatively underexplored—particularly in the context of complex terpene synthesis. Addressing this gap, Park, Han, and co-workers employed their self-developed Cu-catalyzed CDC platform to forge key fragment couplings in the total synthesis of elodeoidins A (**723**) and B (**724**) (Scheme 89).[314] The first CDC transformation utilized tetrabutylammonium decatungstate

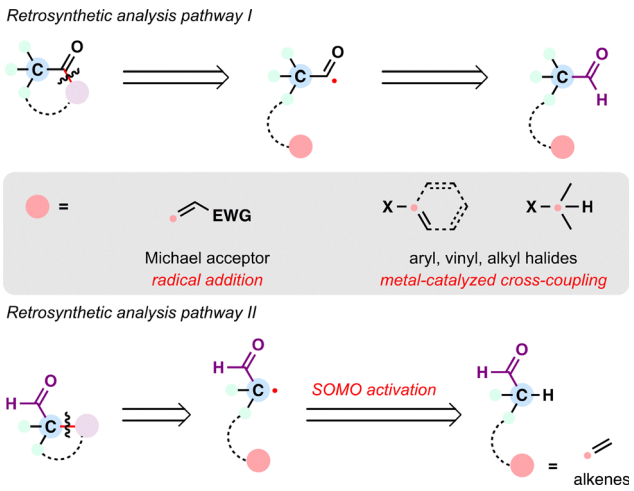

Scheme 88 Modern radical retrosynthesis of C–C bonds from aldehydes.

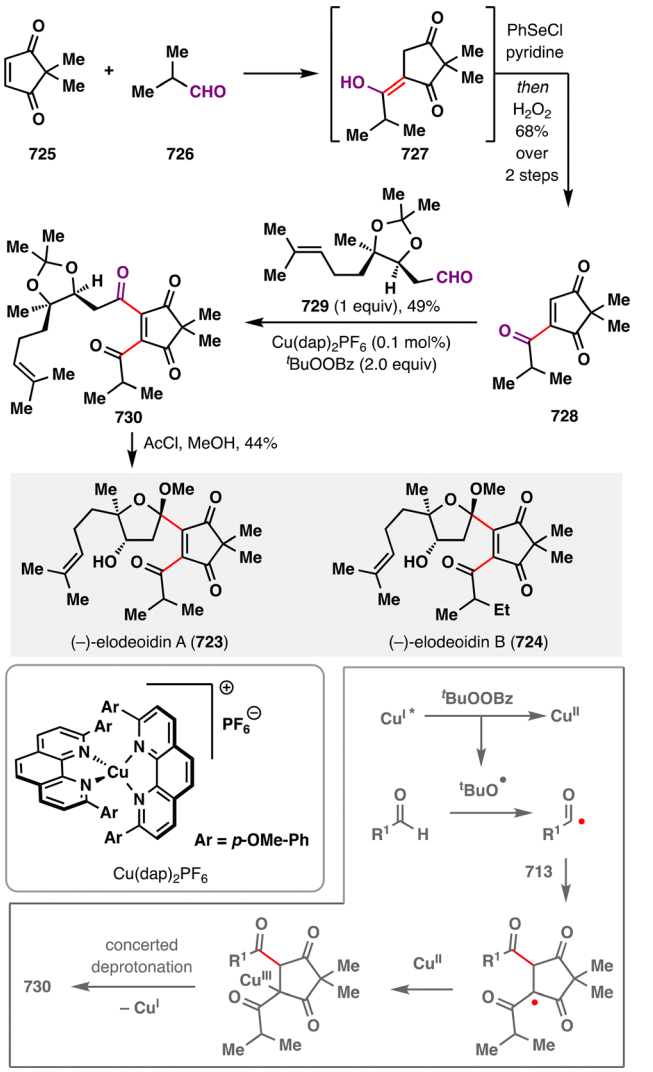

Scheme 89 Total synthesis of (–)-elodeoidins A and B (**723–724**) by Park, Han and co-workers.

(TBADT) as a photocatalyst under 370 nm irradiation to generate conjugated enol intermediate **727** *via* direct coupling of enedione **725** and isobutyraldehyde **726**,[315,316] followed by a selenylation/oxidation sequence to yield enetrione **728** in 68% over two steps. Mechanistically, photoexcited TBADT initiated HAT from aldehyde **726**, generating a ketyl radical that underwent Giese-type radical addition to enedione **725**. Subsequent back-HAT from TBADTH to the resulting radical intermediate enabled catalytic turnover under mild, redox-neutral conditions—well suited for complex molecular settings. Besides, the second CDC event featured a $Cu(dap)_2PF_6$-mediated acylation that formed a key C–C bond in 49% yield. This transformation proceed *via* photoexcitation of $[Cu(I)(dap)_2]^*$, which reduces TBPB to form a *tert*-butoxyl radical. The latter abstracts a hydrogen atom from acetaldehyde **729**, generating a ketyl radical that undergoes a Giese-type addition to enetrione **728**. A subsequent concerted deprotonation furnishes intermediate **730** and regenerates the Cu(i) catalyst. Final treatment with AcCl/MeOH furnished elodeoidins A (**723**) and B (**724**).

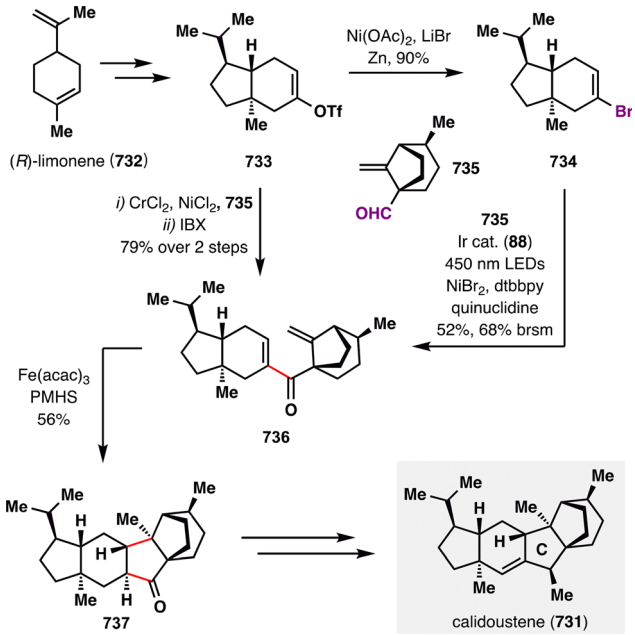

Scheme 90 Total synthesis of (−)-calidoustene (**731**) by Chen, Wang and co-workers.

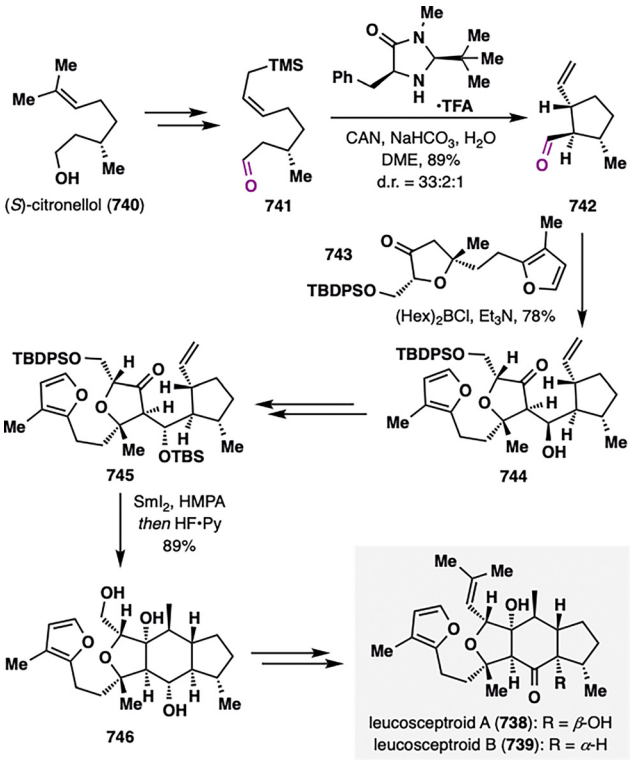

Scheme 91 D. Ma's total synthesis of leucosceptroids A and B (**738–739**).

A similar strategy involving ketyl radical generation from aldehydes was strategically employed by Chen, Wang, and co-workers in their inaugural total synthesis of the complex sesterterpenoid (−)-calidoustene (**731**) (Scheme 90).[317] The key challenge—construction of the sterically congested C-ring—was addressed through a dual-strategy approach. Initially, a traditional NHK coupling of **733** with **735** followed by IBX oxidation of the resulting alcohol provided the dienone intermediate **736** in 79% yield over two steps. However, this route suffered from competitive dimerization side reactions. To overcome this limitation, the team first utilized Reisman's bromination protocol mediated by LiBr/Ni catalysis to afford the corresponding alkenyl bromide in 90% yield.[318] Next, using a metallaphotoredox method developed by MacMillan was implemented, giving the same product **736** with improved selectivity (52% isolated yield, 68% brsm).[319] Mechanistically, photoexcited Ir(III)* oxidize quinuclidine to generate a N-radical cation, which selectively abstract the formyl hydrogen from aldehyde **735** *via* HAT, generating a ketyl radical. This radical is intercepted by a Ni(II) complex formed *via* oxidative addition of Ni(0) to alkenyl bromide **734**, yielding an alkenyl–Ni(III) intermediate that undergo reductive elimination to furnish the desired coupling product **736** in 58% yield. Subsequent transformations, including an anti-Baldwin BROC cyclization, completed the ring closure and finalized the total synthesis of (−)-calidoustene (**731**).

Another milestone in aldehyde activation was MacMillan's development of SOMO catalysis using imidazolidinone organocatalysts. Building on this concept, Ma and co-workers accomplished the first total synthesis of leucosceptroids A (**738**) and B (**739**) through a strategically designed route featuring an enantioselective ring closure enabled by SOMO catalysis (Scheme 91).[320] Specifically, an (*S*)-citronellol-derived aldehyde **741** underwent an efficient intramolecular SOMO-catalyzed allylation, delivering the cyclized product **742** in 89% yield on gram scale with excellent diastereoselectivity (d.r. = 33:2:1). This enantioselective aldehyde–ene cyclization proceeded *via* formation of a chiral enamine intermediate, followed by single-electron oxidation to generate an electrophilic enamine radical cation. Re-face selective radical addition to the tethered olefin furnished an alkyl radical, which was further oxidized to a carbocation *via* a RPCO process. Subsequent desilylation and hydrolysis of the imidazolidinone yielded the cyclization product **742**. Further elaboration involved a highly diastereoselective aldol reaction between chiral aldehyde **743** and functionalized dihydrofuranone **744** (78% yield), followed by a pivotal SmI_2-mediated intramolecular ketyl–olefin radical cyclization efficiently constructed the complex polycyclic core **746** in 89% yield with complete stereocontrol, thereby setting the stage for late-stage modifications *en route* to leucosceptroids A (**738**) and B (**739**). In a parallel advance, S. Li and co-workers also employed an enantioselective SOMO-catalyzed cyclization of commercially available (*S*)-citronellal (**748**) with cat. **749** to afford **750**, thereby setting the stage for the total synthesis of the sesterterpenoid gracilisoid A (**747**) (Scheme 92),[321] further highlighting the utility of SOMO catalysis in assembling architecturally complex terpenoids.

Lei and co-workers achieved the total synthesis of (+)-*ent*-kauradienone (**751**) and (−)-jungermannenone C (**752**) by strategically employing a tandem SOMO-catalyzed aldehyde polycyclization (Scheme 93).[322] Treatment of precursor **753** with imidazolidinone organocatalyst *ent*-**749** and Cu(II) enabled

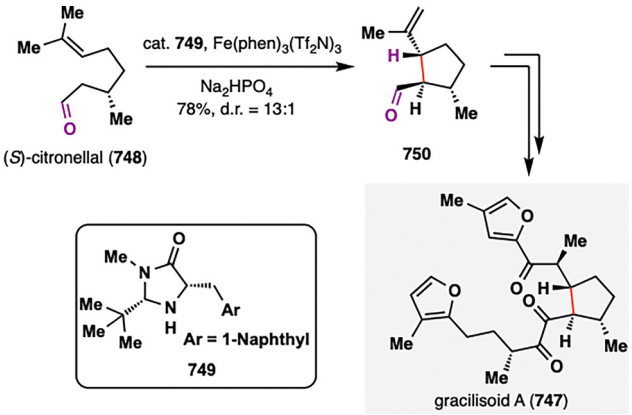

Scheme 92 Total synthesis of gracilisoid A by S. Li and co-workers (**747**).

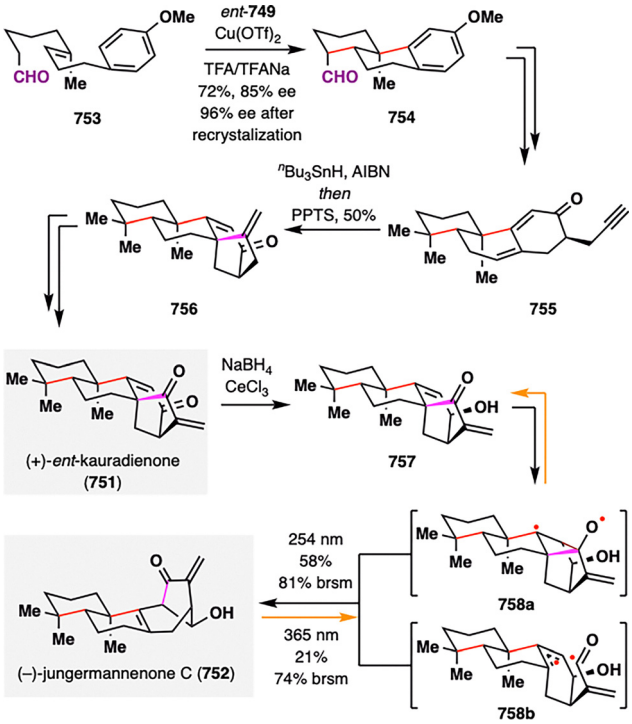

Scheme 93 Total synthesis of *ent*-kauradienone (**751**) and jungermannenone C (**752**) by Lei, Li, and co-workers.

efficient enantioselective cyclization, furnishing tricyclic aldehyde **754** in 72% yield with 85% ee (further upgraded to 96% ee *via* recrystallization). The *ent*-kaurane core was then constructed *via* a highly selective tin-mediated radical 1,6-dienyne cyclization of **755**, which selectively formed the bicyclo[3.2.1]octene scaffold **756**. **756** could be further elaborated to (+)-*ent*-kauradienone (**751**). Luche reduction of (+)-*ent*-kauradienone (**751**) afforded intermediate **757**, which underwent UV-induced (254 nm) radical-mediated rearrangement through **758a** and **758b** to deliver (−)-jungermannenone C (**752**) in 58% yield. Notably, this transformation was shown to be thermodynamically reversible: irradiation at 365 nm enabled the back-conversion of **752** to **757** in 21% yield, underscoring the equilibrium nature of this structural interconversion.

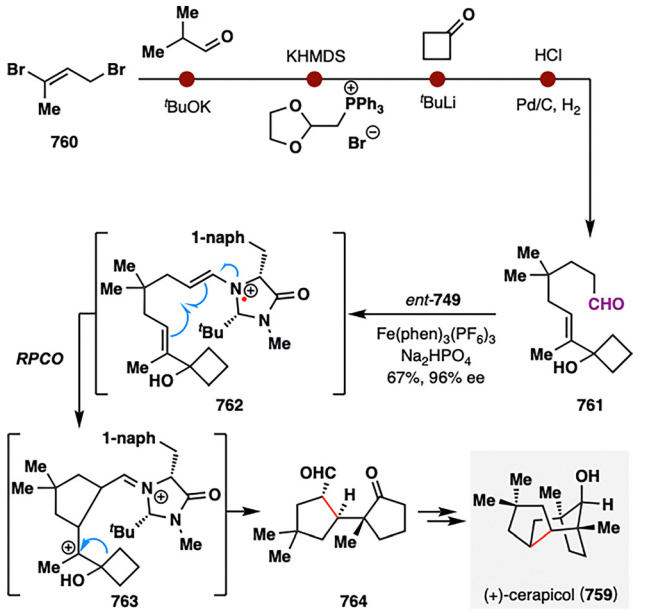

Scheme 94 Total synthesis of (+)-cerapicol (**759**) by Zhang and Tu.

Inspired by MacMillan's pioneering work on aldehyde organo-SOMO catalysis, Tu, Zhang, and co-workers developed a tandem enantioselective aldehyde α-alkylation/semipinacol rearrangement strategy that enabled the efficient construction of synthetically challenging α-quaternary 1,5-dicarbonyl scaffolds.[323] This approach was elegantly demonstrated in their concise total synthesis of (+)-cerapicol (**759**) (Scheme 94). The synthesis commenced with α-allylation of isobutyraldehyde using (*E*)-1,3-dibromobut-2-ene (**760**), followed by a sequence of Wittig homologation, nucleophilic addition, acetal deprotection, and regioselective hydrogenation to furnish aldehyde **761**. The key transformation employed imidazolidinone organocatalyst *ent*-**749** to promote a gram-scale, enantioselective tandem α-alkylation/oxidative RPCO/semipinacol rearrangement of allylic alcohol **761**, delivering the pivotal intermediate **764** in 67% yield with excellent enantioselectivity (96% ee). This cascade strategy not only provided an efficient solution to constructing all-carbon quaternary stereocenters but also enabled the streamlined synthesis of (+)-cerapicol (**759**), highlighting the versatility and synthetic utility of SOMO-catalyzed transformations in the context of complex molecule assembly.

While previous approaches to SOMO activation typically relied on stoichiometric metal oxidants, Xuan, Ding, and co-workers applied a recent method developed by Macmillan that combined photoredox catalysis and organocatalysis to achieve the enantioselective α-alkylation of aldehydes without the requirement of stoichiometric oxidants.[309] This strategy was applied in their asymmetric total synthesis of three pleurotin natural products (**765–767**),[324] originally isolated from the fungus *Pleurotus griseus*,[325] and featuring several innovative transformations that address key stereochemical challenges (Scheme 95). The synthesis began with a regioselective ozonolysis of a trisubstituted alkene **768**, followed by intramolecular aldol condensation, and reduction to furnish allylic alcohol

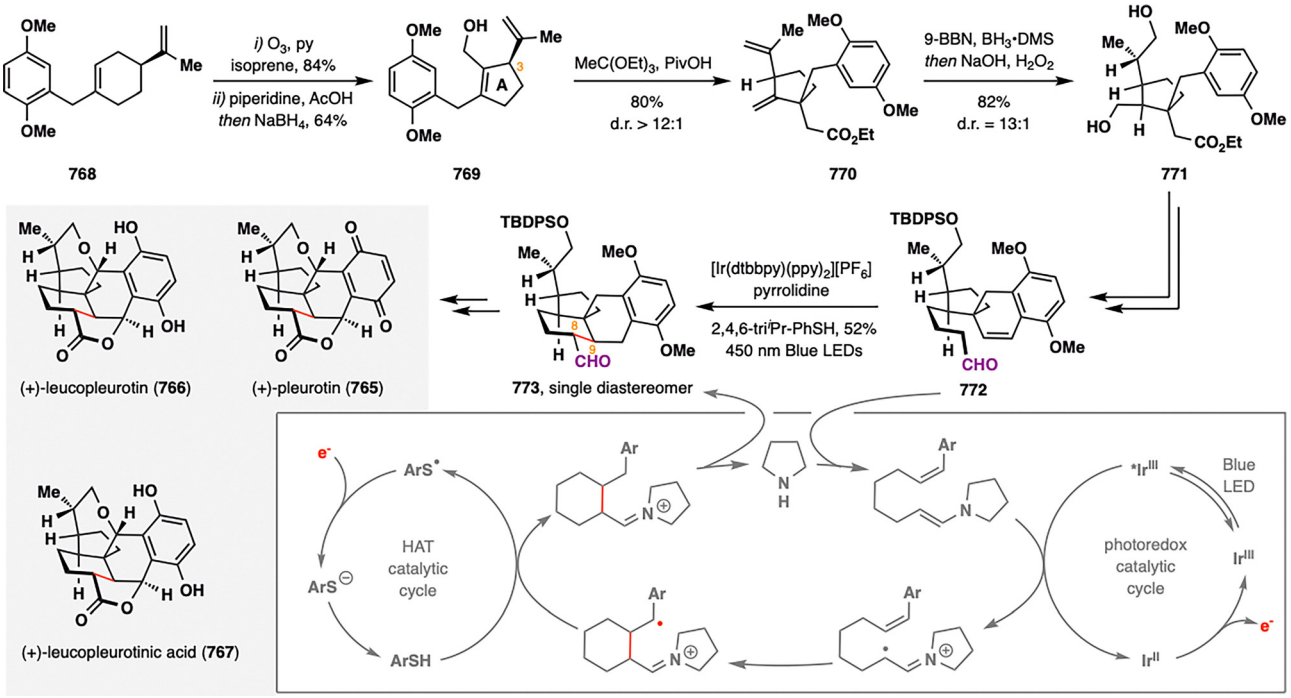

Scheme 95 Total synthesis of pleurotins (**765–767**) by Ding and Xuan.

769. A particularly noteworthy Johnson–Claisen rearrangement of **769** proceeded with excellent diastereoselectivity (d.r. > 12:1) and high yield (80%, gram scale), delivering diene **770**. Subsequent hydroboration–oxidation furnished diol **771**, which was further elaborated to aldehyde **772**. Application of MacMillan's dual photoredox–organocatalytic system to **772** enabled stereocontrolled α-alkylation, affording **773** as a single diastereomer in 52% yield, which set the stage for downstream elaboration to complete the total synthesis of pleurotin congeners **765–767**.

Mechanistically, the α-alkylation is initiated by condensation of the pyrrolidine catalyst with the aldehyde substrate to generate an enamine (Scheme 95). Upon photoexcitation, the Ir^{III}* catalyst undergoes single-electron transfer (SET) from the enamine, affording an enaminyl radical and reduced Ir^{II}. The resulting radical undergoes a 6-*exo*-trig cyclization, forging a new C–C bond and simultaneously establishing a stereocenter while generating a benzylic radical. HAT from ArSH then furnishes an iminium ion, which hydrolyzes to release the pyrrolidine catalyst and the α-alkylated aldehyde. Finally, the thiyl radical formed in the HAT step is reduced by Ir^{II} and protonated to regenerate both the ground-state Ir^{III} photocatalyst and the thiol catalyst.

Collectively, these modern strategies utilizing aldehyde—direct C–H functionalization to ketyl radicals and SOMO-enabled α-radical generation—significantly expand the synthetic chemist's arsenal for terpenoid construction. They circumvent the need for stoichiometric organometallic reagents, unlock novel retrosynthetic disconnections, and provide robust solutions for assembling the intricate and stereochemically demanding architectures characteristic of bioactive terpenoid natural products.

7. Ketone derivatives as radical precursors

Alcohol functionalities, particularly tertiary alcohols, represent foundational handles for radical-based disconnections of to ketones in complex molecule assembly (Scheme 96). Like aldehydes, ketones primarily generate nucleophilic ketyl radicals *via* single-electron reduction, classically employing samarium diiodide (SmI_2). The diverse reactivity of ketyl radicals has been extensively cataloged in contemporary reviews.[302–306] Notably, Procter's comprehensive recent tutorial reviews provide authoritative survey of modern generation methods (*e.g.*, photoredox catalysis) and their evolving synthetic applications.[326–331] This section highlights a complementary, strategically powerful approach: the ketyl radical-mediated skeletal reorganization pioneered by Takatori *et al.*[332] This method efficiently converts fused bicyclo[4.2.0] frameworks into synthetically challenging bicyclo[3.2.1] architectures through a SmI_2-induced 1,2-rearrangement with ring expansion.

Its significant recent adoption in terpenoid synthesis—demonstrating robust efficiency in forging key polycyclic

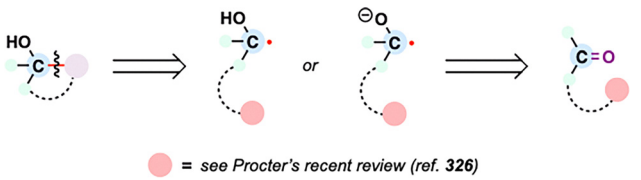

Scheme 96 Radical retrosynthesis of C–C bonds from ketone based on recent studies.

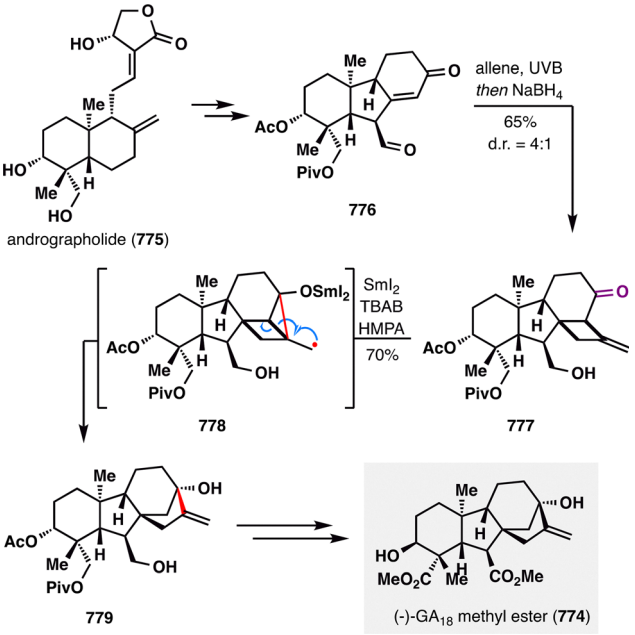

Scheme 97 Dai's total synthesis of (−)-GA_{18} methyl ester (**774**).

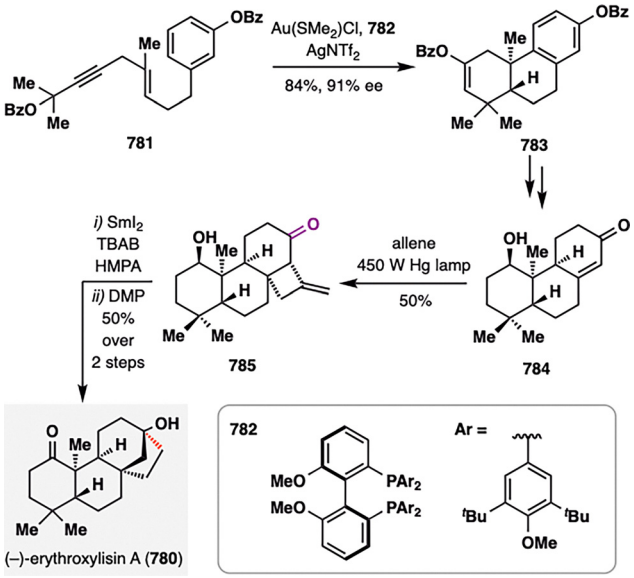

Scheme 98 Total synthesis of (−)-erythroxylisin A (**780**) by Wang and co-workers.

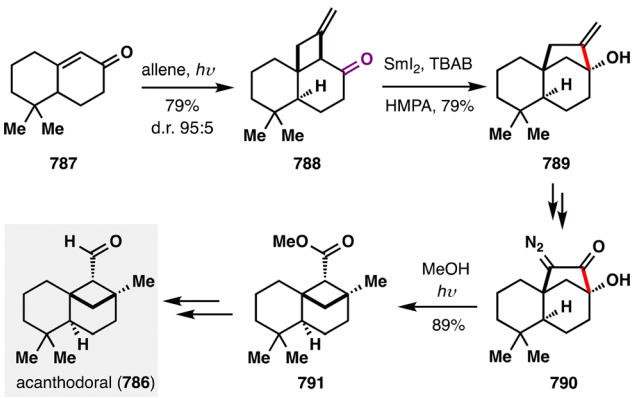

Scheme 99 Kalesse's total synthesis of acanthodoral (**786**).

intermediates—motivates focused discussion here, with mechanistic principles exemplified by Dai's synthesis of (−)-GA_{18} methyl ester (**774**),[333] a member of the gibberellin (GA) family of plant hormones that regulate growth and development (Scheme 97).[334] Given the importance of GAs in agricultural and biochemical research, synthetic access to these compounds is of considerable value. In this work, Dai and co-workers reported a concise nine-step total synthesis of (−)-GA_{18} methyl ester (**774**), starting from the inexpensive and readily available diterpenoid andrographolide (**775**). Their strategy merged photochemical [2+2] cyclization with a SmI_2-mediated radical addition/fragmentation cascade to construct the methylenebicyclo[3.2.1]-octanol motif—a central feature of the gibberellin scaffold—in 70% yield from intermediate **777**. Mechanistically, SET from SmI_2 to the carbonyl group of **777** generated an α-alkoxy radical, which underwent a 3-*exo*-trig cyclization onto the adjacent alkene to form intermediate **778**. A subsequent radical ring expansion of **778** relieved ring strain, furnishing the methylenebicyclo[3.2.1]-octanol framework. This transformation effectively set the stage for final manipulations, ultimately delivering (−)-GA_{18} methyl ester (**774**).

Notably, Wang and co-workers employed a related radical-based skeletal rearrangement strategy to construct the methylenebicyclo[3.2.1]octanol core in their total synthesis of (−)-erythroxylisin A (**780**) (Scheme 98).[335] The enone precursor **784** was synthesized from **783**, which in turn was assembled *via* a Au-catalyzed asymmetric polyene cyclization of alkyne **781**—a key transformation establishing the tricyclic framework. Subsequent exposure of enone **784** to allene under photoirradiation conditions furnished strained cyclobutene **785**, which then underwent a SmI_2-mediated radical addition/fragmentation cascade. Final oxidation with DMP delivered the target natural product (−)-erythroxylisin A (**780**).

Similarly, Kalesse and co-workers applied a comparable sequence, combining photoinduced [2+2] cycloaddition with SmI_2-mediated radical addition/fragmentation cascade to access methylenebicyclo[3.2.1]octanol intermediate **789**, as shown in Scheme 99.[336] This species subsequently underwent diazo formation followed by a photoinduced Wolff rearrangement to achieve a ring contraction, thereby forging the bicyclo[3.1.1]-heptane core in **791** and setting the stage for final elaborations *en route* to acanthodoral (**786**).

Notably, in all three total synthesis described above, the SmI_2-triggered radical addition/fragmentation was strategically employed at a late stage, underscoring its exceptional chemoselectivity, mildness, and compatibility with complex, functionally dense molecular architectures.

8. Alkanes as radical precursors

The direct functionalization of aliphatic C–H bonds has become a powerful strategy for late-stage diversification and

improved step- and atom-economy in complex molecule synthesis.[12,337–339] Among methods for C–H activation, HAT has gained prominence by generating carbon-centered radicals under mild, tunable conditions. Unlike classical two-electron pathways, HAT can achieve C–H functionalization without requiring prefunctionalization, enabling unique modifications of complex molecular architectures.

Recent advances in photocatalysis, electrochemistry, and biocatalysis have dramatically expanded the HAT toolbox. Photocatalytic HAT enables selective activation of aliphatic C–H bonds under visible light,[11,340] and electrochemical strategies offer scalable, redox-economical radical generation.[238,341–344] Engineered enzymes can perform highly site- and stereoselective HAT-mediated oxidations.[345–348] Collectively, these developments have elevated HAT from a mechanistic curiosity to a powerful platform for constructing complex targets, including terpenoid frameworks.

In retrosynthetic analysis, leveraging HAT of alkanes to formally disconnect a C–X bond into a C(sp^3)–H bond presents both conceptual opportunities and practical challenges. The ubiquity of aliphatic C–H bonds demands precise control of selectivity—dictated by factors such as bond dissociation energies (BDEs), steric and electronic environments, and the presence of directing groups that facilitate intramolecular HAT. Consequently, no structural pattern can be generalized to use HAT disconnections; instead, effective retrosynthetic design requires detailed molecular analysis and careful reaction condition optimization. In terpenoid synthesis (Scheme 100), key HAT-initiated transformations include C–H oxidation (*e.g.*, hydroxylation, carboxylation),[238,349] C(sp^3)–C(sp^3) desaturation,[350] stereocenter epimerization,[351] alkene isomerization,[352] radical addition,[353] and radical-mediated skeletal rearrangements.[354]

An alkane C–H functionalization strategy enabled by amidyl radicals was strategically employed by Sarpong and co-workers in their unified approach to functionalized camphor derivatives (**85**, **792**, and **793**)—a class of versatile chiral building blocks long valued in organic synthesis (Scheme 101).[353] The C8-functionalization transformation hinged on a 1,5-HAT process initiated from an amidyl radical, which was generated from camphor-derived aminonitrile **795** *via* photoexcited Ir(III)*-catalyzed oxidation. The resulting C8-centered primary radical then underwent a Giese-type conjugate addition to MVK, affording adduct **798**, which enabled streamlined access to several structural intricate sesquiterpenoids, including copacamphor (**792**), longicamphor (**793**), and longiborneol (**85**).

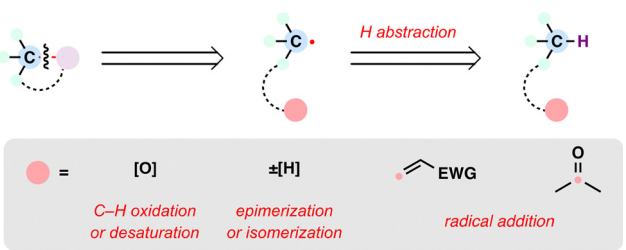

Scheme 100 Modern radical retrosynthesis using alkane as radical precursors.

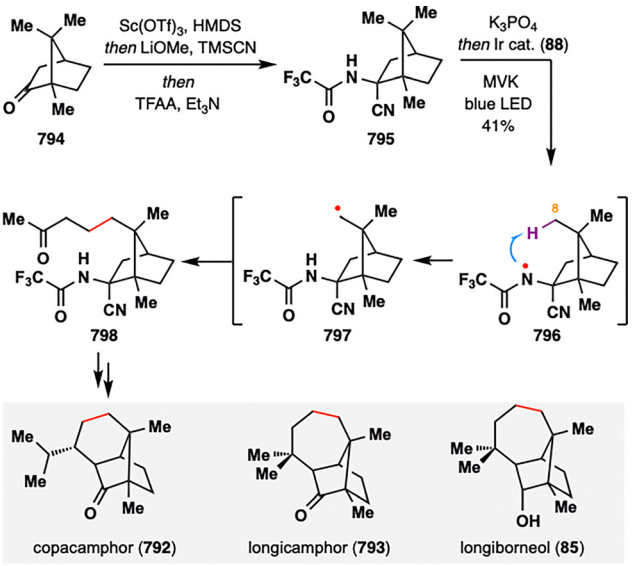

Scheme 101 Sarpong's total synthesis of copacamphor (**792**), longicamphor (**793**), and longiborneol (**85**).

While previous efforts in C–H activation have predominantly relied on heteroatom-initiated intramolecular 1,5-HAT processes, Luo and co-workers achieved a photo-induced direct C–H activation to trigger a Dowd–Beckwith rearrangement, serving as a pivotal step in the total synthesis of (+)-kobusine (**799**) and (+)-spirasine IX (**800**)—two polycyclic C_{20}-diterpenoid alkaloids renowned for their intricate cage-like architectures (Scheme 102).[354] Specifically, upon irradiation, the photoexcited TBADT undervent HAT reversibly with C12–H bond of

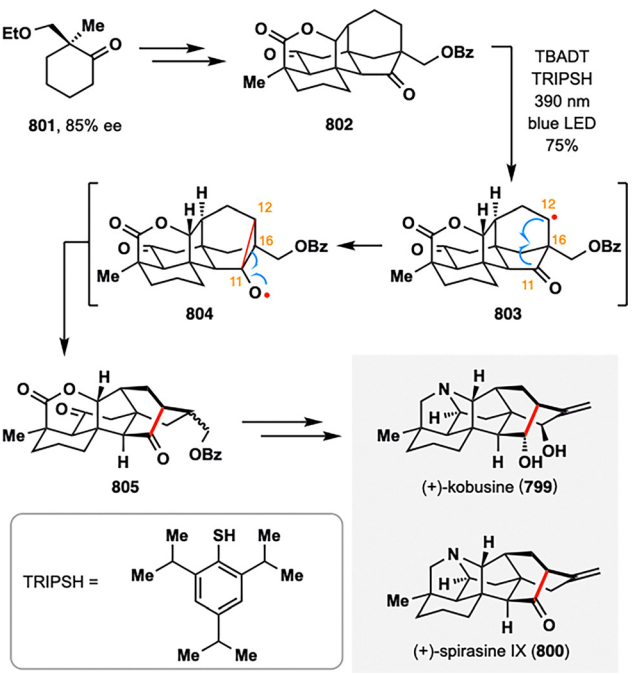

Scheme 102 Luo's total synthesis of (+)-kobusine (**799**) and (+)-spirasine IX (**800**).

precursor **802**, generating a carbon-centered radical intermediate **803**. This radical underwent a 3-*exo*-trig cyclization to furnish intermediate **804**, which then engaged in a Dowd–Beckwith rearrangement to forge the characteristic hetisine skeleton **805** efficiently. This strategically executed skeletal rearrangement laid the foundation for a concise total synthesis of both natural products **799** and **800** through subsequent functional group manipulations, showcasing the synthetic power of HAT-driven transformations in constructing highly complex diterpenoid frameworks.

9. Conclusion and outlook

Radical retrosynthesis has emerged as a powerful and conceptually distinct platform for the synthesis of complex terpenoid natural products. By reconceiving bond disconnections in terms of radical fragments, this strategy enables synthetic solutions that circumvent the limitations of traditional polar approaches—facilitating late-stage functionalization, efficient quaternary center construction, and modular assembly of polycyclic scaffolds. In this review, we have summarized the recent applications of diverse classes of radical precursors—including alkenes, carboxylic acids, organohalides, alcohol derivatives, aldehydes, ketones, and alkanes—in the context of terpenoid synthesis. Particular emphasis has been placed on how each precursor class has been transformed through newly developed radical processes to enable bond-forming reactions that are well-suited to the densely functionalized and stereochemically rich nature of terpenoid frameworks.

These advances have been driven by a wave of methodological innovation over the past decade. Developments in photoredox catalysis, electrochemical activation, MHAT, redox-active ester chemistry, and HAT based C–H functionalization have significantly expanded the repertoire of radical generation and reactivity under synthetically useful conditions. In terpenoid contexts, such tools have enabled installation of quaternary stereocenters, ring constructions, and skeletal rearrangements with improved efficiency and convergence. By organizing the discussion around radical precursor classes and mapping them to representative reaction modes, this review provides a conceptual and practical framework for integrating radical retrosynthetic logic into the total synthesis of architecturally intricate terpenoid natural products.

Looking forward, the broader integration of radical retrosynthesis into complex molecule synthesis will benefit from continued advances on multiple fronts. Asymmetric radical transformations, though rapidly developing, remain underutilized in total synthesis and demand expansion beyond substrate-controlled systems. The rational design of radical cascade reactions also holds great promise for enhancing step economy, particularly in the assembly of polycyclic terpenoid frameworks. In addition, while radical additions to alkenes provide a valuable strategy for constructing quaternary carbon centers, further development of alternative approaches—such as S_H2-based couplings and other non-Giese-type mechanisms—will be critical for expanding structural diversity and stereochemical control. Finally, achieving higher levels of regio- and chemoselectivity in C–H functionalization remains a key goal, one that will enable more precise and programmable bond disconnections. Continued innovation in these areas will further establish radical retrosynthesis as a central and enabling logic in the synthesis of architecturally complex natural products. We hope that the ideas outlined in this review will inspire practitioners to think beyond conventional retrosynthetic paradigms and to embrace the unique reactivity of radicals as a foundation for creative and efficient synthesis.

Conflicts of interest

There are no conflicts to declare.

Data availability

No primary research results, software or code have been included and no new data were generated or analysed as part of this review.

Acknowledgements

We are grateful to all members of our laboratory for their support in gathering and surveying the pertinent literature. Financial support was provided by the National Natural Science Foundation of China (grant no. 22171025), MOST of China, and Tsinghua Institute of Multidisciplinary Biomedical Research, Tsinghua University.

References

1 E. J. Corey, *Chem. Soc. Rev.*, 1988, **17**, 111–133.
2 E. J. Corey and X.-M. Cheng, *Logic of chemical synthesis*, Wiley, New York, New ed., 1995.
3 J. M. Smith, S. J. Harwood and P. S. Baran, *Acc. Chem. Res.*, 2018, **51**, 1807–1817.
4 S. L. Shevick, C. V. Wilson, S. Kotesova, D. Kim, P. L. Holland and R. A. Shenvi, *Chem. Sci.*, 2020, **11**, 12401–12422.
5 S. A. Green, S. W. M. Crossley, J. L. M. Matos, S. Vásquez-Céspedes, S. L. Shevick and R. A. Shenvi, *Acc. Chem. Res.*, 2018, **51**, 2628–2640.
6 S. W. M. Crossley, C. Obradors, R. M. Martinez and R. A. Shenvi, *Chem. Rev.*, 2016, **116**, 8912–9000.
7 S. Murarka, *Adv. Synth. Catal.*, 2018, **360**, 1735–1753.
8 S. Karmakar, A. Silamkoti, N. A. Meanwell, A. Mathur and A. K. Gupta, *Adv. Synth. Catal.*, 2021, **363**, 3693–3736.
9 A. Y. Chan, I. B. Perry, N. B. Bissonnette, B. F. Buksh, G. A. Edwards, L. I. Frye, O. L. Garry, M. N. Lavagnino, B. X. Li, Y. Liang, E. Mao, A. Millet, J. V. Oakley, N. L. Reed, H. A. Sakai, C. P. Seath and D. W. C. MacMillan, *Chem. Rev.*, 2022, **122**, 1485–1542.
10 L. E. Ehehalt, O. M. Beleh, I. C. Priest, J. M. Mouat, A. K. Olszewski, B. N. Ahern, A. R. Cruz, B. K. Chi, A. J. Castro, K. Kang, J. Wang and D. J. Weix, *Chem. Rev.*, 2024, **124**, 13397–13569.

11 L. Capaldo, D. Ravelli and M. Fagnoni, *Chem. Rev.*, 2022, **122**, 1875–1924.
12 S. Sarkar, K. P. S. Cheung and V. Gevorgyan, *Chem. Sci.*, 2020, **11**, 12974–12993.
13 S. Mondal, F. Dumur, D. Gigmes, M. P. Sibi, M. P. Bertrand and M. Nechab, *Chem. Rev.*, 2022, **122**, 5842–5976.
14 K. Hung, X. Hu and T. J. Maimone, *Nat. Prod. Rep.*, 2018, **35**, 174–202.
15 K. J. Romero, M. S. Galliher, D. A. Pratt and C. R. J. Stephenson, *Chem. Soc. Rev.*, 2018, **47**, 7851–7866.
16 A. Frank and M. Groll, *Chem. Rev.*, 2017, **117**, 5675–5703.
17 E. C. Cherney and P. S. Baran, *Isr. J. Chem.*, 2011, **51**, 391–405.
18 E. Goyer, C. Lavaud and G. Massiot, *Nat. Prod. Rep.*, 2023, **40**, 1071–1077.
19 R. B. Clayton, *Q. Rev. Chem. Soc.*, 1965, **19**, 168–200.
20 J. Gershenzon and N. Dudareva, *Nat. Chem. Biol.*, 2007, **3**, 408–414.
21 Y. Wang and J. Gui, *Chem. Soc. Rev.*, 2025, **54**, 6807–6831.
22 A. Kanwal, M. Bilal, N. Rasool, M. Zubair, S. A. A. Shah and Z. A. Zakaria, *Pharmaceuticals*, 2022, **15**, 1392.
23 W. P. Thomas and S. V. Pronin, *Acc. Chem. Res.*, 2021, **54**, 1347–1359.
24 Y. Chen, J. Zhao, S. Li and J. Xu, *Nat. Prod. Rep.*, 2019, **36**, 263–288.
25 J. Justicia, L. Álvarez De Cienfuegos, A. G. Campaña, D. Miguel, V. Jakoby, A. Gansäuer and J. M. Cuerva, *Chem. Soc. Rev.*, 2011, **40**, 3525.
26 D. Urabe, T. Asaba and M. Inoue, *Chem. Rev.*, 2015, **115**, 9207–9231.
27 C. N. Stout and H. Renata, *Acc. Chem. Res.*, 2021, **54**, 1143–1156.
28 Z. G. Brill, M. L. Condakes, C. P. Ting and T. J. Maimone, *Chem. Rev.*, 2017, **117**, 11753–11795.
29 S. P. Pitre, N. A. Weires and L. E. Overman, *J. Am. Chem. Soc.*, 2019, **141**, 2800–2813.
30 C. P. Jasperse, D. P. Curran and T. L. Fevig, *Chem. Rev.*, 1991, **91**, 1237–1286.
31 G. J. Rowlands, *Tetrahedron*, 2009, **65**, 8603–8655.
32 G. J. Rowlands, *Tetrahedron*, 2010, **66**, 1593–1636.
33 T. Yoshimitsu, *Chem. Rec.*, 2014, **14**, 268–279.
34 M. Yan, J. C. Lo, J. T. Edwards and P. S. Baran, *J. Am. Chem. Soc.*, 2016, **138**, 12692–12714.
35 R. W. Hoffmann, *Chem. Soc. Rev.*, 2016, **45**, 577–583.
36 Y. Li, X. Lu and Y. Fu, *CCS Chem.*, 2024, **6**, 1130–1156.
37 S. H. Kyne, G. Lefèvre, C. Ollivier, M. Petit, V.-A. Ramis Cladera and L. Fensterbank, *Chem. Soc. Rev.*, 2020, **49**, 8501–8542.
38 S. Isayama and T. Mukaiyama, *Chem. Lett*, 1989, **18**, 569–572.
39 I. Tabushi and N. Koga, *J. Am. Chem. Soc.*, 1979, **101**, 6456–6458.
40 S. Inoki, K. Kato, T. Takai, S. Isayama, T. Yamada and T. Mukaiyama, *Chem. Lett*, 1989, **18**, 515–518.
41 T. Mukaiyama, S. Isayama, S. Inoki, K. Kato, T. Yamada and T. Takai, *Chem. Lett.*, 1989, 449–452.
42 B. Gaspar and E. M. Carreira, *J. Am. Chem. Soc.*, 2009, **131**, 13214–13215.
43 J. Waser and E. M. Carreira, *Angew. Chem., Int. Ed.*, 2004, **43**, 4099–4102.
44 J. Waser and E. M. Carreira, *J. Am. Chem. Soc.*, 2004, **126**, 5676–5677.
45 J. Waser, H. Nambu and E. M. Carreira, *J. Am. Chem. Soc.*, 2005, **127**, 8294–8295.
46 J. Waser, B. Gaspar, H. Nambu and E. M. Carreira, *J. Am. Chem. Soc.*, 2006, **128**, 11693–11712.
47 B. Gaspar and E. M. Carreira, *Angew. Chem., Int. Ed.*, 2007, **46**, 4519–4522.
48 B. Gaspar and E. M. Carreira, *Angew. Chem., Int. Ed.*, 2008, **47**, 5758–5760.
49 J. E. Sears and D. L. Boger, *Acc. Chem. Res.*, 2015, **48**, 653–662.
50 H. Ishikawa, D. A. Colby and D. L. Boger, *J. Am. Chem. Soc.*, 2008, **130**, 420–421.
51 H. Ishikawa, D. A. Colby, S. Seto, P. Va, A. Tam, H. Kakei, T. J. Rayl, I. Hwang and D. L. Boger, *J. Am. Chem. Soc.*, 2009, **131**, 4904–4916.
52 E. K. Leggans, T. J. Barker, K. K. Duncan and D. L. Boger, *Org. Lett.*, 2012, **14**, 1428–1431.
53 D. C. Eisenberg and J. R. Norton, *Isr. J. Chem.*, 1991, **31**, 55–66.
54 Y. Hu, A. P. Shaw, D. P. Estes and J. R. Norton, *Chem. Rev.*, 2016, **116**, 8427–8462.
55 L. Tang, E. T. Papish, G. P. Abramo, J. R. Norton, M.-H. Baik, R. A. Friesner and A. Rappé, *J. Am. Chem. Soc.*, 2003, **125**, 10093–10102.
56 J. Choi, L. Tang and J. R. Norton, *J. Am. Chem. Soc.*, 2006, **129**, 234–240.
57 J. L. Kuo, J. Hartung, A. Han and J. R. Norton, *J. Am. Chem. Soc.*, 2015, **137**, 1036–1039.
58 J. C. Lo, D. Kim, C.-M. Pan, J. T. Edwards, Y. Yabe, J. Gui, T. Qin, S. Gutiérrez, J. Giacoboni, M. W. Smith, P. L. Holland and P. S. Baran, *J. Am. Chem. Soc.*, 2017, **139**, 2484–2503.
59 J. C. Lo, Y. Yabe and P. S. Baran, *J. Am. Chem. Soc.*, 2014, **136**, 1304–1307.
60 J. C. Lo, J. Gui, Y. Yabe, C.-M. Pan and P. S. Baran, *Nature*, 2014, **516**, 343–348.
61 H. T. Dao, C. Li, Q. Michaudel, B. D. Maxwell and P. S. Baran, *J. Am. Chem. Soc.*, 2015, **137**, 8046–8049.
62 J. Gui, C.-M. Pan, Y. Jin, T. Qin, J. C. Lo, B. J. Lee, S. H. Spergel, M. E. Mertzman, W. J. Pitts, T. E. La Cruz, M. A. Schmidt, N. Darvatkar, S. R. Natarajan and P. S. Baran, *Science*, 2015, **348**, 886–891.
63 L. Kong, X. Gan, V. A. Van Der Puyl Lovett and R. A. Shenvi, *J. Am. Chem. Soc.*, 2024, **146**, 2351–2357.
64 S. A. Green, J. L. M. Matos, A. Yagi and R. A. Shenvi, *J. Am. Chem. Soc.*, 2016, **138**, 12779–12782.
65 S. A. Green, S. Vásquez-Céspedes and R. A. Shenvi, *J. Am. Chem. Soc.*, 2018, **140**, 11317–11324.
66 J. L. M. Matos, S. Vásquez-Céspedes, J. Gu, T. Oguma and R. A. Shenvi, *J. Am. Chem. Soc.*, 2018, **140**, 16976–16981.

67 S. L. Shevick, C. Obradors and R. A. Shenvi, *J. Am. Chem. Soc.*, 2018, **140**, 12056–12068.
68 S. A. Green, T. R. Huffman, R. O. McCourt, V. van der Puyl and R. A. Shenvi, *J. Am. Chem. Soc.*, 2019, **141**, 7709–7714.
69 X. Gan, B. Zhang, N. Dao, C. Bi, M. Pokle, L. Kan, M. R. Collins, C. C. Tyrol, P. N. Bolduc, M. Nicastri, Y. Kawamata, P. S. Baran and R. Shenvi, *Science*, 2024, **384**, 113–118.
70 X. Ma and S. B. Herzon, *Beilstein J. Org. Chem.*, 2018, **14**, 2259–2265.
71 S. M. King, X. Ma and S. B. Herzon, *J. Am. Chem. Soc.*, 2014, **136**, 6884–6887.
72 X. Ma and S. B. Herzon, *Chem. Sci.*, 2015, **6**, 6250–6255.
73 X. Ma, H. Dang, J. A. Rose, P. Rablen and S. B. Herzon, *J. Am. Chem. Soc.*, 2017, **139**, 5998–6007.
74 D. E. Essayan, M. J. Schubach, J. M. Smoot, T. Puri and S. V. Pronin, *J. Am. Chem. Soc.*, 2024, **146**, 18224–18229.
75 E. E. Touney, N. J. Foy and S. V. Pronin, *J. Am. Chem. Soc.*, 2018, **140**, 16982–16987.
76 C. A. Discolo, E. E. Touney and S. V. Pronin, *J. Am. Chem. Soc.*, 2019, **141**, 17527–17532.
77 L.-J. Li, Y. He, Y. Yang, J. Guo, Z. Lu, C. Wang, S. Zhu and S.-F. Zhu, *CCS Chem.*, 2024, **6**, 537–584.
78 Y. Wang, Y. He and S. Zhu, *Acc. Chem. Res.*, 2022, **55**, 3519–3536.
79 G. Zhang and Q. Zhang, *Chem. Catal.*, 2023, **3**, 100526.
80 J. Wu and Z. Ma, *Org. Chem. Front.*, 2021, **8**, 7050–7076.
81 D. T. George, E. J. Kuenstner and S. V. Pronin, *J. Am. Chem. Soc.*, 2015, **137**, 15410–15413.
82 B. Huang, C.-J. Xiao, Z.-Y. Huang, X.-Y. Tian, X. Cheng, X. Dong and B. Jiang, *Org. Lett.*, 2014, **16**, 3552–3555.
83 W. Cao, H. Deng, Y. Sun, B. Liu and S. Qin, *Chem. – Eur. J.*, 2018, **24**, 9120–9129.
84 H. Deng, W. Cao, R. Liu, Y. Zhang and B. Liu, *Angew. Chem., Int. Ed.*, 2017, **56**, 5849–5852.
85 Z. Lu, X. Zhang, Z. Guo, Y. Chen, T. Mu and A. Li, *J. Am. Chem. Soc.*, 2018, **140**, 9211–9218.
86 D. Leonori and V. K. Aggarwal, *Acc. Chem. Res.*, 2014, **47**, 3174–3183.
87 K. Nozaki, K. Oshima and K. Utimoto, *Tetrahedron Lett.*, 1988, **29**, 1041–1044.
88 P. Hu, H. M. Chi, K. C. DeBacker, X. Gong, J. H. Keim, I. T. Hsu and S. A. Snyder, *Nature*, 2019, **569**, 703–707.
89 Y. Matsuda and I. Abe, *Nat. Prod. Rep.*, 2016, **33**, 26–53.
90 J. Li, F. Li, E. King-Smith and H. Renata, *Nat. Chem.*, 2020, **12**, 173–179.
91 J. Kobayashi and T. Kubota, *Nat. Prod. Rep.*, 2009, **26**, 936.
92 G. Xu, J. Wu, L. Li, Y. Lu and C. Li, *J. Am. Chem. Soc.*, 2020, **142**, 15240–15245.
93 P. Magnus, J. Lacour, I. Coldham, B. Mugrage and W. B. Bauta, *Tetrahedron*, 1995, **51**, 11087–11110.
94 K. B. Sharpless, T. Hori, L. K. Truesdale and C. O. Dietrich, *J. Am. Chem. Soc.*, 1976, **98**, 269–271.
95 J. Li, F. Chen and H. Renata, *J. Am. Chem. Soc.*, 2022, **144**, 19238–19242.
96 C. Petrier, C. Dupuy and J. L. Luche, *Tetrahedron Lett.*, 1986, **27**, 3149–3152.
97 R. F. Lusi, G. Sennari and R. Sarpong, *J. Am. Chem. Soc.*, 2022, **144**, 17277–17294.
98 R. F. Lusi, G. Sennari and R. Sarpong, *Nat. Chem.*, 2022, **14**, 450–456.
99 F. A. Bermejo, A. Fernández Mateos, A. Marcos Escribano, R. Martín Lago, L. Mateos Burón, M. Rodríguez López and R. Rubio González, *Tetrahedron*, 2006, **62**, 8933–8942.
100 O. Goethe, A. Heuer, X. Ma, Z. Wang and S. B. Herzon, *Nat. Prod. Rep.*, 2019, **36**, 220–247.
101 N. J. Foy and S. V. Pronin, *J. Am. Chem. Soc.*, 2022, **144**, 10174–10179.
102 W. Cao, Z. Wang, Y. Hao, T. Wang, S. Fu and B. Liu, *Angew. Chem., Int. Ed.*, 2023, **62**, e202305516.
103 A. Heidbreder and J. Mattay, *Tetrahedron Lett.*, 1992, **33**, 1973–1976.
104 X.-H. Zhao, L.-L. Meng, X.-T. Liu, P.-F. Shu, C. Yuan, X.-T. An, T.-X. Jia, Q.-Q. Yang, X. Zhen and C.-A. Fan, *J. Am. Chem. Soc.*, 2023, **145**, 311–321.
105 P. S. Rao, K. G. Sarma and T. R. Seshadri, *Curr. Sci.*, 1965, **34**, 9–11.
106 X. Chen, W. Yao, H. Zheng, H. Wang, P.-P. Zhou, D.-Y. Zhu and S.-H. Wang, *J. Am. Chem. Soc.*, 2023, **145**, 13549–13555.
107 X.-H. Tian, L.-L. Hong, W.-H. Jiao and H.-W. Lin, *Nat. Prod. Rep.*, 2023, **40**, 718–749.
108 Y. Huang, Q. Gu, Q. Chao, H. Xiao and H. Lu, *Angew. Chem., Int. Ed.*, 2025, **64**, e202507638.
109 B. Xu, C. Liu and M. Dai, *J. Am. Chem. Soc.*, 2022, **144**, 19700–19703.
110 B. Khatri Chhetri, S. Lavoie, A. M. Sweeney-Jones, N. Mojib, V. Raghavan, K. Gagaring, B. Dale, C. W. McNamara, K. Soapi, C. L. Quave, P. L. Polavarapu and J. Kubanek, *J. Org. Chem.*, 2019, **84**, 8531–8541.
111 N. Germain and A. Alexakis, *Chem. – Eur. J.*, 2015, **21**, 8597–8606.
112 C. H. Oh, H. H. Jung, K. S. Kim and N. Kim, *Angew. Chem., Int. Ed.*, 2003, **42**, 805–808.
113 K. Du, P. Guo, Y. Chen, Z. Cao, Z. Wang and W. Tang, *Angew. Chem., Int. Ed.*, 2015, **54**, 3033–3037.
114 M. Fadel and E. M. Carreira, *J. Am. Chem. Soc.*, 2023, **145**, 8332–8337.
115 R. J. Ferreira, G. Spengler, A. Orthaber, D. J. V. A. Dos Santos and M.-J. U. Ferreira, *Org. Lett.*, 2021, **23**, 274–278.
116 H. Wang, L. Wei, J. Huang, L. Wang, H. Peng, H. Jiang, J. Wu and Z. Ma, *Angew. Chem., Int. Ed.*, 2025, **64**, e202507961.
117 H. H. Patel and M. S. Sigman, *J. Am. Chem. Soc.*, 2015, **137**, 3462–3465.
118 W. Zhao, R. Al-Ahmad and M. Dai, *J. Am. Chem. Soc.*, 2025, **147**, 32365–32369.
119 Y.-P. Liu, Q. Dai, W.-X. Wang, J. He, Z.-H. Li, T. Feng and J.-K. Liu, *J. Nat. Prod.*, 2020, **83**, 1725–1729.
120 B. Xu, W. Xun, S. Su and H. Zhai, *Angew. Chem., Int. Ed.*, 2020, **59**, 16475–16479.
121 R. Uchida, S. Yokota, D. Matsuda, A. Matsumoto, S. Iwamoto, H. Onodera, Y. Takahashi and H. Tomoda, *J. Antibiot.*, 2014, **67**, 777–781.

122 H. Taguchi, M. Kawaguchi, T. Nagamitsu and M. Ohtawa, *Org. Biomol. Chem.*, 2023, **21**, 6129–6133.
123 G. Huang, X. Zhang, Y.-C. Gu and J. Gui, *J. Am. Chem. Soc.*, 2025, **147**, 20239–20245.
124 J. Li, H. Tang, T. Kurtán, A. Mándi, C.-L. Zhuang, L. Su, G.-L. Zheng and W. Zhang, *J. Nat. Prod.*, 2018, **81**, 1645–1650.
125 J. Gong, P. Sun, N. Jiang, R. Riccio, G. Lauro, G. Bifulco, T.-J. Li, W. H. Gerwick and W. Zhang, *Org. Lett.*, 2014, **16**, 2224–2227.
126 M. Saladrigas, E. Gómez-Bengoa, J. Bonjoch and B. Bradshaw, *Chem. – Eur. J.*, 2023, **29**, e202203286.
127 X. Fang, N. Zhang, S.-C. Chen and T. Luo, *J. Am. Chem. Soc.*, 2022, **144**, 2292–2300.
128 P. W. Brian and J. G. Mcgowan, *Nature*, 1945, **156**, 144–145.
129 J. S. Moffatt, J. D. Bu'Lock and T. H. Yuen, *J. Chem. Soc. D*, 1969, 839a.
130 Y. Ji, Z. Xin, H. He and S. Gao, *J. Am. Chem. Soc.*, 2019, **141**, 16208–16212.
131 W. Gao, C. Chai, Y. He, F. Li, X. Hao, F. Cao, L. Gu, J. Liu, Z. Hu and Y. Zhang, *Org. Lett.*, 2019, **21**, 8469–8472.
132 T. Amagata, M. Doi, M. Tohgo, K. Minoura and A. Numata, *Chem. Commun.*, 1999, 1321–1322.
133 T. Amagata, M. Tanaka, T. Yamada, M. Doi, K. Minoura, H. Ohishi, T. Yamori and A. Numata, *J. Nat. Prod.*, 2007, **70**, 1731–1740.
134 P. Chen, C. Wang, R. Yang, H. Xu, J. Wu, H. Jiang, K. Chen and Z. Ma, *Angew. Chem., Int. Ed.*, 2021, **60**, 5512–5518.
135 L. Canonica, B. Danieli, G. Lesma and G. Palmisano, *J. Chem. Soc., Chem. Commun.*, 1985, 1321–1322.
136 K. Yu, F. Yao, Q. Zeng, H. Xie and H. Ding, *J. Am. Chem. Soc.*, 2021, **143**, 10576–10581.
137 A. Ulubelen, H. K. Desai, S. K. Srivastava, B. P. Hart, J.-C. Park, B. S. Joshi, S. W. Pelletier, A. H. Meriçli, F. Meriçli and R. Ilarslan, *J. Nat. Prod.*, 1996, **59**, 360–366.
138 V. B. Birman, E. W. Uffman, H. Jiang, X. Li and C. J. Kilbane, *J. Am. Chem. Soc.*, 2004, **126**, 12226–12227.
139 S. Dall'Acqua, B. B. Shrestha, M. B. Gewali, P. K. Jha, M. Carrara and G. Innocenti, *Nat. Prod. Commun.*, 2008, **3**, 1985–1989.
140 J. Liu and D. Ma, *Angew. Chem., Int. Ed.*, 2018, **57**, 6676–6680.
141 F. F. Fleming, J. Guo, Q. Wang and D. Weaver, *J. Org. Chem.*, 1999, **64**, 8568–8575.
142 K. Iwasaki, K. K. Wan, A. Oppedisano, S. W. M. Crossley and R. A. Shenvi, *J. Am. Chem. Soc.*, 2014, **136**, 1300–1303.
143 C. Zhou, W. Qin, C. Tu, Y. Chen, S. Fu and B. Liu, *Angew. Chem., Int. Ed.*, 2025, **64**, e202503943.
144 H. Hussain, J. Xiao, A. Ali, I. R. Green and B. Westermann, *Nat. Prod. Rep.*, 2023, **40**, 412–451.
145 R. Wittenberg, J. Srogl, M. Egi and L. S. Liebeskind, *Org. Lett.*, 2003, **5**, 3033–3035.
146 R. J. Wiles and G. A. Molander, *Isr. J. Chem.*, 2020, **60**, 281–293.
147 N. Müller, T. Magauer and O. Kováč, *J. Org. Chem.*, 2025, **90**, 5083–5092.
148 L. Pitzer, J. L. Schwarz and F. Glorius, *Chem. Sci.*, 2019, **10**, 8285–8291.
149 T. Long, S. He and C. Li, *Chin. J. Org. Chem.*, 2025, **45**, 748–763.
150 X. Li, Z. Chang, S. Duan and Z. Xie, *Angew. Chem., Int. Ed.*, 2025, **64**, e202416211.
151 F. Tang, Z.-C. Zhang, Z.-L. Song, Y.-H. Li, Z.-H. Zhou, J.-J. Chen and Z. Yang, *J. Am. Chem. Soc.*, 2025, **147**, 4731–4735.
152 C. P. Ting, G. Xu, X. Zeng and T. J. Maimone, *J. Am. Chem. Soc.*, 2016, **138**, 14868–14871.
153 M. Elkin, S. M. Szewczyk, A. C. Scruse and T. R. Newhouse, *J. Am. Chem. Soc.*, 2017, **139**, 1790–1793.
154 F. Yang and J. A. Porco, *J. Am. Chem. Soc.*, 2022, **144**, 12970–12978.
155 Y. Zhang, Y. Ji, I. Franzoni, C. Guo, H. Jia, B. Hong and H. Li, *Angew. Chem., Int. Ed.*, 2021, **60**, 14869–14874.
156 G. Xu, M. Elkin, D. J. Tantillo, T. R. Newhouse and T. J. Maimone, *Angew. Chem., Int. Ed.*, 2017, **56**, 12498–12502.
157 H. Shigehisa, T. Aoki, S. Yamaguchi, N. Shimizu and K. Hiroya, *J. Am. Chem. Soc.*, 2013, **135**, 10306–10309.
158 L. K. Johnson, S. W. Niman, D. Vrubliauskas and C. D. Vanderwal, *Org. Lett.*, 2021, **23**, 9569–9573.
159 D. Vrubliauskas, B. M. Gross and C. D. Vanderwal, *J. Am. Chem. Soc.*, 2021, **143**, 2944–2952.
160 D. Vrubliauskas and C. D. Vanderwal, *Angew. Chem., Int. Ed.*, 2020, **59**, 6115–6121.
161 Y. Zhao, J. Hu, R. Chen, F. Xiong, H. Xie and H. Ding, *J. Am. Chem. Soc.*, 2022, **144**, 2495–2500.
162 G. Schoenn, C. Kouklovsky, R. Guillot, T. Magauer and G. Vincent, *Angew. Chem., Int. Ed.*, 2025, **64**, e202505270.
163 D. J. Schatz, E. J. Kuenstner, D. T. George and S. V. Pronin, *Nat. Prod. Rep.*, 2022, **39**, 946–968.
164 W. P. Thomas and S. V. Pronin, *J. Am. Chem. Soc.*, 2022, **144**, 118–122.
165 W. P. Thomas, D. J. Schatz, D. T. George and S. V. Pronin, *J. Am. Chem. Soc.*, 2019, **141**, 12246–12250.
166 N. A. Godfrey, D. J. Schatz and S. V. Pronin, *J. Am. Chem. Soc.*, 2018, **140**, 12770–12774.
167 G. Liu, Z. Zhang, S. Fu and B. Liu, *Org. Lett.*, 2021, **23**, 290–295.
168 H.-M. Chung, J.-H. Su, T.-L. Hwang, J.-J. Li, J.-J. Chen, Y.-H. Chen, Y.-C. Chang, Y.-D. Su, Y.-H. Chen, L.-S. Fang, J.-H. Sheu, W.-H. Wang and P.-J. Sung, *Tetrahedron*, 2013, **69**, 2740–2744.
169 X. Gan, S. Kotesova, A. Castanedo, S. A. Green, S. L. B. Møller and R. A. Shenvi, *J. Am. Chem. Soc.*, 2023, **145**, 15714–15720.
170 L. G. Faqueti, I. V. Farias, E. C. Sabedot, F. Delle Monache, A. San Feliciano, I. T. A. Schuquel, V. Cechinel-Filho, A. Bella Cruz and C. Meyre-Silva, *J. Agric. Food Chem.*, 2015, **63**, 8151–8155.
171 S. W. M. Crossley, F. Barabé and R. A. Shenvi, *J. Am. Chem. Soc.*, 2014, **136**, 16788–16791.
172 G. H. Harris, K. Hoogsteen, K. C. Silverman, S. L. Raghoobar, G. F. Bills, R. B. Lingham, J. L. Smith, H. W. Dougherty, C. Cascales and F. Peláez, *Tetrahedron*, 1993, **49**, 2139–2144.

173 C. Y. Bemis, C. N. Ungarean, A. S. Shved, C. S. Jamieson, T. Hwang, K. S. Lee, K. N. Houk and D. Sarlah, *J. Am. Chem. Soc.*, 2021, **143**, 6006–6017.
174 L. Pan, F. Schneider, M. Ottenbruch, R. Wiechert, T. List, P. Schoch, B. Mertes and T. Gaich, *Nature*, 2024, **632**, 543–549.
175 P. Zhang, Y. Li, Z. Yan, J. Gong and Z. Yang, *J. Org. Chem.*, 2019, **84**, 15958–15971.
176 P.-P. Zhang, Z.-M. Yan, Y.-H. Li, J.-X. Gong and Z. Yang, *J. Am. Chem. Soc.*, 2017, **139**, 13989–13992.
177 S. Shen, H. Zhu, D. Chen, D. Liu, L. V. Ofwegen, P. Proksch and W. Lin, *Tetrahedron Lett.*, 2012, **53**, 5759–5762.
178 J. H. Dworkin, B. W. Dehnert and O. Kwon, *Trends in Chem.*, 2023, **5**, 174–200.
179 M. Šimek, J. H. Dworkin and O. Kwon, *Acc. Chem. Res.*, 2025, **58**, 1547–1561.
180 A. J. Smaligo, M. Swain, J. C. Quintana, M. F. Tan, D. A. Kim and O. Kwon, *Science*, 2019, **364**, 681–685.
181 A. J. Smaligo and O. Kwon, *Org. Lett.*, 2019, **21**, 8592–8597.
182 A. J. Smaligo, J. Wu, N. R. Burton, A. S. Hacker, A. C. Shaikh, J. C. Quintana, R. Wang, C. Xie and O. Kwon, *Angew. Chem., Int. Ed.*, 2020, **59**, 1211–1215.
183 B. W. Dehnert, J. H. Dworkin and O. Kwon, *Synthesis*, 2024, 71–86.
184 M. Swain, G. Sadykhov, R. Wang and O. Kwon, *Angew. Chem., Int. Ed.*, 2020, **59**, 17565–17571.
185 M. Swain, T. B. Bunnell, J. Kim and O. Kwon, *J. Am. Chem. Soc.*, 2022, **144**, 14828–14837.
186 D. E. Kim, Y. Zhu, S. Harada, I. Aguilar, A. E. Cuomo, M. Wang and T. R. Newhouse, *J. Am. Chem. Soc.*, 2023, **145**, 4394–4399.
187 M. Liu, P. Li, X. Tang, X. Luo, K. Liu, Y. Zhang, Q. Wang and G. Li, *J. Org. Chem.*, 2021, **86**, 970–979.
188 T. Kobayashi, R. Sugitate, K. Uchida, Y. Kawamoto and H. Ito, *Org. Lett.*, 2024, **26**, 1803–1806.
189 T. Kobayashi, F. Hayano, A. Kamiya, Y. Kawamoto and H. Ito, *Org. Lett.*, 2024, **26**, 5105–5109.
190 S. L. Schreiber, *J. Am. Chem. Soc.*, 1980, **102**, 6163–6165.
191 J. Ji, J. Chen, S. Qin, W. Li, J. Zhao, G. Li, H. Song, X.-Y. Liu and Y. Qin, *J. Am. Chem. Soc.*, 2023, **145**, 3903–3908.
192 F.-P. Wang and Q.-H. Chen, *The Alkaloids: Chem. Bio.*, Elsevier, 2010, vol. 69, pp. 1–577.
193 L.-P. Zhong, C. Gudeman, J. Zhen, O. A. Wanasinghe, J. Hellmig, M. J. E. Collins, J. Bacsa, A. Adibekian and M. Dai, *J. Am. Chem. Soc.*, 2025, **147**, 28589–28594.
194 J. Hu, Z.-X. Zou, Y. Chen, S. Li, X. Gao, Z. Liu, Y. Wang, H. Liu and W. Zhang, *J. Nat. Prod.*, 2022, **85**, 1967–1975.
195 S. B. Beil, T. Q. Chen, N. E. Intermaggio and D. W. C. MacMillan, *Acc. Chem. Res.*, 2022, **55**, 3481–3494.
196 T. Kato, K. Hagiwara and M. Inoue, *Chem. Pharm. Bull.*, 2024, **72**, 767–771.
197 M. Nagatomo, D. Kamimura, Y. Matsui, K. Masuda and M. Inoue, *Chem. Sci.*, 2015, **6**, 2765–2769.
198 G. Laudadio, M. D. Palkowitz, T. El-Hayek Ewing and P. S. Baran, *ACS Med. Chem. Lett.*, 2022, **13**, 1413–1420.
199 C. R. Jamison and L. E. Overman, *Acc. Chem. Res.*, 2016, **49**, 1578–1586.
200 S. P. Pitre and L. E. Overman, *Chem. Rev.*, 2022, **122**, 1717–1751.
201 L. Huang, A. M. Olivares and D. J. Weix, *Angew. Chem., Int. Ed.*, 2017, **56**, 11901–11905.
202 J. M. Smith, T. Qin, R. R. Merchant, J. T. Edwards, L. R. Malins, Z. Liu, G. Che, Z. Shen, S. A. Shaw, M. D. Eastgate and P. S. Baran, *Angew. Chem., Int. Ed.*, 2017, **56**, 11906–11910.
203 D. M. Kitcatt, S. Nicolle and A.-L. Lee, *Chem. Soc. Rev.*, 2022, **51**, 1415–1453.
204 G. Pratsch, G. L. Lackner and L. E. Overman, *J. Org. Chem.*, 2015, **80**, 6025–6036.
205 T. Qin, L. R. Malins, J. T. Edwards, R. R. Merchant, A. J. E. Novak, J. Z. Zhong, R. B. Mills, M. Yan, C. Yuan, M. D. Eastgate and P. S. Baran, *Angew. Chem., Int. Ed.*, 2017, **56**, 260–265.
206 L. Chu, C. Ohta, Z. Zuo and D. W. C. MacMillan, *J. Am. Chem. Soc.*, 2014, **136**, 10886–10889.
207 M. J. Schnermann and L. E. Overman, *Angew. Chem., Int. Ed.*, 2012, **51**, 9576–9580.
208 K. Okada, K. Okamoto, N. Morita, K. Okubo and M. Oda, *J. Am. Chem. Soc.*, 1991, **113**, 9401–9402.
209 M. J. Schnermann and L. E. Overman, *J. Am. Chem. Soc.*, 2011, **133**, 16425–16427.
210 M. R. Garnsey, Y. Slutskyy, C. R. Jamison, P. Zhao, J. Lee, Y. H. Rhee and L. E. Overman, *J. Org. Chem.*, 2018, **83**, 6958–6976.
211 D. S. Müller, N. L. Untiedt, A. P. Dieskau, G. L. Lackner and L. E. Overman, *J. Am. Chem. Soc.*, 2015, **137**, 660–663.
212 F. Gao and A. H. Hoveyda, *J. Am. Chem. Soc.*, 2010, **132**, 10961–10963.
213 D. J. Tao, Y. Slutskyy and L. E. Overman, *J. Am. Chem. Soc.*, 2016, **138**, 2186–2189.
214 Z.-K. Wan, H. Choi, F.-A. Kang, K. Nakajima, D. Demeke and Y. Kishi, *Org. Lett.*, 2002, **4**, 4431–4434.
215 Y. Okanishi, T. Ishikawa, T. Jinnouchi, S. Hayashi, T. Takanami, H. Aoyama and T. Yoshimitsu, *J. Org. Chem.*, 2023, **88**, 1085–1092.
216 K. D. Wellington, R. C. Cambie, P. S. Rutledge and P. R. Bergquist, *J. Nat. Prod.*, 2000, **63**, 79–85.
217 X. Li, Y. Zhang, Z. Zhang and J. Wu, *Org. Chem. Front.*, 2024, **11**, 3939–3945.
218 X. Li, Z. Zhang and J. Wu, *Angew. Chem., Int. Ed.*, 2025, **64**, e202500341.
219 Z. Cao, W. Sun, J. Zhang, J. Zhuo, S. Yang, X. Song, Y. Ma, P. Lu, T. Han and C. Li, *Nat. Commun.*, 2024, **15**, 6052.
220 L. Li, Y. Yao and N. Fu, *Eur. J. Org. Chem.*, 2023, **26**, e202300166.
221 J. C. Beck, C. R. Lacker, L. M. Chapman and S. E. Reisman, *Chem. Sci.*, 2019, **10**, 2315–2319.
222 Y. Hikone, T. Kato, M. Nagatomo and M. Inoue, *Org. Lett.*, 2022, **24**, 929–933.
223 M. Hergenhahn, W. Adolf and E. Hecker, *Tetrahedron Lett.*, 1975, **16**, 1595–1598.
224 Y. Imamura, K. Takaoka, Y. Komori, M. Nagatomo and M. Inoue, *Angew. Chem., Int. Ed.*, 2023, **62**, e202219114.
225 D. Kuwana, Y. Komori, M. Nagatomo and M. Inoue, *J. Org. Chem.*, 2022, **87**, 730–736.

226 J. Taguchi, S. Fukaya, H. Fujino and M. Inoue, *J. Am. Chem. Soc.*, 2024, **146**, 34221–34230.
227 Y. Imamura, S. Yoshioka, M. Nagatomo and M. Inoue, *Angew. Chem., Int. Ed.*, 2019, **58**, 12159–12163.
228 T. Watanabe, K. Oga, H. Matoba, M. Nagatomo and M. Inoue, *J. Am. Chem. Soc.*, 2023, **145**, 25894–25902.
229 M. M. Logan, T. Toma, R. Thomas-Tran and J. Du Bois, *Science*, 2016, **354**, 865–869.
230 Y. Watanabe, K. Sakata, D. Urabe, K. Hagiwara and M. Inoue, *J. Org. Chem.*, 2023, **88**, 17479–17484.
231 T. Tokuyama, J. Daly, B. Witkop, I. L. Karle and J. Karle, *J. Am. Chem. Soc.*, 1968, **90**, 1917–1918.
232 J. Cornella, J. T. Edwards, T. Qin, S. Kawamura, J. Wang, C.-M. Pan, R. Gianatassio, M. Schmidt, M. D. Eastgate and P. S. Baran, *J. Am. Chem. Soc.*, 2016, **138**, 2174–2177.
233 J. T. Edwards, R. R. Merchant, K. S. McClymont, K. W. Knouse, T. Qin, L. R. Malins, B. Vokits, S. A. Shaw, D.-H. Bao, F.-L. Wei, T. Zhou, M. D. Eastgate and P. S. Baran, *Nature*, 2017, **545**, 213–218.
234 J. Lu, Y. Yao, L. Li and N. Fu, *J. Am. Chem. Soc.*, 2023, **145**, 26774–26782.
235 S. J. Harwood, M. D. Palkowitz, C. N. Gannett, P. Perez, Z. Yao, L. Sun, H. D. Abruña, S. L. Anderson and P. S. Baran, *Science*, 2022, **375**, 745–752.
236 H. Chen, S. Sun and X. Liao, *Org. Lett.*, 2019, **21**, 3625–3630.
237 S. K. Pedersen, S. Clementson, K. El-Chami, J. L. Kristensen and M. Jessing, *Chem. – Eur. J.*, 2023, **29**, e202300265.
238 Y. Kawamata, M. Yan, Z. Liu, D.-H. Bao, J. Chen, J. T. Starr and P. S. Baran, *J. Am. Chem. Soc.*, 2017, **139**, 7448–7451.
239 R. R. Merchant, K. M. Oberg, Y. Lin, A. J. E. Novak, J. Felding and P. S. Baran, *J. Am. Chem. Soc.*, 2018, **140**, 7462–7465.
240 H. Kim, J. B. Baker, S.-U. Lee, Y. Park, K. L. Bolduc, H.-B. Park, M. G. Dickens, D.-S. Lee, Y. Kim, S. H. Kim and J. Hong, *J. Am. Chem. Soc.*, 2009, **131**, 3192–3194.
241 J. Gu, K. Rodriguez, Y. Kanda, S. Yang, M. Ociepa, H. Wilke, A. Abrishami, L. Joergensen, T. Skak-Nielsen, J. Chen and P. Baran, *Proc. Natl. Acad. Sci. U. S. A.*, 2022, **119**, e2200814119.
242 D. D. Bikle, *Chem. Bio.*, 2014, **21**, 319–329.
243 A. J. Rodriguez, M. S. Pokle, G. L. Barnes and P. S. Baran, *J. Am. Chem. Soc.*, 2025, **147**, 16781–16785.
244 L. Zhang, M. Zhao, M. Pu, Z. Ma, J. Zhou, C. Chen, Y.-D. Wu, Y. R. Chi and J. S. Zhou, *J. Am. Chem. Soc.*, 2022, **144**, 20249–20257.
245 B. Qin, A. Szyperek and M. Tomanik, *J. Am. Chem. Soc.*, 2025, **147**, 31221–31227.
246 J. Wang, T. Qin, T. Chen, L. Wimmer, J. T. Edwards, J. Cornella, B. Vokits, S. A. Shaw and P. S. Baran, *Angew. Chem., Int. Ed.*, 2016, **55**, 9676–9679.
247 M. Zhang, H. Fan, Y. Wang and J. Gui, *Org. Lett.*, 2022, **24**, 7383–7387.
248 J. Zhang, Z. Li, J. Zhuo, Y. Cui, T. Han and C. Li, *J. Am. Chem. Soc.*, 2019, **141**, 8372–8380.
249 K. M. M. Huihui, J. A. Caputo, Z. Melchor, A. M. Olivares, A. M. Spiewak, K. A. Johnson, T. A. DiBenedetto, S. Kim, L. K. G. Ackerman and D. J. Weix, *J. Am. Chem. Soc.*, 2016, **138**, 5016–5019.
250 N. Suzuki, J. L. Hofstra, K. E. Poremba and S. E. Reisman, *Org. Lett.*, 2017, **19**, 2150–2153.
251 Y.-M. Yan, J. Ai, L. Zhou, A. C. K. Chung, R. Li, J. Nie, P. Fang, X.-L. Wang, J. Luo, Q. Hu, F.-F. Hou and Y.-X. Cheng, *Org. Lett.*, 2013, **15**, 5488–5491.
252 A. Rode, N. Müller, O. Kováč, K. Wurst and T. Magauer, *Org. Lett.*, 2024, **26**, 9017–9021.
253 J. Choi and G. C. Fu, *Science*, 2017, **356**, eaaf7230.
254 M. H. Shaw, J. Twilton and D. W. C. MacMillan, *J. Org. Chem.*, 2016, **81**, 6898–6926.
255 C.-L. Sun and Z.-J. Shi, *Chem. Rev.*, 2014, **114**, 9219–9280.
256 W. Xue, X. Jia, X. Wang, X. Tao, Z. Yin and H. Gong, *Chem. Soc. Rev.*, 2021, **50**, 4162–4184.
257 G. C. Fu, *ACS Cent. Sci.*, 2017, **3**, 692–700.
258 M. Durandetti, J.-Y. Nédélec and J. Périchon, *J. Org. Chem.*, 1996, **61**, 1748–1755.
259 D. A. Everson, R. Shrestha and D. J. Weix, *J. Am. Chem. Soc.*, 2010, **132**, 920–921.
260 X. Yu, T. Yang, S. Wang, H. Xu and H. Gong, *Org. Lett.*, 2011, **13**, 2138–2141.
261 A. H. Cherney, N. T. Kadunce and S. E. Reisman, *J. Am. Chem. Soc.*, 2013, **135**, 7442–7445.
262 M. Menger, D. Lentz and M. Christmann, *J. Org. Chem.*, 2018, **83**, 6793–6797.
263 P. Luo, W. Xia, S. L. Morris-Natschke, K.-H. Lee, Y. Zhao, Q. Gu and J. Xu, *J. Nat. Prod.*, 2017, **80**, 1679–1683.
264 A. Ahmad and A. C. B. Burtoloso, *Org. Lett.*, 2019, **21**, 6079–6083.
265 B. Yan, M. Zhou, J. Li, X. Li, S. He, J. Zuo, H. Sun, A. Li and P. Puno, *Angew. Chem., Int. Ed.*, 2021, **133**, 12969–12977.
266 K. A. Johnson, S. Biswas and D. J. Weix, *Chem. – Eur. J.*, 2016, **22**, 7399–7402.
267 W. Zhu, Q. Yin, Z. Lou and M. Yang, *Nat. Commun.*, 2022, **13**, 6633.
268 X.-B. Yan, C.-L. Li, W.-J. Jin, P. Guo and X.-Z. Shu, *Chem. Sci.*, 2018, **9**, 4529–4534.
269 Y. Wang, Y. Su and Y. Jia, *J. Am. Chem. Soc.*, 2023, **145**, 9459–9463.
270 I. I. Rodríguez, A. D. Rodríguez and H. Zhao, *J. Org. Chem.*, 2009, **74**, 7581–7584.
271 B. B. Snider, J. E. Merritt, M. A. Dombroski and B. O. Buckman, *J. Org. Chem.*, 1991, **56**, 5544–5553.
272 J. M. R. Narayanam and C. R. J. Stephenson, *Chem. Soc. Rev.*, 2011, **40**, 102–113.
273 D. Staveness, I. Bosque and C. R. J. Stephenson, *Acc. Chem. Res.*, 2016, **49**, 2295–2306.
274 Z. Zhang, W. Zhang, J. Tang, J. Che, Z. Zhang, J. Chen and Z. Yang, *J. Org. Chem.*, 2023, **88**, 10539–10554.
275 W. Zhang, Z. Zhang, J.-C. Tang, J.-T. Che, H.-Y. Zhang, J.-H. Chen and Z. Yang, *J. Am. Chem. Soc.*, 2020, **142**, 19487–19492.
276 Z.-J. Xu, X.-Y. Liu, M.-Z. Zhu, Y.-L. Xu, Y. Yu, H.-R. Xu, A.-X. Cheng and H.-X. Lou, *Org. Lett.*, 2021, **23**, 9073–9077.
277 J. Xiao, H. Wu, J.-R. Liang, P. Wu, C. Guo, Y.-W. Wang, Z.-Y. Wang and Y. Peng, *Org. Lett.*, 2024, **26**, 3481–3486.

278 G. V. Ramakrishna, L. P. Pop, Z. Latif, H. K. V. Suryadevara, L. Santo and F. Romiti, *J. Am. Chem. Soc.*, 2023, **145**, 20062–20072.
279 Z. Wang, H. Yin and G. C. Fu, *Nature*, 2018, **563**, 379–383.
280 Z. Wang, Z.-P. Yang and G. C. Fu, *Nat. Chem.*, 2021, **13**, 236–242.
281 G. V. Ramakrishna, Z. Latif and F. Romiti, *J. Am. Chem. Soc.*, 2025, **147**, 4613–4623.
282 H. Wang, X. Zhang and P. Tang, *Chem. Sci.*, 2017, **8**, 7246–7250.
283 D. A. Powell, T. Maki and G. C. Fu, *J. Am. Chem. Soc.*, 2005, **127**, 510–511.
284 J. Zhang, X. Luo, J. Zhang and C. Li, *J. Am. Chem. Soc.*, 2025, **147**, 5933–5942.
285 Z. Dong and D. W. C. MacMillan, *Nature*, 2021, **598**, 451–456.
286 Z. Li, W. Sun, X. Wang, L. Li, Y. Zhang and C. Li, *J. Am. Chem. Soc.*, 2021, **143**, 3536–3543.
287 J. Wang, J. Zhao and H. Gong, *Chem. Commun.*, 2017, **53**, 10180–10183.
288 K. Komeyama, R. Ohata, S. Kiguchi and I. Osaka, *Chem. Commun.*, 2017, **53**, 6401–6404.
289 J. Liu, C. Yang, X. Lu, Z. Zhang, L. Xu, M. Cui, X. Lu, B. Xiao, Y. Fu and L. Liu, *Chem. – Eur. J.*, 2014, **20**, 15334–15338.
290 G. A. Molander, K. M. Traister and B. T. O'Neill, *J. Org. Chem.*, 2015, **80**, 2907–2911.
291 L. K. G. Ackerman, L. L. Anka-Lufford, M. Naodovic and D. J. Weix, *Chem. Sci.*, 2015, **6**, 1115–1119.
292 Y. Ye, H. Chen, J. L. Sessler and H. Gong, *J. Am. Chem. Soc.*, 2019, **141**, 820–824.
293 C. C. Nawrat, C. R. Jamison, Y. Slutskyy, D. W. C. MacMillan and L. E. Overman, *J. Am. Chem. Soc.*, 2015, **137**, 11270–11273.
294 T. K. Allred, A. P. Dieskau, P. Zhao, G. L. Lackner and L. E. Overman, *Angew. Chem., Int. Ed.*, 2020, **59**, 6268–6272.
295 T. K. Allred, A. P. Dieskau, P. Zhao, G. L. Lackner and L. E. Overman, *J. Org. Chem.*, 2020, **85**, 15532–15551.
296 J. Wu, J. Bao, J. Deng, H. Tian and J. Gui, *J. Am. Chem. Soc.*, 2025, **147**, 30599–30605.
297 Y.-P. Song and N.-Y. Ji, *Nat. Prod. Bioprospect.*, 2024, **14**, 14.
298 J. Zhuo, C. Zhu, J. Wu, Z. Li and C. Li, *J. Am. Chem. Soc.*, 2022, **144**, 99–105.
299 O. Vyhivskyi and O. Baudoin, *J. Am. Chem. Soc.*, 2024, **146**, 11486–11492.
300 M. Kosugi, K. Kurino, K. Takayama and T. Migita, *J. Organomet. Chem.*, 1973, **56**, C11–C13.
301 G. E. Keck and J. B. Yates, *J. Am. Chem. Soc.*, 1982, **104**, 5829–5831.
302 M. M. Heravi and A. Nazari, *RSC Adv.*, 2022, **12**, 9944–9994.
303 D. J. Edmonds, D. Johnston and D. J. Procter, *Chem. Rev.*, 2004, **104**, 3371–3404.
304 K. C. Nicolaou, S. P. Ellery and J. S. Chen, *Angew. Chem., Int. Ed.*, 2009, **48**, 7140–7165.
305 T. Nakata, *Chem. Soc. Rev.*, 2010, **39**, 1955–1972.
306 Y. Gao and D. Ma, *Nat. Synth.*, 2022, **1**, 275–288.
307 B.-C. Hong and R. R. Indurmuddam, *Org. Biomol. Chem.*, 2024, **22**, 3799–3842.
308 S. Le, J. Li, J. Feng, Z. Zhang, Y. Bai, Z. Yuan and G. Zhu, *Nat. Commun.*, 2022, **13**, 4734.
309 A. G. Capacci, J. T. Malinowski, N. J. McAlpine, J. Kuhne and D. W. C. MacMillan, *Nat. Chem.*, 2017, **9**, 1073–1077.
310 S. Rendler and D. W. C. MacMillan, *J. Am. Chem. Soc.*, 2010, **132**, 5027–5029.
311 P. V. Pham, K. Ashton and D. W. C. MacMillan, *Chem. Sci.*, 2011, **2**, 1470–1473.
312 R. J. Comito, F. G. Finelli and D. W. C. MacMillan, *J. Am. Chem. Soc.*, 2013, **135**, 9358–9361.
313 C.-J. Li, *Acc. Chem. Res.*, 2009, **42**, 335–344.
314 C. Lee, G. Kang, J. You, T. Kim, H.-S. Lee, Y. Park and S. Han, *JACS Au*, 2025, **5**, 1096–1103.
315 S. Esposti, D. Dondi, M. Fagnoni and A. Albini, *Angew. Chem., Int. Ed.*, 2007, **46**, 2531–2534.
316 D. Gorbachev, E. Smith, S. P. Argent, G. N. Newton and H. W. Lam, *Chem. – Eur. J.*, 2022, **28**, e202201478.
317 W. Yao, Z. Liu, H. Ling, H. Wang, H. Zheng, S.-H. Wang, D.-Y. Zhu, S.-Y. Zhang and X. Chen, *J. Am. Chem. Soc.*, 2025, **147**, 15963–15969.
318 J. L. Hofstra, K. E. Poremba, A. M. Shimozono and S. E. Reisman, *Angew. Chem., Int. Ed.*, 2019, **58**, 14901–14905.
319 X. Zhang and D. W. C. MacMillan, *J. Am. Chem. Soc.*, 2017, **139**, 11353–11356.
320 S. Guo, J. Liu and D. Ma, *Angew. Chem., Int. Ed.*, 2015, **54**, 1298–1301.
321 Y. Zheng, L. Teng, T. Zhou, Z. Liu, K. Guo, H. Li, T. Li, L. Wang, Y. Liu and S. Li, *Angew. Chem., Int. Ed.*, 2025, **64**, e202421497.
322 B. Hong, W. Liu, J. Wang, J. Wu, Y. Kadonaga, P.-J. Cai, H.-X. Lou, Z.-X. Yu, H. Li and X. Lei, *Chem*, 2019, **5**, 1671–1681.
323 J. Yang, X. Zhang, F. Zhang, S. Wang, Y. Tu, Z. Li, X. Wang and H. Wang, *Angew. Chem., Int. Ed.*, 2020, **59**, 8471–8475.
324 Y. Gao, Q. Xia, A. Zhu, W. Mao, Y. Mo, H. Ding and J. Xuan, *J. Am. Chem. Soc.*, 2024, **146**, 18230–18235.
325 W. J. Robbins, F. Kavanagh and A. Hervey, *Proc. Natl. Acad. Sci. U. S. A.*, 1947, **33**, 171–176.
326 Á. Péter, S. Agasti, O. Knowles, E. Pye and D. J. Procter, *Chem. Soc. Rev.*, 2021, **50**, 5349–5365.
327 M. Szostak, M. Spain and D. J. Procter, *Chem. Soc. Rev.*, 2013, **42**, 9155–9183.
328 M. Szostak, N. J. Fazakerley, D. Parmar and D. J. Procter, *Chem. Rev.*, 2014, **114**, 5959–6039.
329 X. Just-Baringo and D. J. Procter, *Acc. Chem. Res.*, 2015, **48**, 1263–1275.
330 M. P. Plesniak, H.-M. Huang and D. J. Procter, *Nat. Rev. Chem.*, 2017, **1**, 0077.
331 H.-M. Huang, M. H. Garduño-Castro, C. Morrill and D. J. Procter, *Chem. Soc. Rev.*, 2019, **48**, 4626–4638.
332 K. Takatori, S. Ota, K. Tendo, K. Matsunaga, K. Nagasawa, S. Watanabe, A. Kishida, H. Kogen and H. Nagaoka, *Org. Lett.*, 2017, **19**, 3763–3766.
333 L. Li, W. Liang, M. E. Rivera, Y.-C. Wang and M. Dai, *J. Am. Chem. Soc.*, 2023, **145**, 53–57.
334 J. R. Annand, A. R. Henderson, K. S. Cole, A. J. Maurais, J. Becerra, Y. Liu, E. Weerapana, A. N. Koehler, A. K. Mapp

and C. S. Schindler, *ACS Med. Chem. Lett.*, 2020, **11**, 1913–1918.
335 T.-L. Zheng, C.-Y. Huo, W. Bao, X.-T. Xu, W.-H. Dai, F. Cheng, D.-S. Duan, L.-L. Yang, X.-M. Zhang, D.-Y. Zhu and S.-H. Wang, *Org. Lett.*, 2023, **25**, 7476–7480.
336 A. Eggert, K. T. Schuppe, H. L. S. Fuchs, M. Brönstrup and M. Kalesse, *Org. Lett.*, 2024, **26**, 2893–2896.
337 D. L. Golden, S.-E. Suh and S. S. Stahl, *Nat. Rev. Chem.*, 2022, **6**, 405–427.
338 H. Yi, G. Zhang, H. Wang, Z. Huang, J. Wang, A. K. Singh and A. Lei, *Chem. Rev.*, 2017, **117**, 9016–9085.
339 L. Stateman, K. Nakafuku and D. Nagib, *Synthesis*, 2018, **50**, 1569–1586.
340 L. Capaldo and D. Ravelli, *Eur. J. Org. Chem.*, 2017, 2056–2071.
341 Y. Wang, S. Dana, H. Long, Y. Xu, Y. Li, N. Kaplaneris and L. Ackermann, *Chem. Rev.*, 2023, **123**, 11269–11335.
342 M. D. Kärkäs, *Chem. Soc. Rev.*, 2018, **47**, 5786–5865.
343 C. Ma, P. Fang and T.-S. Mei, *ACS Catal.*, 2018, **8**, 7179–7189.
344 M. Munda, S. Niyogi, K. Shaw, S. Kundu, R. Nandi and A. Bisai, *Org. Biomol. Chem.*, 2022, **20**, 727–748.
345 S. Chakrabarty, Y. Wang, J. C. Perkins and A. R. H. Narayan, *Chem. Soc. Rev.*, 2020, **49**, 8137–8155.
346 J. C. Lewis, P. S. Coelho and F. H. Arnold, *Chem. Soc. Rev.*, 2011, **40**, 2003–2021.
347 F. Li, X. Zhang and H. Renata, *Curr. Opin. Chem. Biol.*, 2019, **49**, 25–32.
348 Y. Nakano, K. F. Biegasiewicz and T. K. Hyster, *Curr. Opin. Chem. Biol.*, 2019, **49**, 16–24.
349 I. Bakanas, R. F. Lusi, S. Wiesler, J. Hayward Cooke and R. Sarpong, *Nat. Rev. Chem.*, 2023, **7**, 783–799.
350 Y. Shen, L. Li, X. Xiao, S. Yang, Y. Hua, Y. Wang, Y. Zhang and Y. Zhang, *J. Am. Chem. Soc.*, 2021, **143**, 3256–3263.
351 J. F. Hoskin and E. J. Sorensen, *J. Am. Chem. Soc.*, 2022, **144**, 14042–14046.
352 B. Xu, Z. Zhang and M. Dai, *J. Am. Chem. Soc.*, 2025, **147**, 17592–17597.
353 G. Sennari, H. Yamagishi and R. Sarpong, *J. Am. Chem. Soc.*, 2024, **146**, 7850–7857.
354 M. Deng, F. Wu, T. Liu, Z. Jiang and T. Luo, *J. Am. Chem. Soc.*, 2025, **147**, 8132–8137.

